AD-A148 771 ACOUSTIC RADIATION FROM SINGLE AND DOUBLE RIBBED CIRCULAR CYLINDRICAL SHE..(U) PENNSYLVANIA STATE UNIV UNIVERSITY PARK APPLIED RESEARCH LAB.. 1/2

UNCLASSIFIED C B BURROUGHS ET AL. 30 MAR 84 F/G 20/1 NL

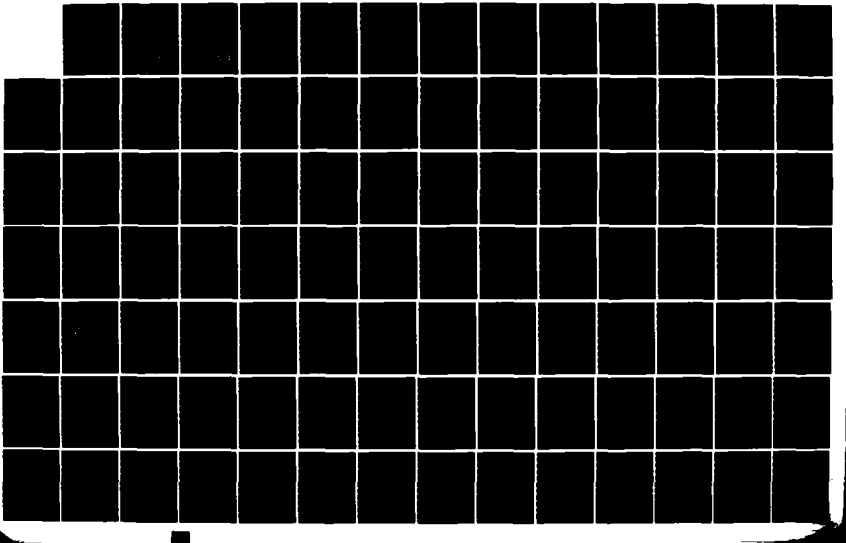

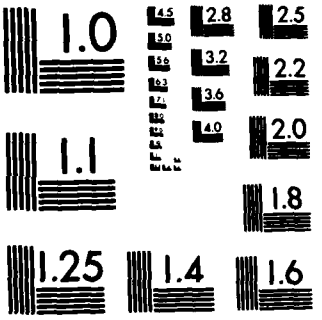

MICROCOPY RESOLUTION TEST CHART
NATIONAL BUREAU OF STANDARDS-1963-A

12

ACOUSTIC RADIATION FROM SINGLE AND DOUBLE RIBBED CIRCULAR CYLINDRICAL SHELLS

C. B. Burroughs, S. I. Hayek,
J. E. Hallander and D. A. Bostian

Technical Memorandum
File No. TM 84-76
30 March 1984
Contract N00024-79-C-6043

Copy No. 11

The Pennsylvania State University
Intercollege Research Programs and Facilities
APPLIED RESEARCH LABORATORY
Post Office Box 30
State College, Pa. 16804

NAVY DEPARTMENT

NAVAL SEA SYSTEMS COMMAND

ACOUSTIC RADIATION FROM SINGLE AND DOUBLE RIBBED CIRCULAR CYLINDRICAL SHELLS

C. B. Burroughs. S. I. Hayek,
J. E. Hallander and D. A. Bostian

Technical Memorandum
File No. TM 84-76
30 March 1984
Contract N00024-79-C-6043

Copy No. 11

The Pennsylvania State University
Intercollege Research Programs and Facilities
APPLIED RESEARCH LABORATORY
Post Office Box 30
State College, PA 16804

NAVY DEPARTMENT

NAVAL SEA SYSTEMS COMMAND

UNCLASSIFIED

SECURITY CLASSIFICATION OF THIS PAGE (When Data Entered)

REPORT DOCUMENTATION PAGE		READ INSTRUCTIONS BEFORE COMPLETING FORM
1. REPORT NUMBER 84-76	2. GOVT ACCESSION NO.	3. RECIPIENT'S CATALOG NUMBER
4. TITLE (and Subtitle) ACOUSTIC RADIATION FROM SINGLE AND DOUBLE RIBBED CIRCULAR CYLINDRICAL SHELLS		5. TYPE OF REPORT & PERIOD COVERED Technical Memorandum 6. PERFORMING ORG. REPORT NUMBER
7. AUTHOR(s) C. B. Burroughs, S. I. Hayek, J. E. Hallander and D. A. Bostian		8. CONTRACT OR GRANT NUMBER(s) N00024-79-C-6043
9. PERFORMING ORGANIZATION NAME AND ADDRESS Applied Research Laboratory Post Office Box 30 State College, PA 16804		10. PROGRAM ELEMENT, PROJECT, TASK AREA & WORK UNIT NUMBERS
11. CONTROLLING OFFICE NAME AND ADDRESS Office of Naval Research [Code 474] 800 North Quincy Street Arlington, VA 22217		12. REPORT DATE 30 March 1984 13. NUMBER OF PAGES 103
14. MONITORING AGENCY NAME & ADDRESS(if different from Controlling Office) Naval Sea Systems Command Department of the Navy Washington, DC 20362		15. SECURITY CLASS. (of this report) Unclassified 15a. DECLASSIFICATION/DOWNGRADING SCHEDULE

16. DISTRIBUTION STATEMENT (of this Report)

Approved for public release. Distribution unlimited.
Per NAVSEA - November 1984

17. DISTRIBUTION STATEMENT (of the abstract entered in Block 20, if different from Report)

18. SUPPLEMENTARY NOTES

19. KEY WORDS (Continue on reverse side if necessary and identify by block number)

acoustic radiation
cylindrical shells

20. ABSTRACT (Continue on reverse side if necessary and identify by block number)

Measurements of the acoustic radiation from single and double ribbed circular cylindrical shells were made on the NUSC Transducer Calibration Platform (TCP) in Lake Seneca, NY. Six different types of mechanical drives were used at each of three locations inside the inner shell. Measurements of the shell vibration and acoustic radiation were made with and without outer shells installed around the inner shell structure. For

DD FORM 1 JAN 73 1473 EDITION OF 1 NOV 65 IS OBSOLETE

UNCLASSIFIED

SECURITY CLASSIFICATION OF THIS PAGE (When Data Entered)

two types of drives, measurements were made with a pressure release layer installed between the inner and outer shell surfaces. Acoustic radiation measurements were made as a function of frequency from 20 to 5,000 Hz and as a function of observation direction at several frequencies for each shell and drive measurement configuration. Measured acoustic radiation data as a function of frequency have been processed. Analysis of the processed data is presented and discussed. It is shown that the location of the drive had a significant effect on the acoustic radiation. The outer shell reduced the acoustic radiation at shell resonant frequencies, but had little effect at other frequencies. The pressure release layer in the double shell had little effect on the acoustic radiation.

From: C. B. Burroughs [2], S. I. Hayek [2], J. E. Hallander and D. A. Bostian

Subject: Acoustic Radiation from Single and Double Ribbed Circular Cylindrical Shells

Abstract: Measurements of the acoustic radiation from single and double ribbed circular cylindrical shells were made on the NUSC Transducer Calibration Platform (TCP) in Lake Seneca, NY. Six different types of mechanical drives were used at each of three locations inside the inner shell. Measurements of the shell vibration and acoustic radiation were made with and without outer shells installed around the inner shell structure. For two types of drives, measurements were made with a pressure release layer installed between the inner and outer shell surfaces. Acoustic radiation measurements were made as a function of frequency from 20 to 5,000 Hz and as a function of observation direction at several frequencies for each shell and drive measurement configuration. Measured acoustic radiation data as a function of frequency have been processed. Analysis of the processed data is presented and discussed. It is shown that the location of the drive had a significant effect on the acoustic radiation. The outer shell reduced the acoustic radiation at shell resonant frequencies, but had little effect at other frequencies. The pressure release layer in the double shell had little effect on the acoustic radiation.

1. Introduction

Acoustic radiation from ribbed elastic structures has been the subject of a number of investigations. Analytic models of acoustic radiation from ribbed infinite plates (i.e., see Refs. [1], [2] and [3]) show that below the critical frequency, where the bending wavenumber is larger than the acoustic wavenumber, the principal mechanisms of acoustic radiation are (1) the conversion of high, non-radiating, subsonic wavenumbers into low, radiating, supersonic wavenumbers by forces applied to the plate by the ribs and on the presence of low, radiating supersonic wavenumbers in the structural nearfield of locally-applied external forces. Thus, the areas near externally-applied forces and ribs become local areas of radiation. For a periodically line-supported plate, peaks in the acoustic radiation are due to the coherent addition of radiation from the array of line supports. By decreasing the area over which structural waves propagate, structural damping decreases the aperture of the array of line support radiators, thus reducing the peaks and valleys in the acoustic radiation as a function of frequency. The same conclusions are applicable to ribbed circular cylindrical shells [4].

The difficulty presented by mixed boundary conditions in analytic models of acoustic radiation from finite plates and cylinders (i.e., see Refs. [5] and [6]) has prevented the same kind of success in identifying the mechanisms of acoustic radiation experienced in the analysis of radiation from infinite plates and cylinders. However, it is well-known that peaks in the acoustic radiation at low frequencies, where the modal density is low, are due to the resonance response of the structure. Several analytic models on resonant frequencies and mode shapes of finite ribbed cylindrical shells, such as those discussed in Ref. [7], are available.

Several questions on the mechanisms of acoustic radiation from finite ribbed cylindrical shells immersed in an inviscid acoustic medium remain unanswered.

For example,

- What is the relation between the resonant mode shape of a fluid-loaded finite cylindrical shell and the acoustic radiation efficiency and directionality pattern?
- What are the effects of drive type (e.g., longitudinal, radial and moment) on acoustic radiation from fluid-loaded, finite, ribbed cylinders?
- How do different types of rib reactive forces (e.g., moment and shear, as well as radial) applied to the shell over finite areas (e.g., where the rib/shell contact area has finite width as well as length around the circumference of the shell) affect the acoustic radiation from finite ribbed cylindrical shells?
- How does an outer concentric shell affect the acoustic radiation from a ribbed cylindrical shell?
- What effect does a pressure release layer have on the acoustic radiation from a fluid-loaded ribbed cylindrical shell?

To begin to address these questions on the mechanisms of acoustic radiation, as well as other questions that may arise later, an extensive measurement program was funded by ONR Code 474 and conducted by ARL/PSU. All of the data in this program has been collected; however not all of the collected data has been processed. Preliminary results, based on the data that has been processed, are presented and discussed in this report. The remaining data are

being processed and will be incorporated in the final report on this measurement program.

Descriptions of the measurements and processed data are given in Section 2. In Section 3, the analysis of the measured data is discussed. Conclusions and recommendations are given in Section 4. The measurement plan is given in Appendix A and a sample run of the data processing and plotting computer program is presented in Appendix B.

2. Description of Measurements

2.1 Shell Assemblies

Single and double shell assemblies were used in the measurements. The single shell assembly consists of five shell sections bolted together end-to-end to make up the 20 ft long single shell assembly. To make the double shell assembly, concentric shells constructed of sheet metal were wrapped around the single shell assembly. A sketch of the double shell assembly is given in Fig. 1. The space between the inner and outer shells is free-flooded. As shown in Fig. 1, bridging the space between the inner and outer shells are sheet metal partitions positioned at every other inner shell rib location. The inner shell assembly is water-tight.

As shown in Fig. 1, each of the five shell sections that make up the single shell assembly have two hand holes. Opposite to the hand holes are two longitudinal rails. Each shell section has five ribs. At both ends of each shell section is a joint band where the shell sections are bolted together. End caps are used to seal the ends of the single shell assembly.

Sketches are given in Figs. 2, 3 and 4 of side, top and end views, respectively, of one of the shell sections that make up the single shell

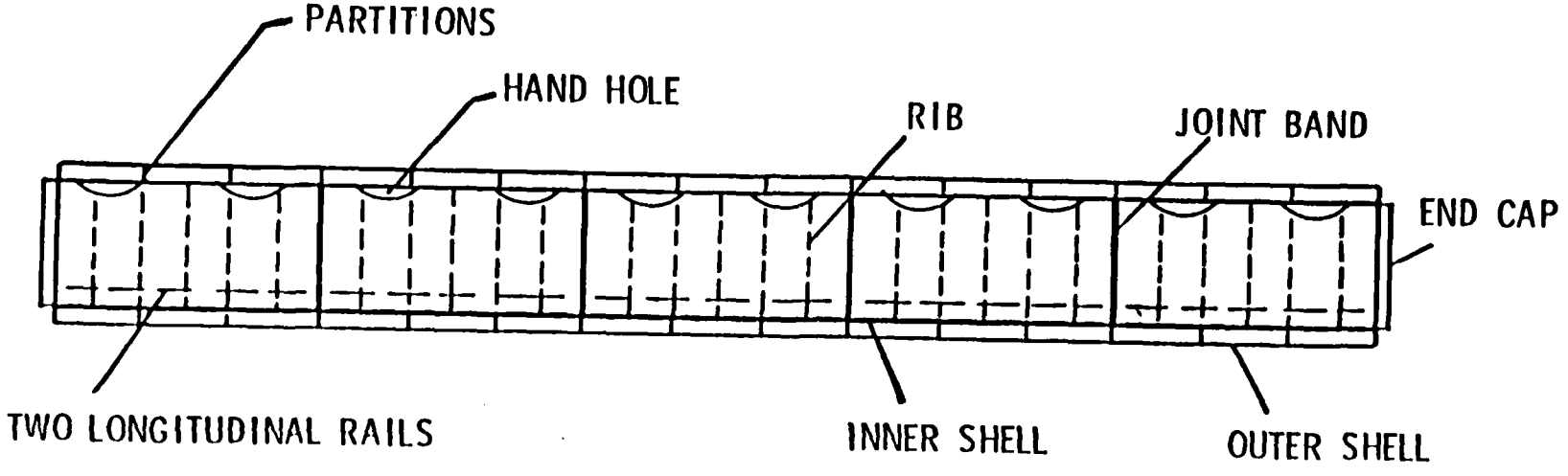

Figure 1. Single and Double Shell Configuration

30 March 1984
CBB:SIH:JEH:DAB:lhz

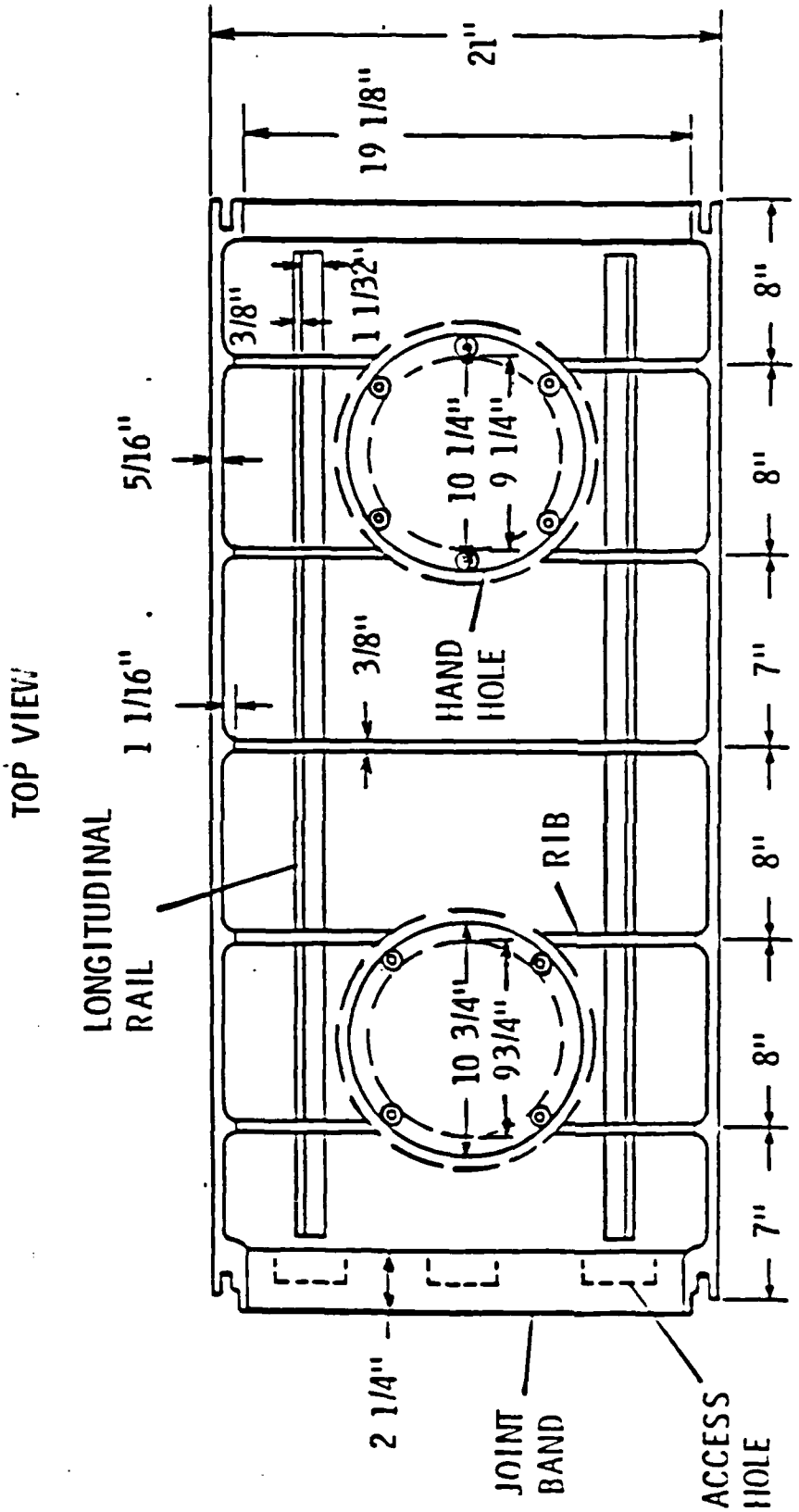

Figure 2. Top View of Shell Section

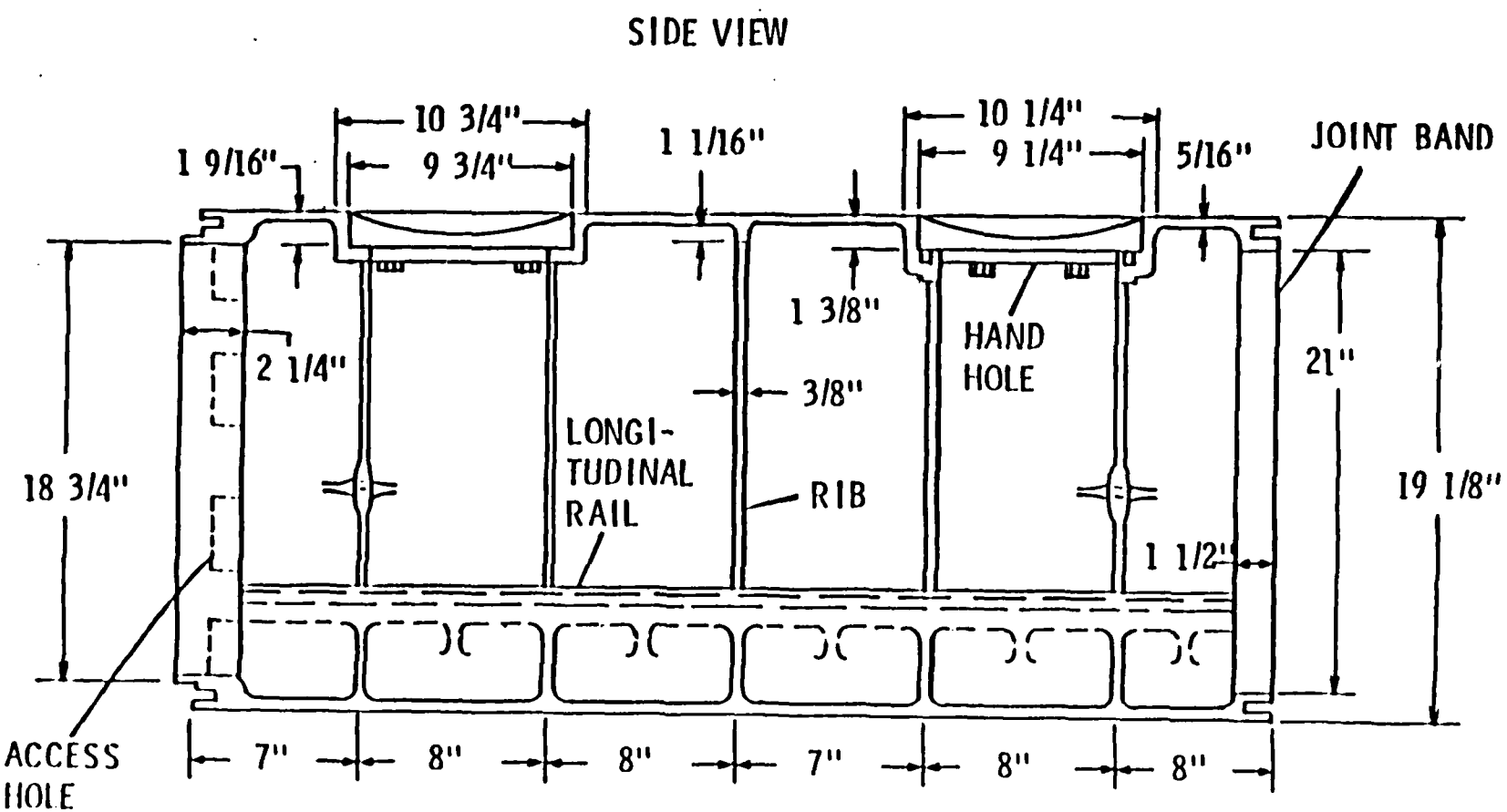

Figure 3. Side View of Shell Section

30 March 1984
CBB:SIH:JEH:DAB:lhz

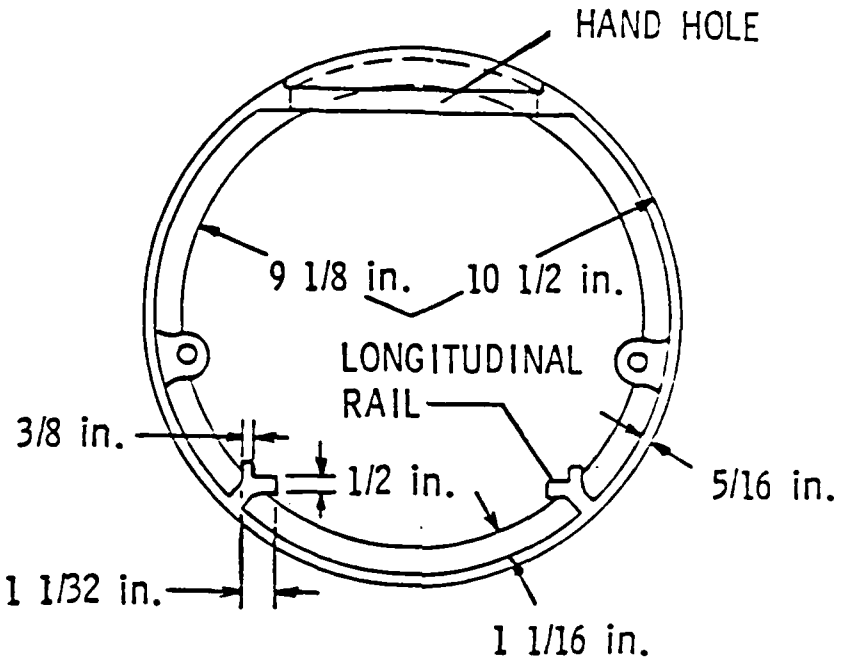

Figure 4. End View of Shell Section

assembly. The shell sections are made of aluminum and each of the shell sections weighs 166 lbs. A sketch of the joint band, showing the coupling of the shell sections, is given in Fig. 5. Shown in Fig. 3 are the two hand holes and the two longitudinal rails running the length of each shell section. The spacing of the five circumferential reinforcing ribs is between seven and eight inches.

Sketches of the two end caps are shown in Figs. 6 and 7. The instrumentation cables penetrate the end cap shown in Fig. 7 and are attached to bars welded to the outside of the end cap.

The outer shell assembly consists of seven shells constructed of 16-gauge (0.05 inch thick) cold rolled steel. The diameter of each of the outer shells is 25 inches and the length is 36 inches. The ribs of the outer shells, referred to as partitions to distinguish them from the inner shell ribs, are also constructed of 16-gauge steel. The height of the partitions is two inches, so that when the outer shells are installed, the partitions are in a tight metal-to-metal contact with the outer surface of the inner shells. The space between the surfaces of the inner and outer shells is two inches and is free-flooded. Since the partitions are located at every other inner shell rib position and the spacing of the inner shell ribs is not constant, the spacing of the partitions varies from 14 to 16 inches.

A clam shell design was used on the outer shells so that they could be easily installed and removed. A piano hinge was used to attach the two halves of the outer shells. Angle irons were attached to the opposite edges on each of the shell halves. The outer shells were opened, wrapped around the inner shell, and closed by bolting the angle irons together to form a tight fit around the inner shell assembly.

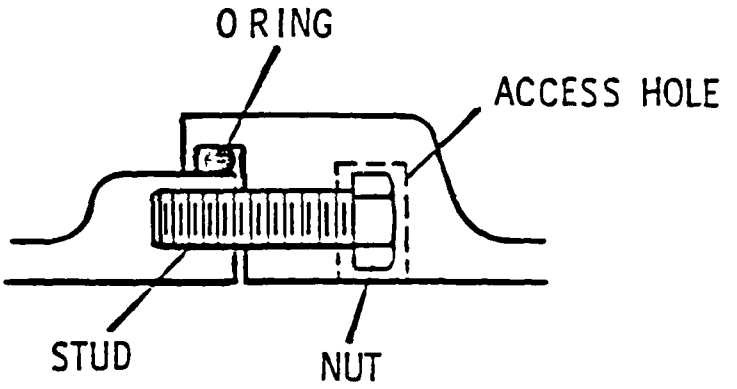

Figure 5. Sketch of Cross-Section of Joint Band

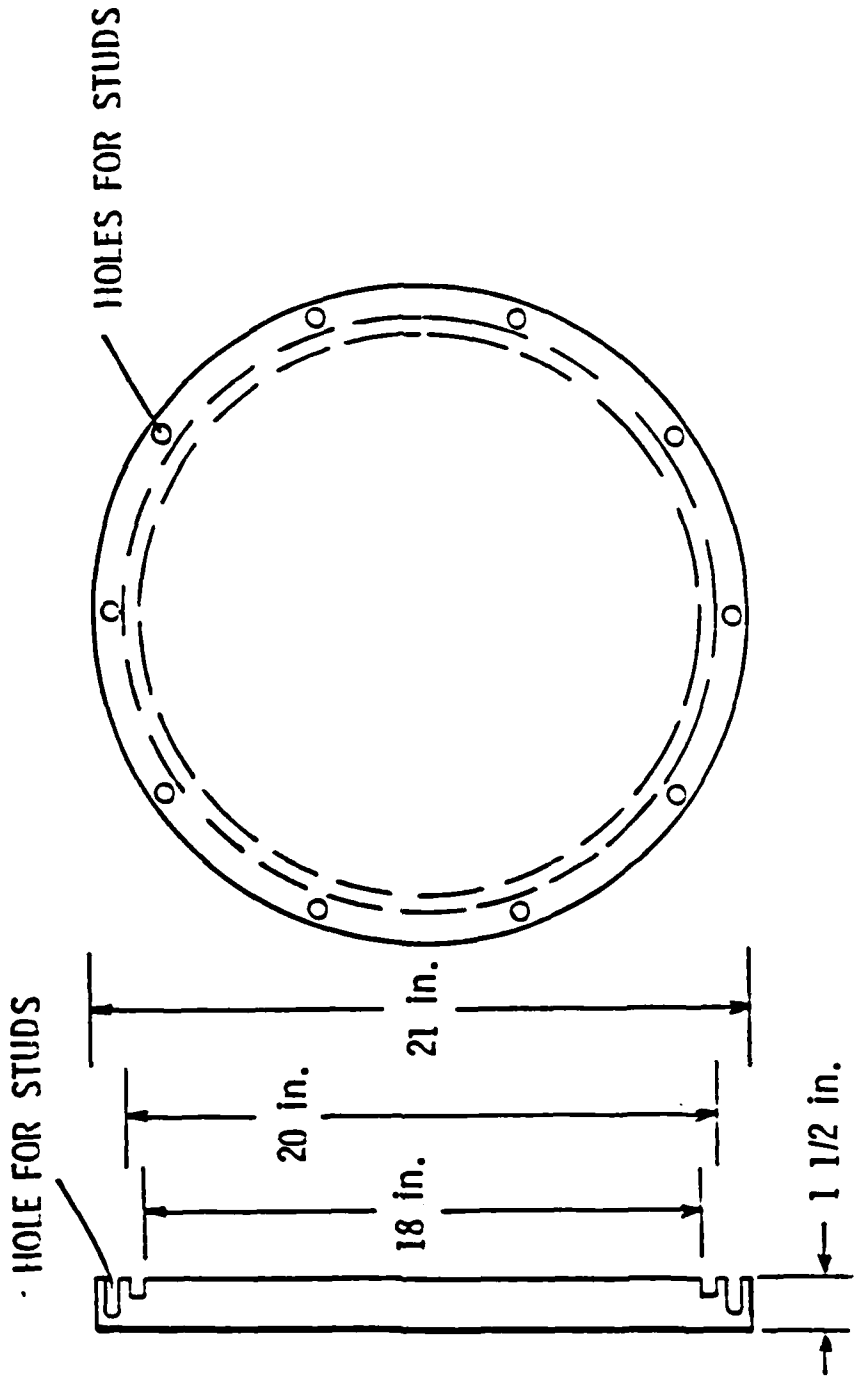

Figure 6. End Caps without Cable Penetrations

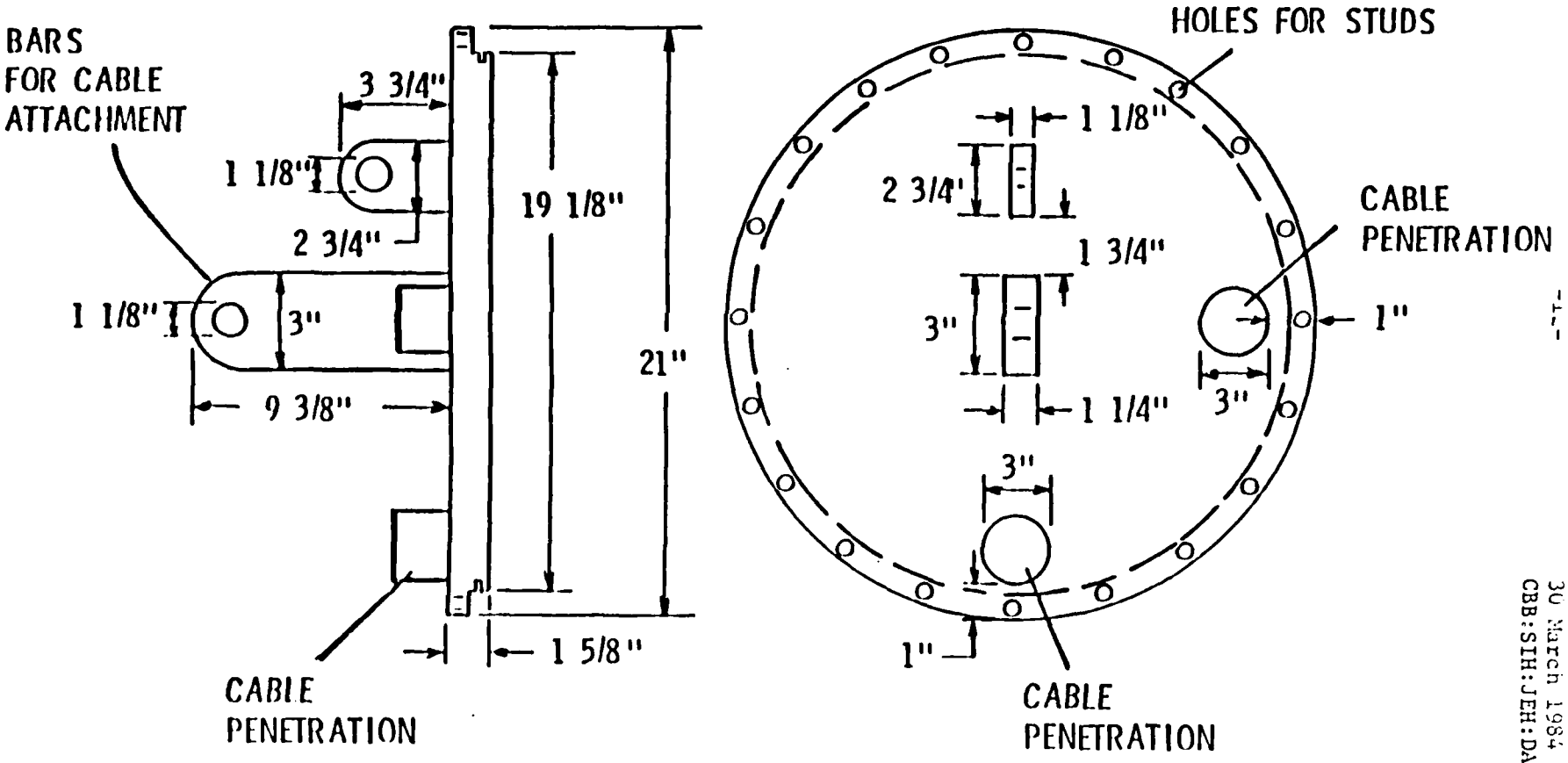

Figure 7. End Caps with Cable Penetrations

30 March 1984
CBB:SIH:JEH:DAB:lhz

After installation around the inner shell assembly, the outer shells were attached to each other with screws around the perimeter.

The pressure release layer installed between the inner and outer shells to investigate the effect of acoustic decoupling on the acoustic radiation from the shell consisted of two layers of closed-cell styrofoam. The inner layer was one inch thick and the outer layer one-half inch thick. The coating covered the middle three of the inner shells of the shell assembly, leaving the two end shells uncovered. The one inch layer was wrapped around the inner shell, followed by the one-half inch layer. Both layers wre pulled tight up against the surface of the inner shell before taping the ends together. One-half inch gaps were left between layer sections for the outer shell partitions. After wrapping the two layers around the inner shells, the outer shells were installed.

2.2 Measurement Instrumentation

The locations of the accelerometers and shakers installed inside the inner shell assembly are shown in Fig. 8. All of the sensors are in the half of the shell assembly opposite to the end with the cable penetrations. The accelerometers are BBN 501s which have internal preamplifiers to reduce cable noise, a frequency response of 4 to 20,000 Hz with a ± 5% maximum variation in sensitivity, and a nominal sensitivity of 10 mV/g. The sensitivity of each accelerometer measured by ARL/PSU before installation inside the shell assembly is given in Table 1. The accelerometers were glued with epoxy to flat spots ground into the inner surface of the inner shell.

Triaxial accelerometers were located at the base of the lower shaker at each of the three shaker locations. These accelerometers were glued to one-half inch cubic aluminum blocks and the blocks glued as close to the base

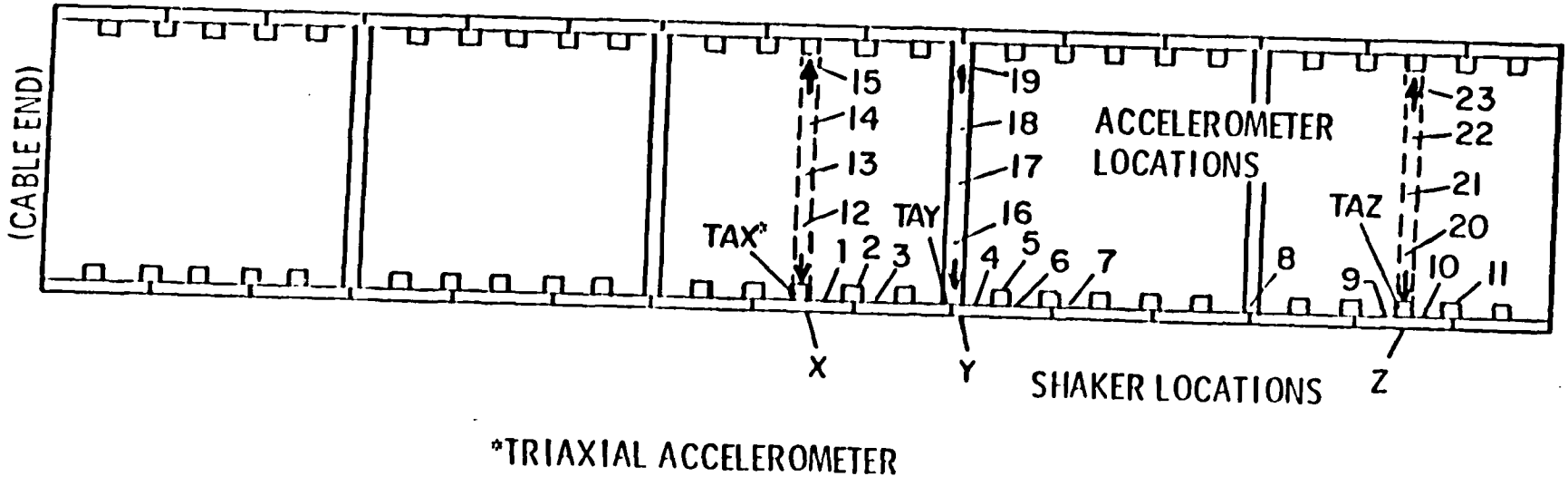

Figure 8. Shaker and Accelerometer Locations

30 March 1984
CDB:SIH:JEH:DAB:lhz

Table 1. Accelerometer Sensitivities

Location	BBN 501 Serial Number	Sensitivity (mV/g)
A1	266	9.31
A2	1435	9.72
A3	292	6.83
A4	524	9.42
A5	051	7.31
A6	528	7.32
A7	464	8.84
A8	1411	9.45
A9	1422	9.43
A10	1444	9.35
A11	215	8.26
A12	182	7.97
A13	503	7.36
A14	253	8.82
A15	030	8.61
A16	513	6.42
A17	221	8.46
A18	216	8.40
A19	080	8.94
A20	216	7.56
A21	296	9.57
A22	056	8.85
A23	250	8.85
TAX(X)*	1402	9.52
TAX(Y)	1429	9.48
TAX(Z)	1446	9.47
TAY(X)	265	8.98
TAY(Y)	406	8.92
TAY(Z)	049	8.92
TAZ(X)	419	7.26
TAX(Y)	214	7.21
TAX(Z)	288	7.23

*Triaxial accelerometer at shaker location X in radial (X) direction [circumferential direction is denoted by (Y) and axial direction by (Z)].

of the shaker mount blocks as possible with one accelerometer oriented radially, one oriented circumferentially, and one oriented axially.

To make the farfield acoustic radiation measurements, two NRL Underwater Sound Reference Division (USRD) Type H56 hydrophones were hung from the NUSC Transducer Calibration Platform (TCP) at Lake Seneca. The sensitivities of these hydrophones are given in Figure 9.

The shakers were Wilcoxon F4 shakers with impedance heads. These shakers have a usable frequency range from 10 to 7,000 Hz. The force and accelerometer signals from the impedance head in each of the shakers were recorded along with the signals from the accelerometers. Sensitivities for the force gauges and accelerometers in the impedance heads are given in Table 2.

To accommodate the different shaker positions required for the different types of shell excitation, i.e., radial, moment and longitudinal drives, three types of shaker mount foundations were used. For the radial drives, two mounting blades were welded to the inner shell surface, one in between the two longitudinal rails (the lower location in Fig. 8) and one between the two hand holes (the upper location in Fig. 8). A sketch of the radial-drive mounting blocks used over a rib at locations X and Z is given in Fig. 10(a). The radial-drive mounting blocks used at location Y on a joint band are sketched in Fig. 10(b). The mounting blocks are aluminum. The shakers were screwed to the mounting blocks with a threaded stud.

For the moment drives, an aluminum bar was mounted to the radial-drive mounting block with four bolts screwed into the four taped holes shown in Fig. 10. A sketch of the moment-drive bar is given in Fig. 11. The mounting arrangement for the circumferential moment drives is shown in

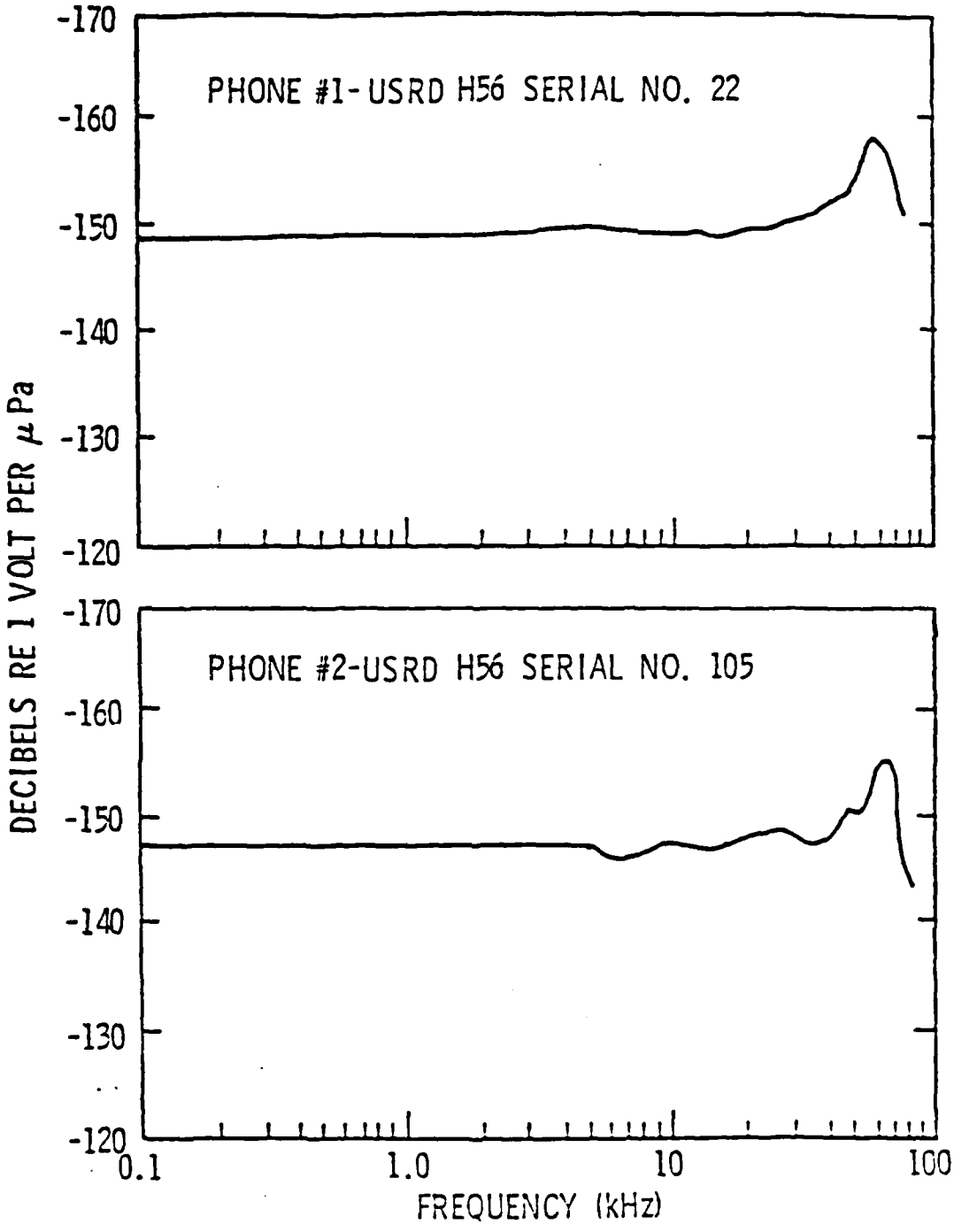

Figure 9. Sensitivities of Hydrophones

Table 2. Sensitivities for Shaker Impedance Heads

Shaker Location	Wilcoxon F4 Serial No.	Force Gauge Sensitivity (mV/lb)	Acceleration Sensitivity (mV/g)
X_1*	73	360	192
X_2	45	375	187
Y_1	9439	354	190
Y_2	9441	359	201
Z_1	----	212	238
Z_2	9440	388	179

*First (lower) shaker at shaker location X (see Fig. 8).

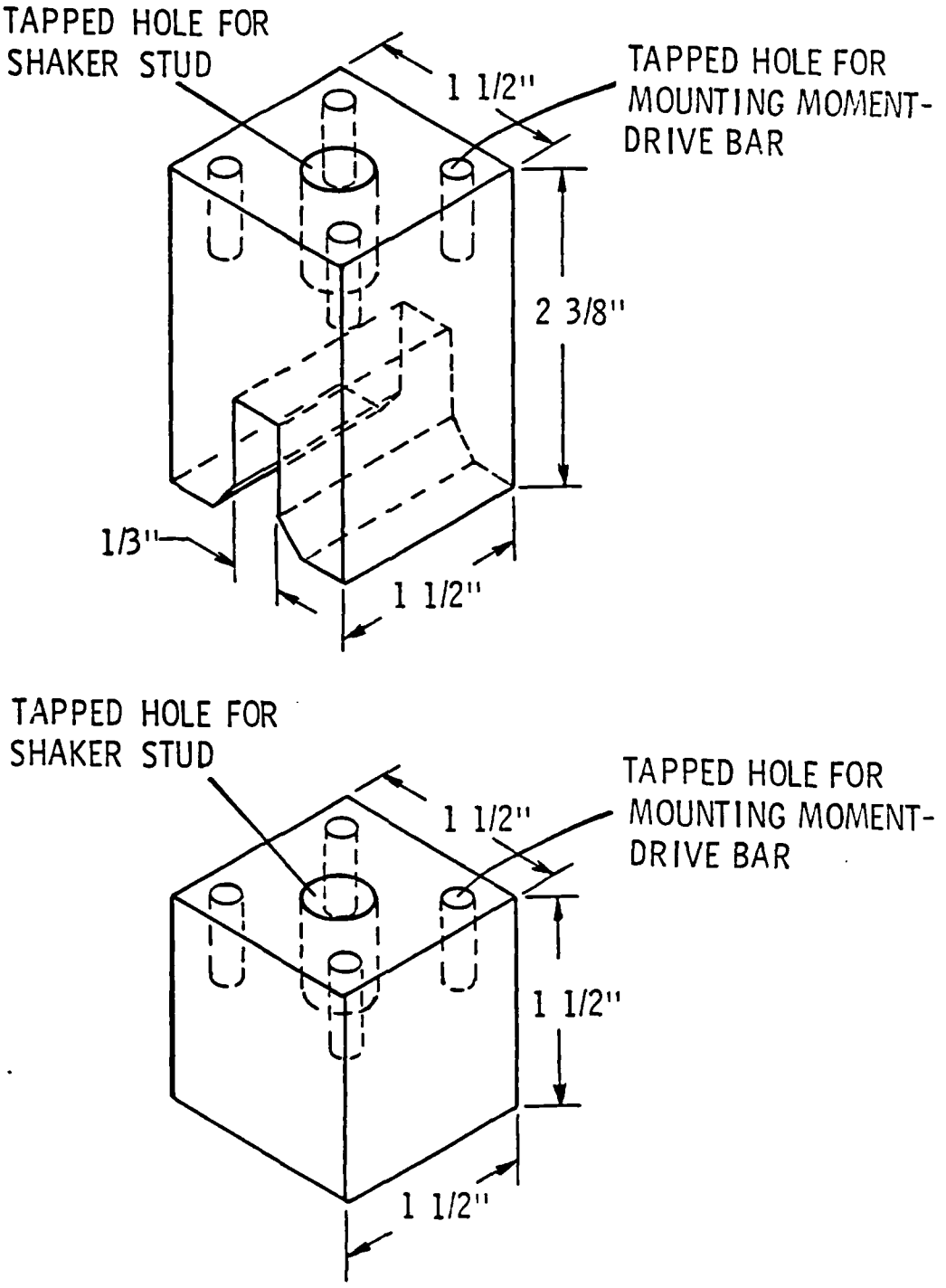

Figure 10. Shaker Mounting Blocks for Radial and Moment Drives

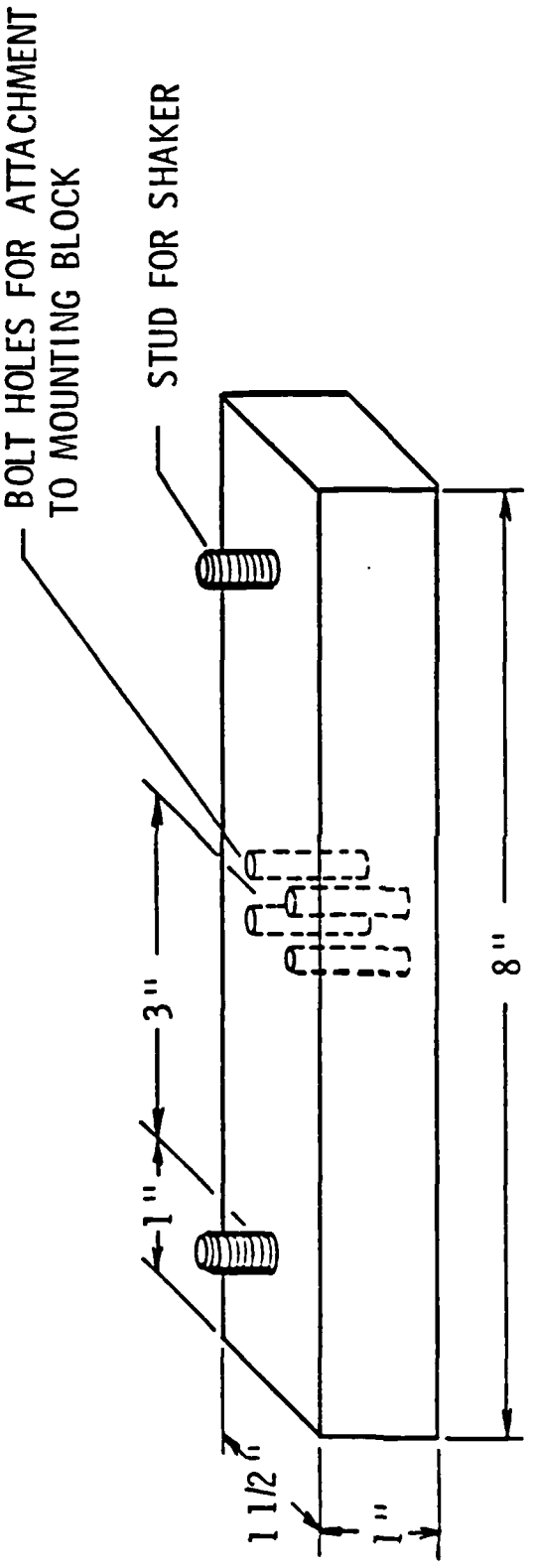

Figure 11. Bar for Moment Drive

Fig. 12. For the axial moment drives, the mounting bar is turned 90° relative to the position shown in Fig. 12, so that it is oriented in the axial direction.

For the longitudinal drives, an aluminum bar was mounted to the inside of the shell across the diameter, as shown in Fig. 13. A sketch of the longitudinal-drive bar is given in Fig. 14. The mounting blocks to which the longitudinal-drive bar was mounted are shown in Fig. 15 for shaker locations X and Z on a rib and for shaker location Y on a joint band. The mounting blocks were welded to the inside surface of the shell. The longitudinal-drive bar was attached to the mounting blocks by drilling holes in the ends of the bar and sliding the bar onto threadless studs rigidly attached to the mounting blocks. This mounting arrangement prevented the transmission of moments by the longitudinal-drive bar to the mounting blocks at the attachment points. As shown in Fig. 13, the shakers were located as close to the ends of the longitudinal-drive bar as possible to maximize the longitudinal component of the shell excitation. The distance from the center of the shaker to the point where the longitudinal-drive bar was attached to the nearest mounting block is 3 1/2 inches. The distance from the center of the moment block stud, to which the longitudinal-drive bar was attached, to midway through the wall of the shell is approximately 1 3/4 inches.

Switching circuitry and preamplifiers were installed inside the shell assembly so that accelerometers, shakers and the gains of the preamplifiers could be remotely selected at the operator's location on the NUSC Transducer Calibration Platform (TCP) when the shell assembly was submerged 245 ft under water at Lake Seneca. For the shakers, the switching was designed so that at each shaker location (X, Y and Z in Fig. 8) one or both of the shakers could

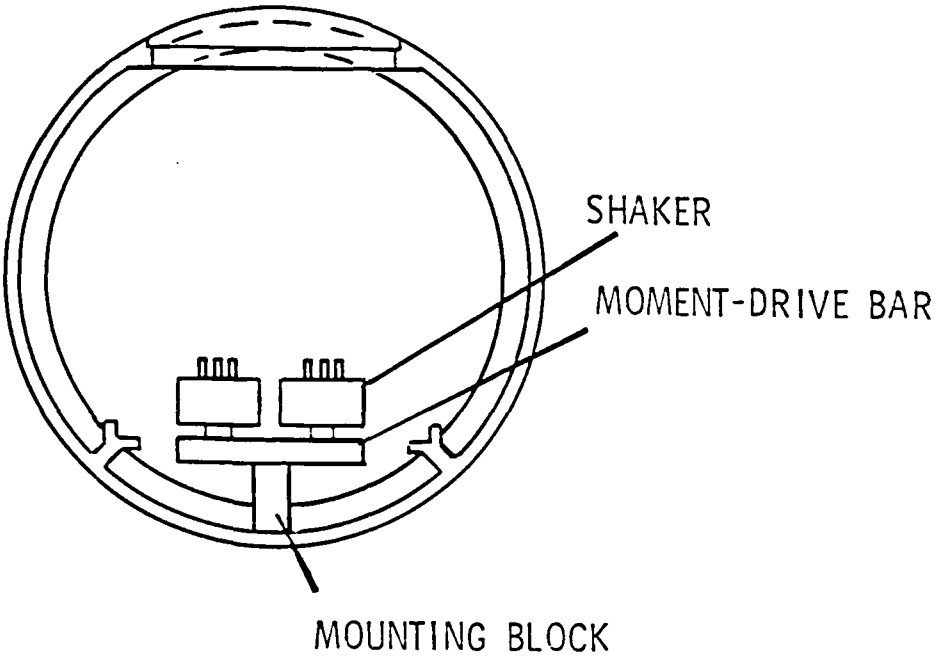

Figure 12. Shaker Mounting Arrangement for Circumferential Moment Drive

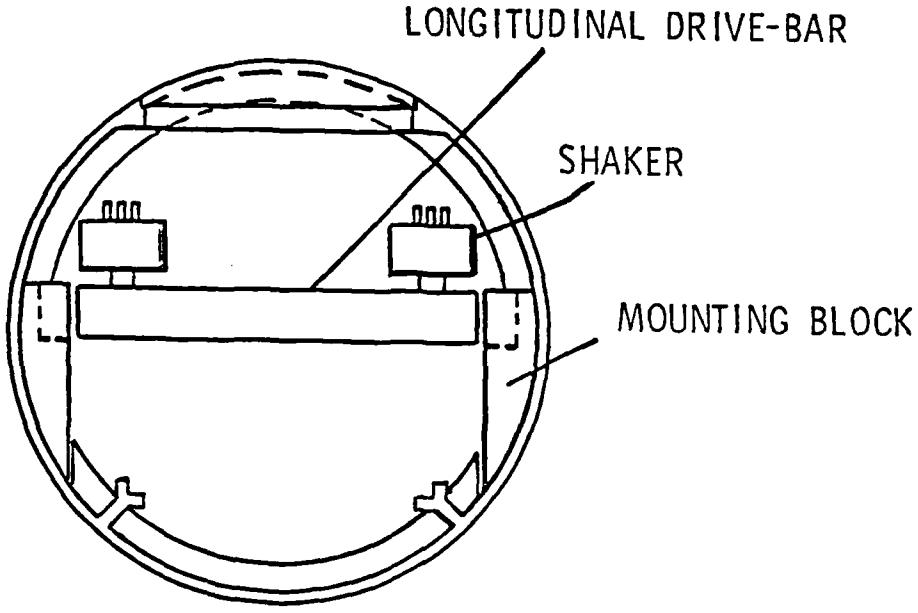

Figure 13. Shaker Mounting Arrangement for Longitudinal Drives

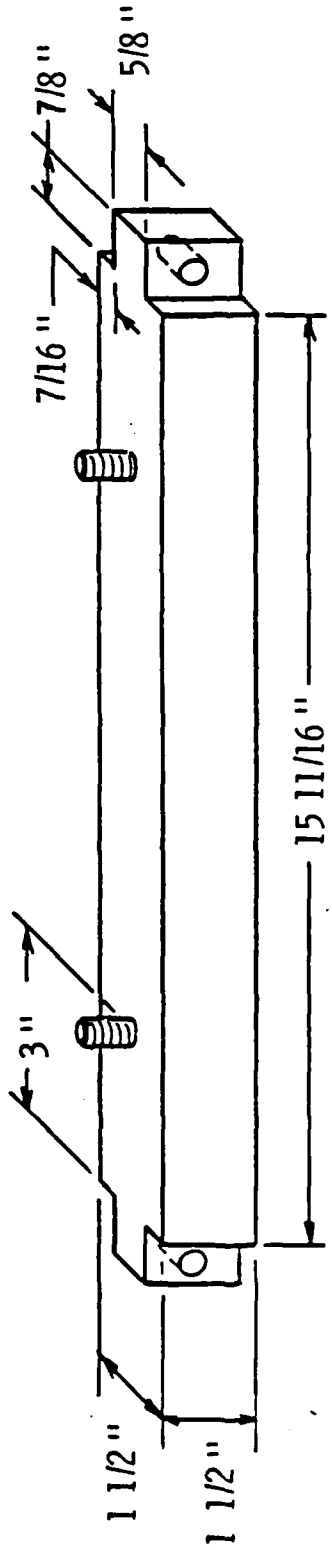

Figure 14. Longitudinal-Drive Bar

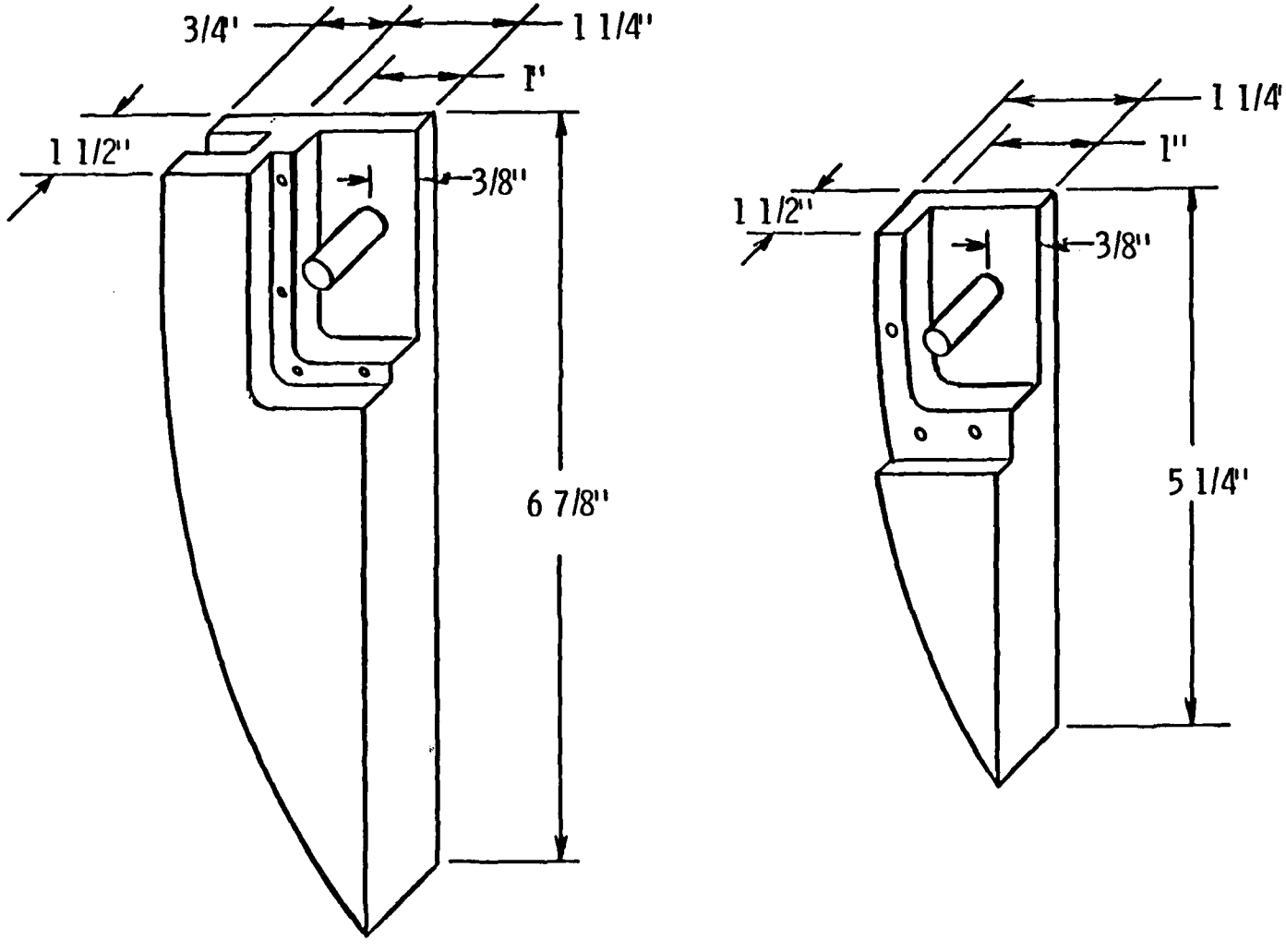

Figure 15. Mounting Blocks for Longitudinal-Drive Bar for Longitudinal Drive

30 March 1984
CBB:SIH:JEH:DAB:lhz

be selected. With two shakers activated, the phases of the two shakers could be switched to be either in phase or out of phase. For the measurement sensors, there were six switching settings, each of which contained a group of eleven sensors inside the shell. The eleven sensors selected by the switching network are those given in Table 3 for tape recorder channels 1 through 7 and 9 through 12.

After passing through the switching network inside the shell assembly, the signals from the accelerometers and impedance heads in the shakers (force and acceleration) were transmitted through 11 preamplifiers inside the shell assembly before transmission to the operator's location on the NUSC TCP through two 300 ft multi-conductor cables. Each of the preamplifier gains could be changed in 6 dB steps from the operator's location on the NUSC TCP.

On the NUSC TCP, the signals were amplified by Ithaco 463 amplifiers before recording the signals on a 14-track Honeywell 1500C FM tape recorder. For each of the six sensor selection switching settings, a list of the signals recorded on the 14 tracks of the tape recorder is given in Table 3. The signals recorded on channels 8, 13 and 14 did not originate inside the shell so that they did not pass through the switching network inside the shell assembly. The signal used to drive the shakers was recorded on channel 8. The output from the two NUSC hydrophones were recorded on channels 13 and 14. During each measurement, the input record and output playback signals from each channel on the tape recorder were displayed one channel at a time on an oscilloscope to check on the quality of the measurement data during recording. On all channels except channel 8, FM Wideband I record cards were used. On channel 8, where the 25 kHz tape recorder servo-drive signal drive as well as the shaker drive signal were recorded, an AM direct-record card was used.

Table 3. Measurement Sensor Selection and Recording Configurations

Tape Recorder Channel No.	C0	C1	C2	C3	C4	C5
1	Force SX_1(1)	Force SX_1	Force SY_1	Force SY_1	Force SZ_1	Force SZ_1
2	Force SX_2	Force SX_2	Force SY_2	Force SY_2	Force SZ_2	Force SZ_2
3	Acc SX_1(2)	A1	Acc SY_1	A1	Acc SZ_1	A1
4	Acc SX_2	A12	Acc SY_2	A16	Acc SZ_2	A20
5	TAX(X)(3)	A15	TAY(X)	A19	TAX(X)	A22
6	TAX(Y)	A13	TAY(Y)	A7	A7	A21
7	TAX(Z)	A4	TAY(Z)	A4	TAZ(Z)	A4
8	Drive Signal	Drive Signal	Drive Signal	Drive Signal	Drive Signal	Drive Signal
9	A2(4)	A8	A2	A8	A2	A8
10	A5	A10	A5	A17	A10	A5
11	A3	A6	A6	A3	A11	A23
12	A9	A14	A9	A18	TAZ(Y)	A9
13	Phone No. 1	Phone No. 1	Phone No. 1	Phone No. 1	Phone No. 1	Phone No. 1
14	Phone No. 2	Phone No. 2	Phone No. 2	Phone No. 2	Phone No. 2	Phone No. 2

(1) Force gauge output from first shaker at location X.
(2) Acceleration output from first shaker at location X.
(3) Triaxial accelerometer at location X (TAX) oriented in the radial (X) direction [circumferential direction is denoted by (Y) and axial direction by (Z)].
(4) Accelerometer located at position 2.

30 March 1984
CBB:SIH:JEH:DAB:lhz

On the tape recorder, the odd-numbered channels were recorded on one head and the even-numbered channels on another head. Therefore, coherent processing should be done only on data recorded on channels that are either both even or odd numbered. In order to compute input power from the shakers, a coherent process between the force and velocity is required. Therefore, the force and acceleration signals from the first shaker impedance head were recorded on odd-numbered channels (channels 1 and 3) and the force and acceleration from the second shaker impedance head on even-numbered channels (channels 2 and 4).

The drive signal was a pure tone generated by a Spectral Dynamics 104A sweep oscillator and amplified by a MacIntosh power amplifier. As data were recorded, the oscillator signal was swept automatically from 20 to 5,000 Hz at a logarithmic sweep rate, so that the sweep rate was lower at the lower frequencies and increased with frequency. Each frequency sweep took approximately five minutes.

2.3 Measurement Configurations

The shell assembly was lowered to a depth of 245 ft by means of 20 ft pipe stringers. One stringer was attached, then the assembly was lowered by the crane on the NUSC TCP before another stringer was added. This process was repeated until the shell was 245 ft below the water surface. The total depth of Lake Seneca at the measurement site is 550 ft.

As shown in Fig. 16, the nominal distances between the shell assembly and the two measurement hydrophones were 45 ft from phone #1 to the center of the shell assembly and 35 ft from phone #2 to the center of the shell. After each time the shell assembly was pulled out of the water to make changes in the shell position or shaker mounts, the hydrophone distances from the shell were

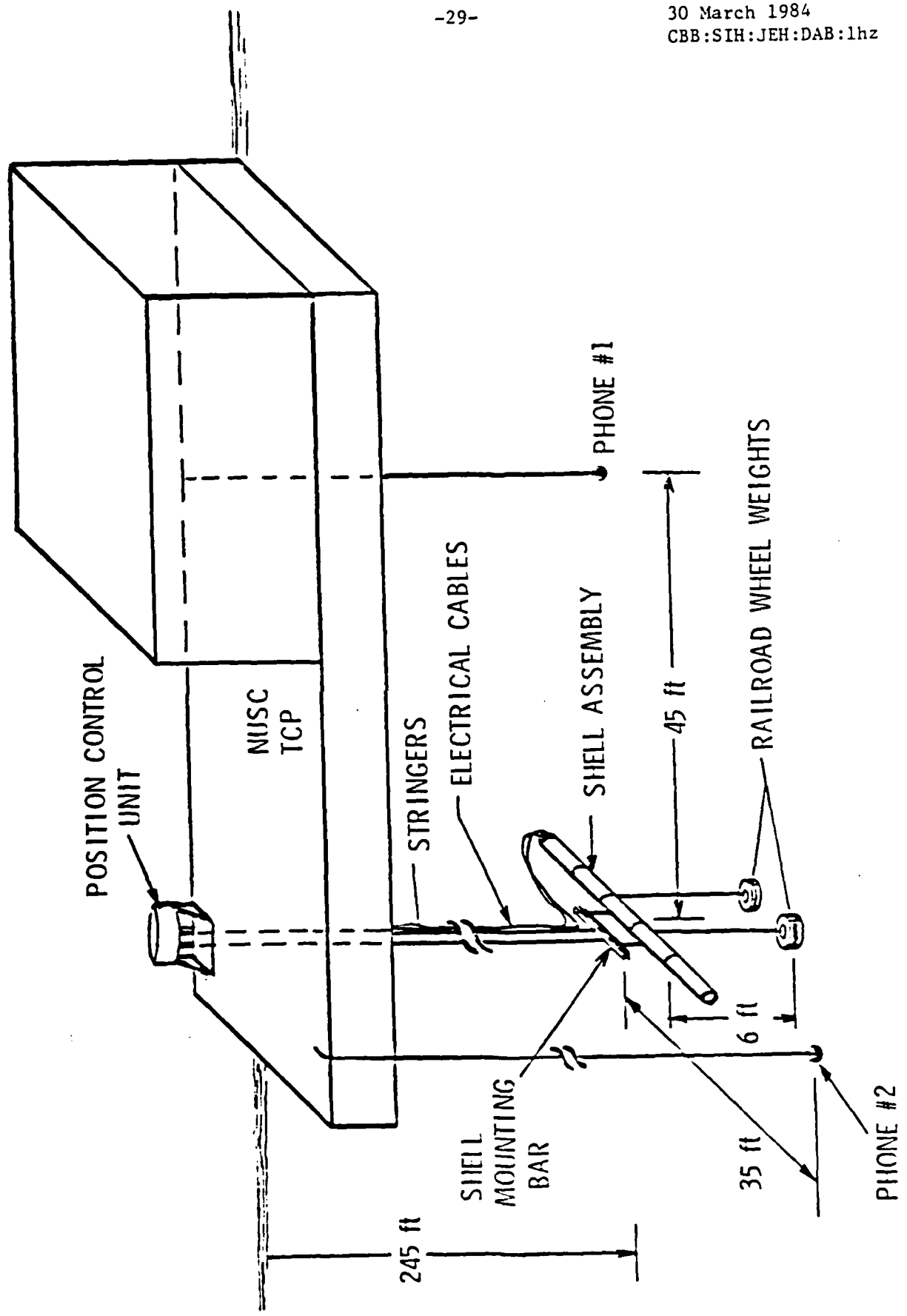

Figure 16. Acoustic Radiation Measurement Configuration

measured using a small pinger source located on one end of the shell. As the frequency of the drive signal was swept from 20 to 5,000 Hz, the shell was positioned as shown in Fig. 16. At selected drive frequencies, the shell was rotated through 180° using the position control unit shown in Fig. 16. A DC voltage signal that was proportional to the position of the control unit was recorded on channel 7 on the tape recorder.

The shell assembly was attached to the stringers by means of an I-beam that spanned the joint bands of the middle shell section. Two brackets were bolted to the joint bands by the joint band bolts. Polyurethane-coated U-shaped bolts were used to attach the I-beam to the shell brackets by means of I-bolts as shown in Fig. 17. Opposite to the I-beam, weights were hung to give the shell assembly negative buoyancy. Each of the two weights consists of two railroad wheels welded together. Each of the two weights weighed 1,250 lbs. The weights were attached to the shell with 6 ft steel cables by brackets bolted to the joint bands of the middle shell section of the shell assembly.

Measurements were conducted with the shell assembly mounted in each of two positions; one with the shakers vertical (ϕ = 0°) and the other (ϕ = 90°) with the shakers horizontal. In the horizontal position, the shaker, which is located between the longitudinal rails, faces phone #1 when the shell rotation position was as shown in Fig. 16. To change the shell mount position, the shell had to be pulled out of the water, rotated about its axial axis 90° and remounted to a second set of mounting brackets. A sketch of both sets of mounting brackets is given in Fig. 18.

A complete list of all the acoustic radiation measurement configurations is given in Appendix A. This list is taken directly from the measurement plan [8], prepared prior to conducting measurements in October to December 1982

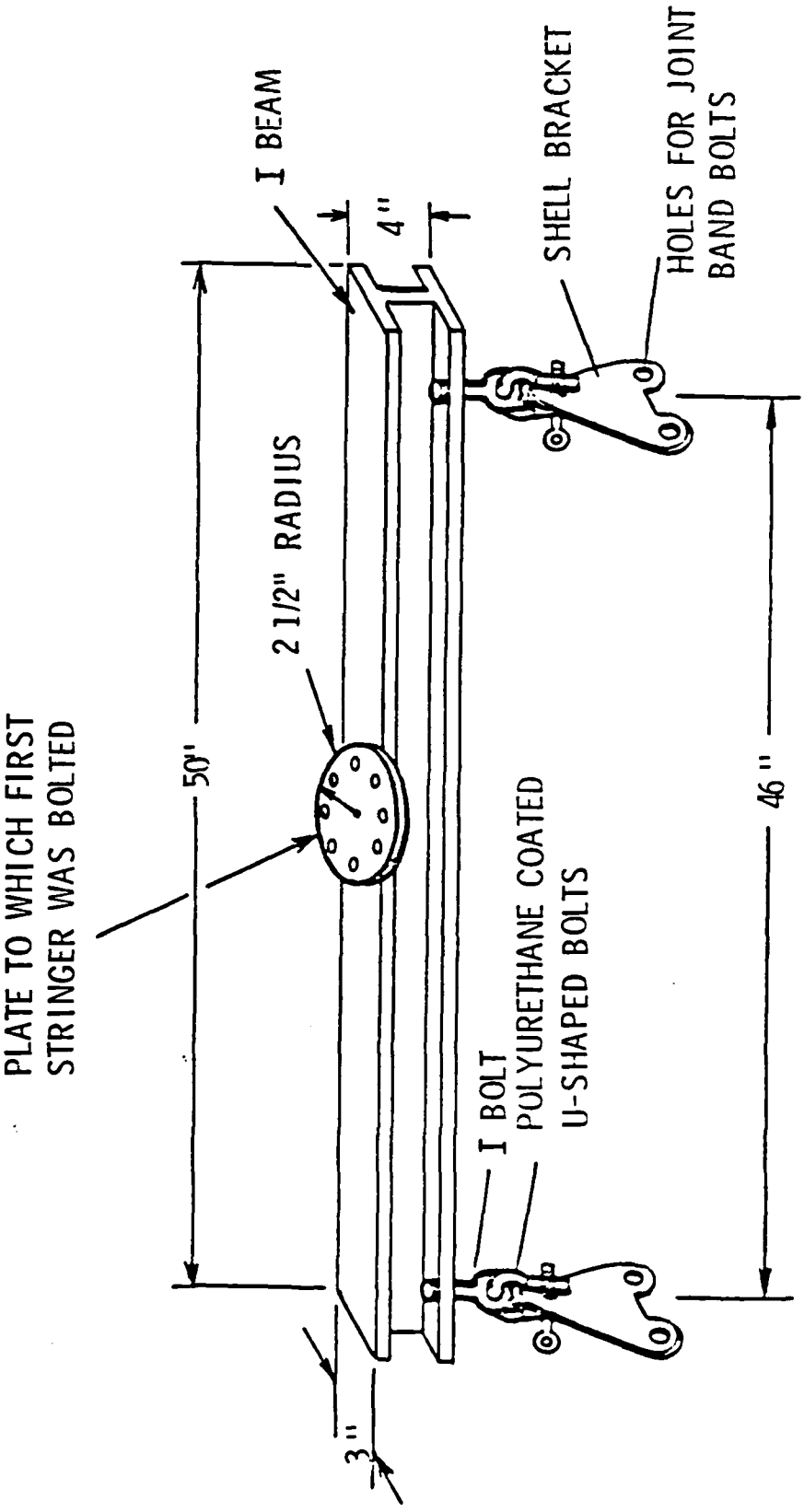

Figure 17. Apparatus for Mounting Shell to Stringers

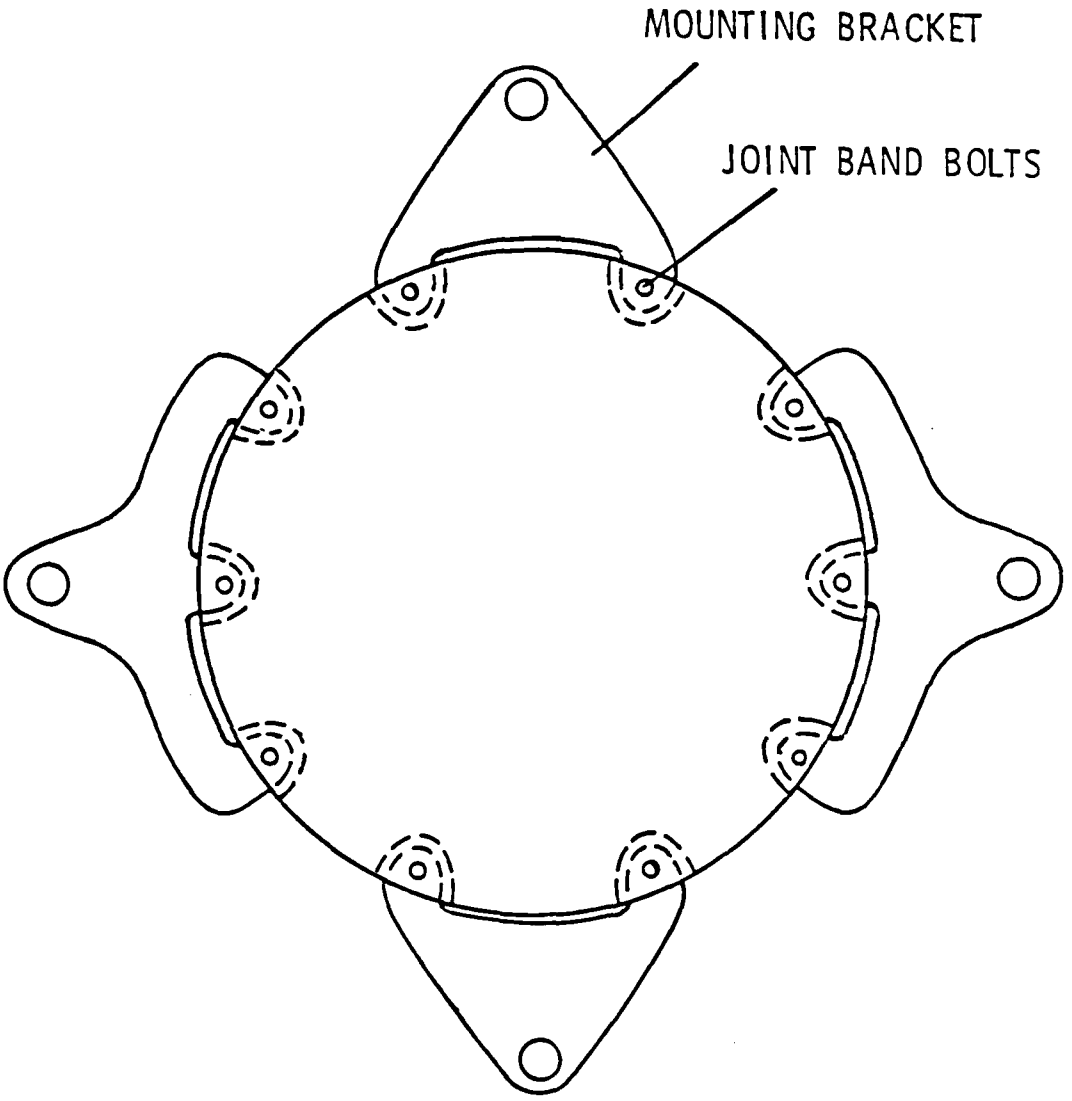

Figure 18. End View of Shell Assembly showing Shell Mounting Brackets Bolted to Joint Bands of Middle Shell Section

when all but the measurements with styrofaom pressure release layer were conducted. The measurements with the closed-cell styrofoam layer were conducted in June 1983. All of the planned measurements, with the following exceptions, were completed.

- The spatial sweeps with the out of phase radial drive at shaker locations Y and Z on the double shell at $\phi = 90°$.
- The spatial sweeps with the single radial drive at shaker locations X and Y on the double shell at $\phi = 90°$ with the styrofoam layers.

A summary of the measurement configurations is given in Table 4. For each shaker location, a different set of accelerometers were recorded; these are illustrated in Fig. 19. For all of the measurements, the force and acceleration levels measured by the impedance heads in the activated shakers and the three signals from the triaxial accelerometer near the base of the lower radial shaker mount were recorded, along with the drive signal and the signals from both hydrophones. For a complete list of the sensors recorded during each of the measurement configurations, refer to Table 3 which lists the recorded sensors for each of the sensor selection switching settings. For shaker location X, sensor selection switching settings C0 and C1 were used, for shaker location Y, settings C2 and C3 were used and for shaker location Z, settings C4 and C5 were used.

2.4 Data Processing

The analog tapes from the 14-channel FM tape recorder were digitized before processing. The digitized data were recorded on digital tape which was read into the ARL VAX computer for processing and plotting. All of the data taken during the acoustic radiation measurements by the impedance heads (force and acceleration) in the active shakers, the accelerometers inside the shell

Table 4. List of Measurement Configurations

Type of Shell	Shaker Locations	Drive Type	Position
Single	X, Y, Z	Radial - Single	ϕ = 0°
Single	X, Y, Z	Radial - Out of Phase	ϕ = 0°
Single	X, Y, Z	Radial - Single	ϕ = 90°
Single	X, Y, Z	Radial - Out of Phase	ϕ = 90°
Double	X, Y, Z	Radial - Single	ϕ = 0°
Double	X, Y, Z	Radial - Out of Phase	ϕ = 0°
Double	X, Y, Z	Radial - Single	ϕ = 90°
Double	X, Y, Z	Radial - Out of Phase	ϕ = 90°
Single	X, Y, Z	Circumferential Moment	ϕ = 0°
Single	X, Y, Z	Circumferential Moment	ϕ = 90°
Double	X, Y, Z	Circumferential Moment	ϕ = 0°
Double	X, Y, Z	Circumferential Moment	ϕ = 90°
Single	X, Y, Z	Axial Moment	ϕ = 0°
Single	X, Y, Z	Axial Moment	ϕ = 90°
Double	X, Y, Z	Axial Moment	ϕ = 0°
Double	X, Y, Z	Axial Moment	ϕ = 90°
Single	X, Y, Z	Longitudinal - In Phase	ϕ = 0°
Single	X, Y, Z	Longitudinal - Out of Phase	ϕ = 0°
Single	X, Y, Z	Longitudinal - In Phase	ϕ = 90°
Single	X, Y, Z	Longitudinal - Out of Phase	ϕ = 90°
Double	X, Y, Z	Longitudinal - In Phase	ϕ = 0°
Double	X, Y, Z	Longitudinal - Out of Phase	ϕ = 0°
Double	X, Y, Z	Longitudinal - In Phase	ϕ = 90°
Double	X, Y, Z	Longitudinal - Out of Phase	ϕ = 90°
Double w/foam	X, Y	Radial - Single	ϕ = 0°
Double w/foam	X, Y	Radial - Single	ϕ = 90°
Double w/foam	X, Y	Circumferential Moment	ϕ = 0°
Double w/foam	X, Y	Circumferential Moment	ϕ = 90°

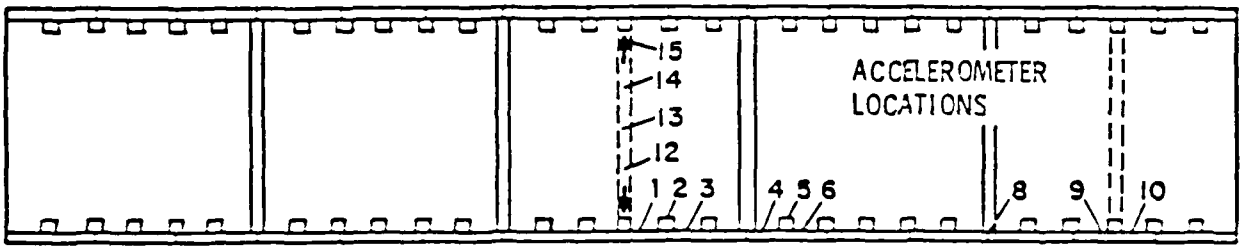

(a) FOR SHAKER LOCATION X- MIDDLE OF SHELL

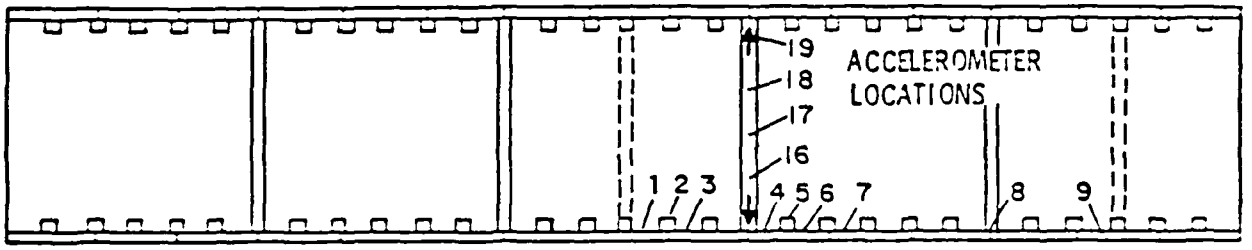

(b) FOR SHAKER LOCATION Y- ON JOINT END

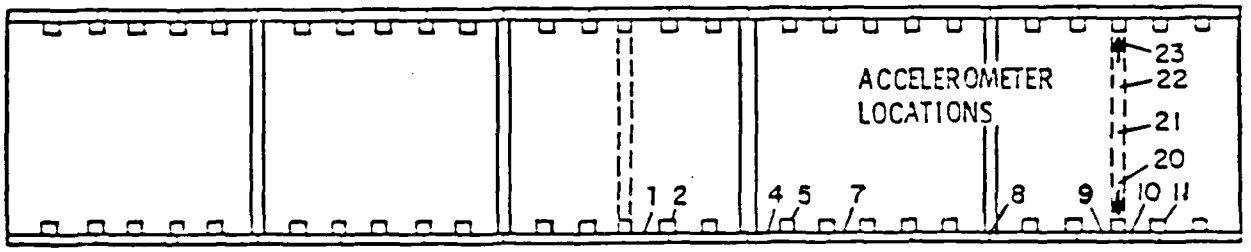

(c) FOR SHAKER LOCATION Z- MIDDLE OF END SHELL

Figure 19. Accelerometers Recorded for each Shaker Location

and the two hydrophones were digitized. Only the digitized data taken by the two hydrophones during the frequency sweeps have been processed and plotted.

The digitization of the data is discussed below in Section 2.4.1 and the processing and plotting of the acoustic radiation data taken during the frequency sweeps is discussed in Section 2.4.2.

2.4.1 Digitization of Data

The 14 channels of analog data recorded by the FM tape recorder were digitized sequentially. A sample of the data from all channels, plus one additional data sample on the shell position during the spatial sweep measurements, constituted one frame of data. The data were digitized at a rate of 2 kHz, so that each data frame took 7.5 milliseconds. A frame of data was taken every 25 milliseconds, or at a rate of 40 frames/second. During digitization, the analog tapes were run at twice the record speed of 15 inches/second so that 40 frames/second is equivalent to 20 frames/second in real time. The data sample rate was higher than the frame rate so that there was some dead time in each frame. A data sample rate higher than the frame rate was used to approximate simultaneous sampling of the data across all channels.

A block diagram of the digitizing instrumentation is given in Fig. 20. The logarithmic amplitude of the analog data on channels 1 through 7 and 9 were detected by the ARL detector, which has a 10 dB/volt sensitivity. The DC voltage outputs from the 8 channels of the ARL detector are digitized by the 10-bit analog-to-digital convertor. With the 10-bit analog-to-digital convertor, operating over a ±5 volt input range, the amplitude resolution is 0.1 dB/bit. Data on the phase of the analog signal were not required, so that it was not necessary to sample as fast as the Nyquist rate. The real-time

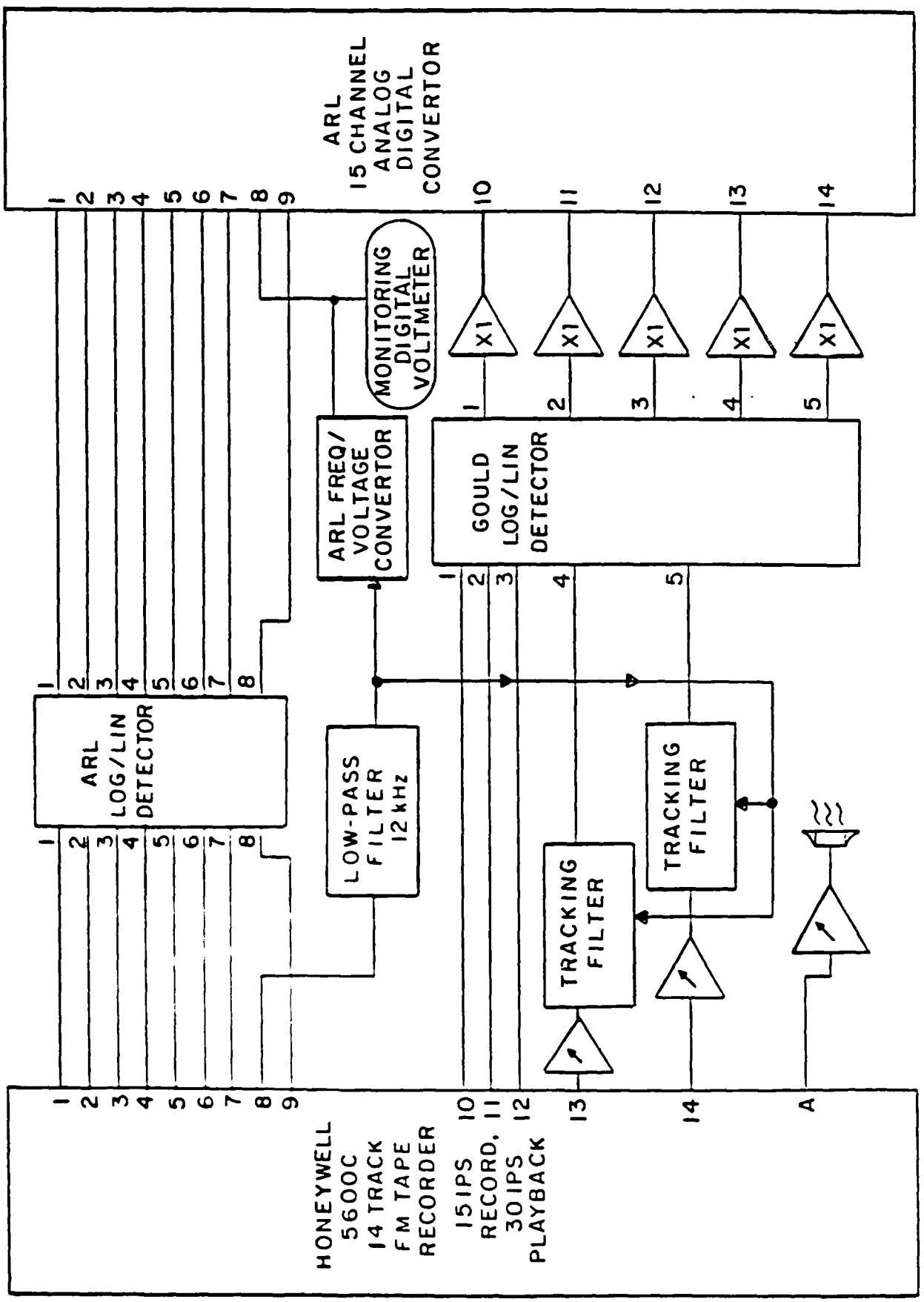

Figure 20. Block Diagram of Data Digitization Instrumentation

frame sample rate of 20 Hz (40 Hz during digitization at twice the record speed) yields about 6,000 samples from each channel for the five minute 20 to 5,000 Hz frequency sweep measurements, or a sample every 0.8 Hz on the average. For the 3 1/2 minute 180° spatial sweep measurements, about 4,200 samples were taken, which averages to one data sample every 0.04 degrees.

As shown in Fig. 20, the log-amplitude of the data from channels 10 through 14 were detected by a Gould detector. The amplifiers on the output from the five channels of the Gould detector had no gain and were used for electronic isolation. The data from the two hydrophones on channels 13 and 14 of the tape recorder contained broadband ambient noise. To reduce the effect of the ambient noise, data from channels 13 and 14 were passed through the Spectral Dynamic 101A tracking filters shown in Fig. 20 before conversion by the Gould log-detector to a DC voltage. The center frequency of the 10 Hz bandwidth filter was controlled by the drive signal taken from channel 8 of the tape recorder. The gains of the preamplifiers on the input to the tracking filters were adjusted to provide 0 dB gains as the signals passed through the filters.

The drive frequency data on channel 8 of the tape recorder were passed through a low pass filter to remove the 25 kHz tape recorder servo-drive signal which was also recorded on channel 8. The ARL frequency/voltage convertor converted the frequency of the signal to a DC voltage. DC voltages from - 5.0 to + 5.0 volts covered the 0 to 10 kHz frequency range during digitization. Thus, the frequency resolution is 1 kHz/volt. With the 10-bit A/D convertor, the digital resolution was 10 Hz/bit during digitization which corresponds to a 5 Hz/bit resolution of the measurement frequency.

A compact digital storage format available at ARL was used to record the data on digital tape. After reading the digital tape, the data required "unscrambling" before processing. The channel address and an identification number for each measurement run were recorded for each data sample. When the identification number reached the maximum of 64 or the end of an analog data tape was reached, a file was ended by a file mark and a new file started.

A one volt RMS signal was recorded on all 14 channels of the tape recorder at several points during the measurements at Lake Seneca. These calibration signals were used to adjust the log-detector input sensitivities to +1.5 volts DC output for a one volt RMS input. Calibration signals of -10 dB re one RMS volt were also recorded on the analog tapes at Lake Seneca. These calibration signals were used to calibrate the sensitivities of the log-detectors to changes in input signal levels. A change of one volt DC corresponded to a 10 dB change in the analog signal level. The calibration signals were digitized and recorded on a separate digital tape. Data from the calibration tape were used to calibrate the data during the data processing and plotting described below in Section 2.4.2. The processed data are referenced back through the data recording, digitizing and processing instrumentation to give an end-to-end calibration that includes all of the electronic instrumentation except the sensors, which were calibrated separately.

2.4.2 Data Calibration, Normalization and Plotting

The digital tapes were read by the ARL VAX computer. All of the data were "unscrambled" and recorded on backup digital tapes. The unscrambled digital tapes from the two hydrophones taken during the frequency sweep measurements

were then processed and plotted. Data on both the signal level and frequency were manipulated before plotting.

Manipulation of the data on the signal level recorded on channels 13 and 14 on the analog tape recorder included the following steps:

- Correction for record amplifier gains.
- Correction for hydrophone sensitivities.
- Normalization for shaker force input level.
- Correction for ambient noise.
- Correction for measurement distance.

Digitizing the data allowed these corrections to be made by the computer, saving considerable data processing time.

Since the signals from the hydrophones did not pass through the electronics inside the shell, there was only one amplifier between a hydrophone and the tape recorder. The gains for the hydrophone amplifiers were set between 40 and 60 dB. To obtain the sound pressure levels at the hydrophones, the gain-corrected data were corrected for the sensitivities of the hydrophones shown in Fig. 9.

The sound pressure levels were normalized to the sum of the forces measured by the impedance heads of the active shakers. These data were taken from channels 1 and 2, corrected for the gains of the amplifiers inside the shell and the amplifiers topside on the NUSC TCP, and for the force gauge sensitivities given in Table 2 to obtain the amplitude of the measured force in pounds. The force in pounds was converted to force in Newtons. The sound pressure level data were then divided by the measured shaker force data to obtain the sound pressure levels per Newton input force.

It is important to note here that the foundations of the shakers were different for different types of drives (see Section 2.2). Therefore, the impedance at the output of the shakers was different for different types of drives, which affected the force applied by the shakers. This means that direct comparisons between the force-normalized sound pressure levels for different types of drives are not valid. Before valid comparisons can be made, corrections for the transmission of the shaker forces through the various shaker mountings should be made. Since the shaker foundations can be easily included in numerical models, the normalized data can be readily used for validation of numerical models. However, the sound pressure levels should be normalized to shaker power input levels before direct comparisons of the measured acoustic radiation levels for different types of drives are made. To compute the shaker input power, the phase between the force and velocity is required. Therefore, the data from the impedance heads in the active shakers would have to be redigitized to include data on the phase between the force and velocity signals.

In order to correct for ambient noise, separate computer files on the levels of the ambient noise were created. Since the ambient noise is broadband, the process used to digitize the data that contained the pure-tone signal could not be used. Instead, a Spectral Dynamics 375 Fast Fourier Transform analyzer was used to measure the ambient noise levels at the beginning of each frequency sweep measurement at drive frequencies below 50 Hz, where the first resonance of the shell occurred. Below 50 Hz, the shell response and radiation efficiency are small so that the signal associated with the acoustic radiation from the shell is much lower than the ambient noise. The bandwidth of the analyzer was 5 Hz over the frequency range 0 to 5 kHz. The ambient noise data were referenced to the one volt RMS calibration signals

before being read directly into the ARL VAX computer. Since the amplifier gains with and without the signal on were the same, no corrections for amplifier gains were required before the ambient noise data in dB re one volt was logarithmically subtracted from the unscrambled data on the levels in dB re one volt measured with the shaker active at frequencies above 50 Hz. Corrections for the difference in the ambient noise bandwidth (5 Hz) and the bandwidth of the tracking filter (10 Hz) were made before subtracting the ambient noise from the measured levels. The ambient noise level in the band that contained the frequency of the drive signal was used to correct the measured level for ambient noise.

If the ambient noise level was within 3 dB of the measured level, the measured level was considered dominated by ambient noise. These data were not plotted. If the ambient noise level was 3 to 10 dB below the measured level, then the measured level was corrected for ambient noise before plotting. If the ambient noise was more than 10 dB below the measured level, no correction for ambient noise was applied. To avoid holes in the plotted data, only data above the highest frequency where the measured levels were dominated by ambient noise were plotted.

Finally, after correcting for amplifier gain, sensor sensitivity, ambient noise and normalizing to shaker input force, the data were corrected for measurement distance to one meter. Thus, the final data on the levels of the acoustic radiation used for plotting are given in terms of sound pressure level in dB re 1 μPa per Newton input force at one meter.

As discussed in Section 2.4.1, the resolution of the digitized frequency data is 5 Hz. Thus, the frequency data was quantified into 5 Hz bins, so that, as the frequency of the analog signal increased, the digital data jumped in 5 Hz steps. Near the frequency steps, the digital data hunted for the

correct frequency, jumping back and forth between bins. Before plotting, the digital frequency data needed smoothing to provide a smooth plot and, more importantly, to increase the frequency resolution and, thereby, the accuracy. Since the drive frequency increased monotonically with time, a running average of the frequency was used to smooth the frequency data. Seventy data points were used in the running average.

3. Analysis

In this section, the analysis of the acoustic radiation data taken during the frequency sweep measurements is discussed. The analysis is limited because neither data on the shell vibration taken during the frequency sweep measurements or data on the acoustic radiation patterns and shell vibration taken during the spatial sweep measurements have been processed and plotted. The effect on the acoustic radiation of the following parameters are considered in the analysis of the measured data:

- Repeatability.
- Drive location.
- Addition of the outer shell.
- Addition of the styrofoam pressure release layer in the double shell.
- Directionality of acoustic radiation observed at the locations of the two hydrophones.

As discussed in Section 2.4.2, the data was normalized to the shaker input force and that comparing the normalized acoustic radiation levels for different types of drives may be misleading. Therefore, the analysis does

not include the effect of changes in drive types on the levels of acoustic radiation.

3.1 Repeatability

In order to record all of the accelerometers listed in Table 3, two recordings were required for each measurement configuration. The shaker force from the active shakers and acoustic radiation levels from both hydrophones were recorded in both recordings. Therefore, all acoustic radiation measurements were repeated which presents an opportunity to assess the repeatability of the acoustic radiation data.

The comparisons between repeated measured acoustic radiation data shown in Figs. 21 and 22 are representative of the repeatability of all the measured data. The average levels show excellent repeatability. The fine structure of the acoustic radiation curves also show good repeatability in both level and frequency at points where maximum and minimum radiation occur. The largest differences in the repeated measured data occur at the higher frequencies, above 1,000 Hz. At the higher frequencies, the repeatability where maximum radiation occurs is better than the repeatability where minimum radiation occurs.

As discussed in Section 1, at higher frequencies the principal mechanism of acoustic radiation is wavenumber conversion or scattering at the ribs, so that the shell looks like an array of ring radiators. Minima in the radiation occur at frequencies and observation locations where the radiation from areas around the ribs sum out-of-phase. This addition is sensitive to shell position; a small change in rotation position would significantly affect the out-of-phase addition of the radiation from individual ribs at the measurement hydrophone. The in-phase addition would be less sensitive to

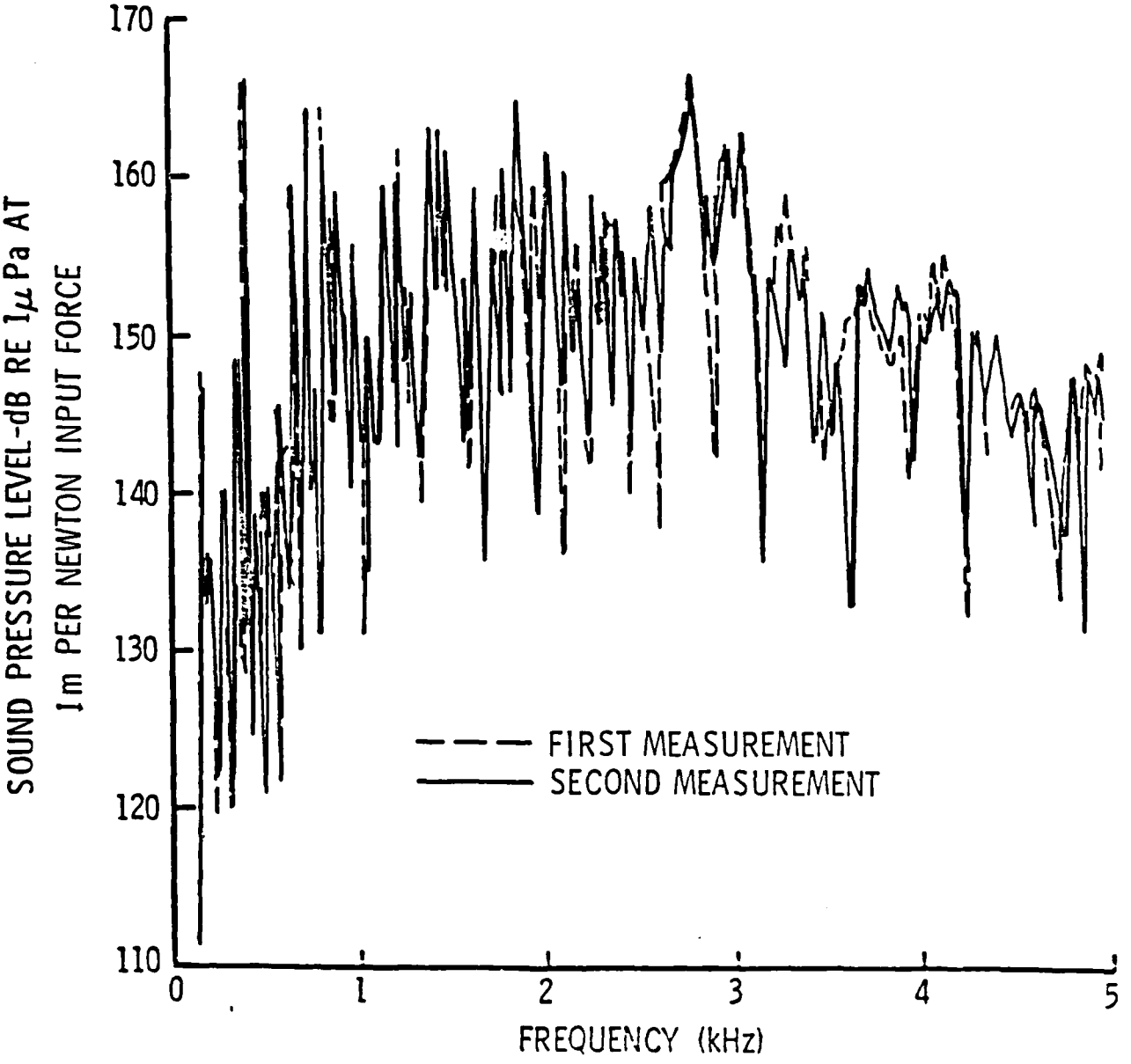

Figure 21. Repeatability of Acoustic Radiation Measurements -- Single Shell with Shaker Vertical (ϕ = 0°), Single Radial Drive in Middle of Shell and Phone No. 1

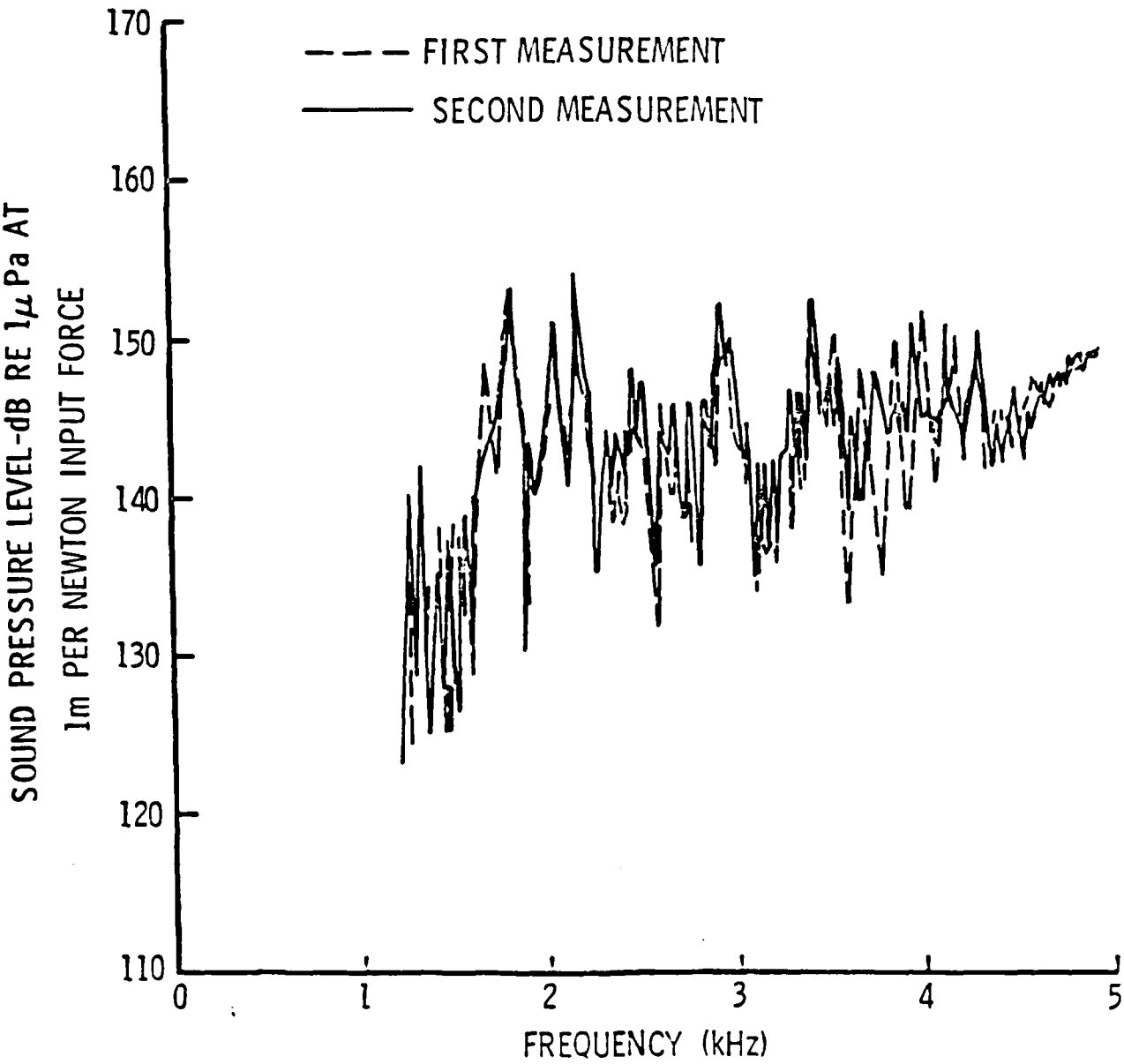

Figure 22. Repeatability of Acoustic Radiation Measurements at Phone No. 2 -- Double Shell with Shakers Horizontal ($\phi = 90°$) and In-Phase Longitudinal Drive in Middle of End Shell

changes in shell position. Thus, shell motion between measurements is likely responsible for the differences in the minimum levels in the repeated measurements, as illustrated in Figs. 21 and 22.

3.2 Drive Location

For each of the six types of drives, three drive locations were used: (1) in the middle of the shell assembly, (2) on the joint band between the middle shell and the adjacent shell and (3) in the middle of the end shell. The effect that the drive location has on the acoustic radiation depends on the type of drive.

For the radial drives, both with a single shaker operating and with both shakers operating out of phase, the acoustic radiation levels with the drive located in the middle of the end shell were higher than the levels for the other two drive locations. A representative comparison of the measured data for different radial drive locations is given in Fig. 23. Also, as shown by the representative data in Fig. 23, the levels with the drive on the joint band are lower in general than the levels with the drive located at the other two locations. The joint band is a more massive structure than the ri[illegible] in the middle of both the middle and end shells, where the two other drives were located. Therefore, the drive impedance on the joint band is probably higher than at the other drive locations so that the applied force for a given shell displacement is higher on the joint band than at the other two drive locations. Because the levels shown in Fig. 23 are normalized to shaker input force and the force-to-velocity ratio is higher on the joint band, the acoustic radiation levels for the joint band drive will be lowered when normalized more than the levels for the other two drive locations.

30 March 1984
CBB:SIH:JEH:DAB:1hz

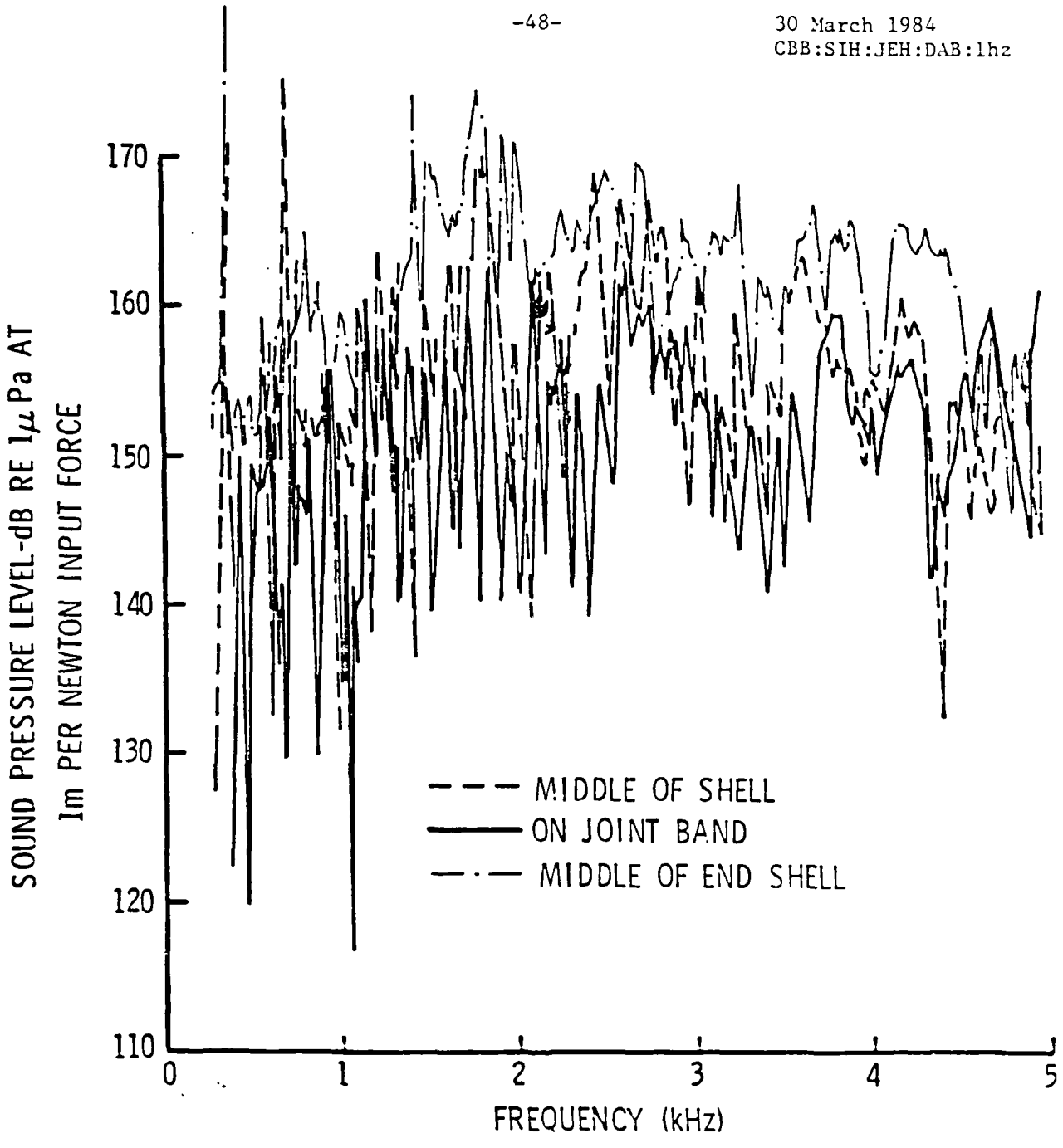

Figure 23. Effect of Drive Location on Acoustic Radiation Levels at Phone No. 1 -- Single Shell with Shakers Horizontal (ϕ = 90°) and Single Radial Drive

The impedances for drive locations in the middle shell and the end shell should be nearly equal; both are located on the middle rib of the shell. At first it appears that because the drive in the end shell is located closer to the massive end cap where more structural scattering and consequently acoustic radiation will occur, the measured acoustic radiation levels for the drive in the end shell are higher than for the drive in the middle shell which is further from the end caps. However, for the other types of drives, particularly the two moment drives, the acoustic radiation levels are not higher for the drive in the end shell. Thus, scattering from the end caps does not appear to be the cause of the higher levels when the drives are located in the end shell.

With the shakers horizontal ($\phi = 90°$), the acoustic radiation is higher when the circumferential moment drive was located in the middle of the middle shell than when the circumferential moment drive was located on either the joint band or the middle of the end shell (see Fig. 24). However, as shown in Fig. 25, when the shell is rotated about the shell axis so that the shakers are vertical, the acoustic radiation levels do not change much with the location of the circumferential moment drive.

As illustrated in Fig. 26, the acoustic radiation levels for the axial moment drives are higher at frequencies below 1.5 kHz when the shakers are located in the middle of the shell assembly. However, above 1.5 kHz, differences in the levels for different drive locations are less.

Representative data for the longitudinal drives at different locations are given in Fig. 27 for the single shell and in Fig. 28 for the double shell. No trends in the data for different longitudinal drive locations are apparent. Since all of the longitudinal drives were applied to nominally-identical longitudinal bars inside the shell at all three locations, the drive input

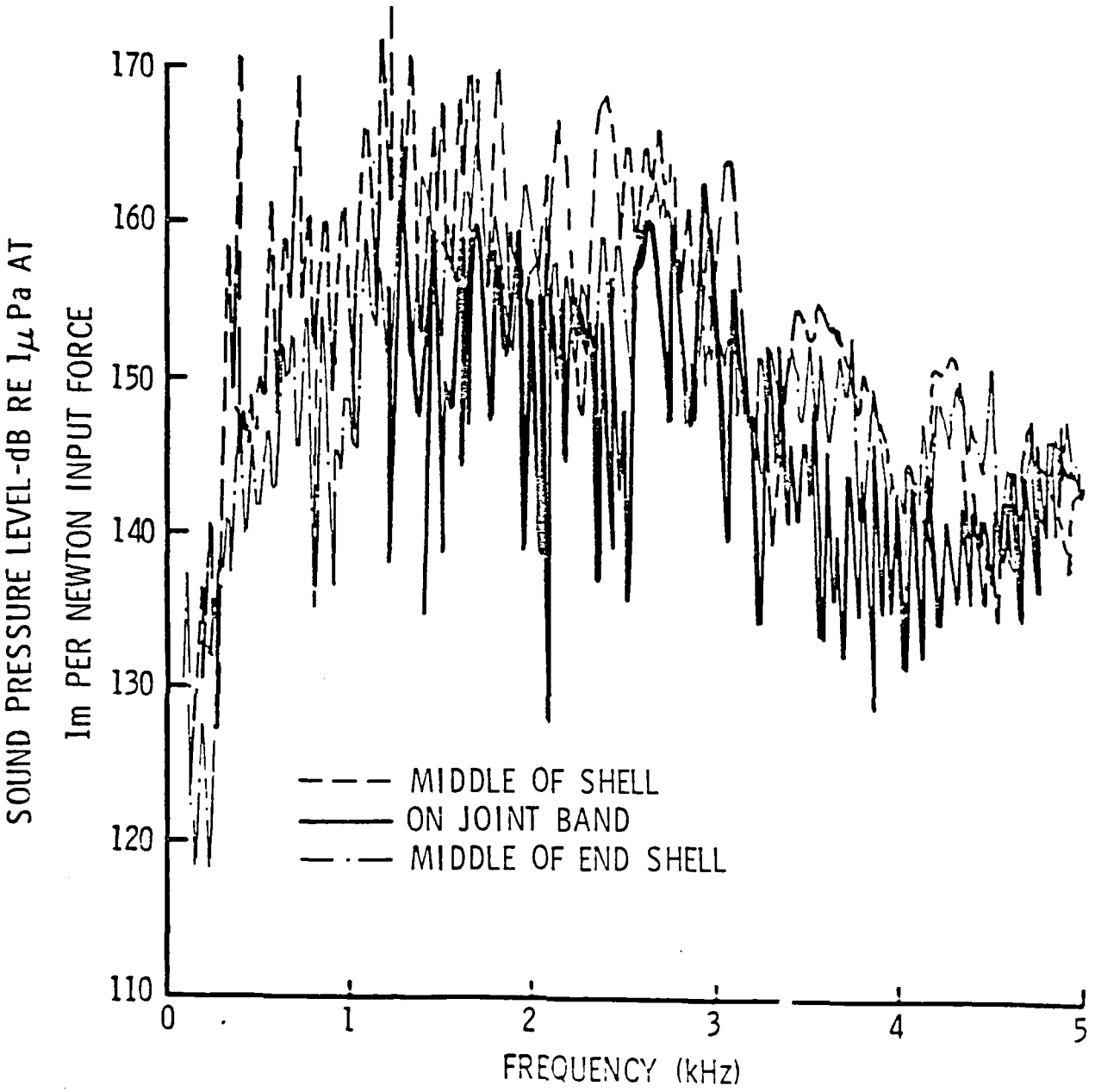

Figure 24. Effect of Drive Location on Acoustic Radiation Levels at Phone No. 1 -- Single Shell with Shaker Horizontal ($\phi = 90°$) and Circumferential Moment Drive

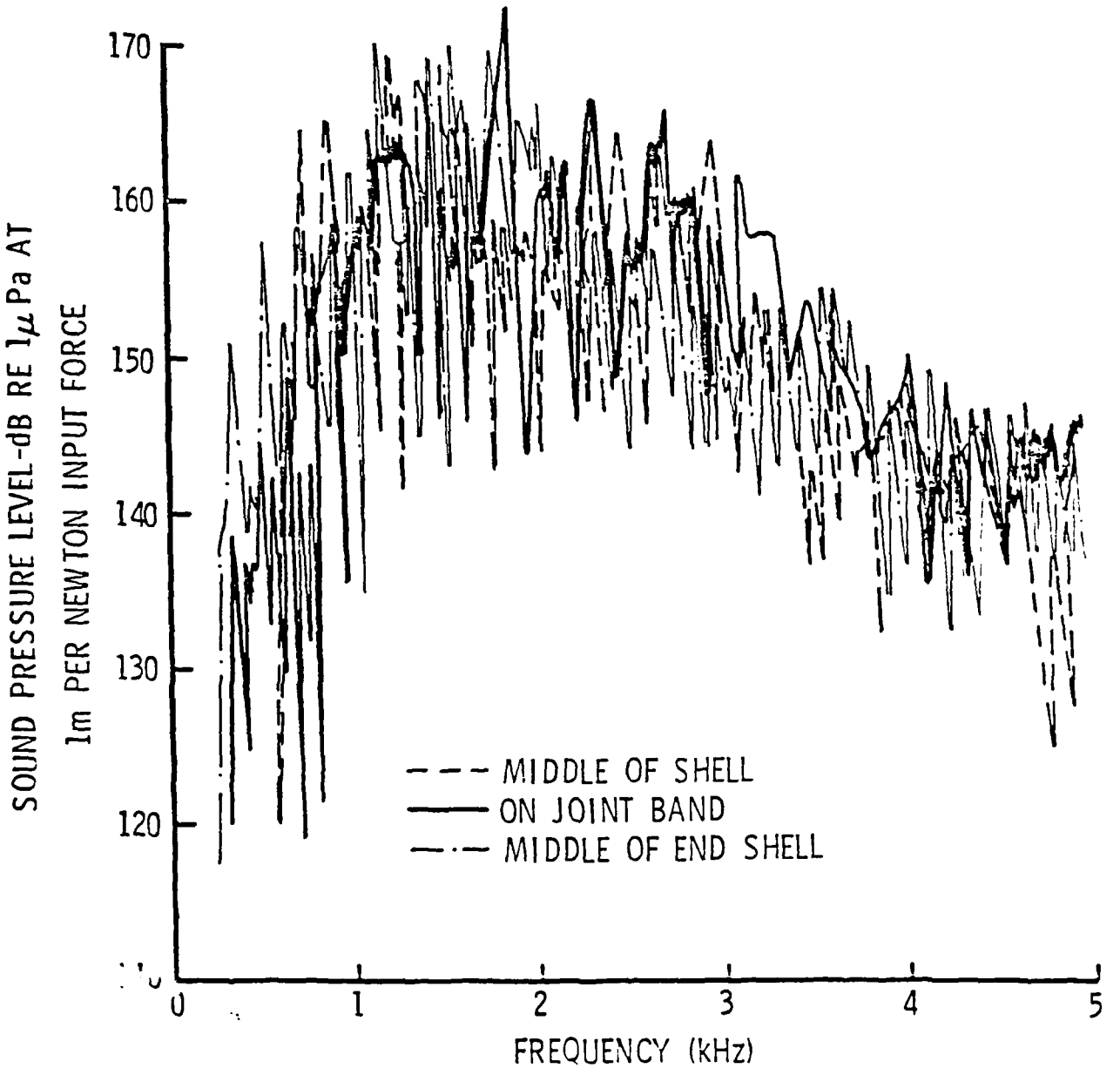

Figure 25. Effect of Drive Location on Acoustic Radiation Levels at Phone No. 1 -- Single Shell with Shakers Vertical (ϕ = 0°) and Circumferential Moment Drive

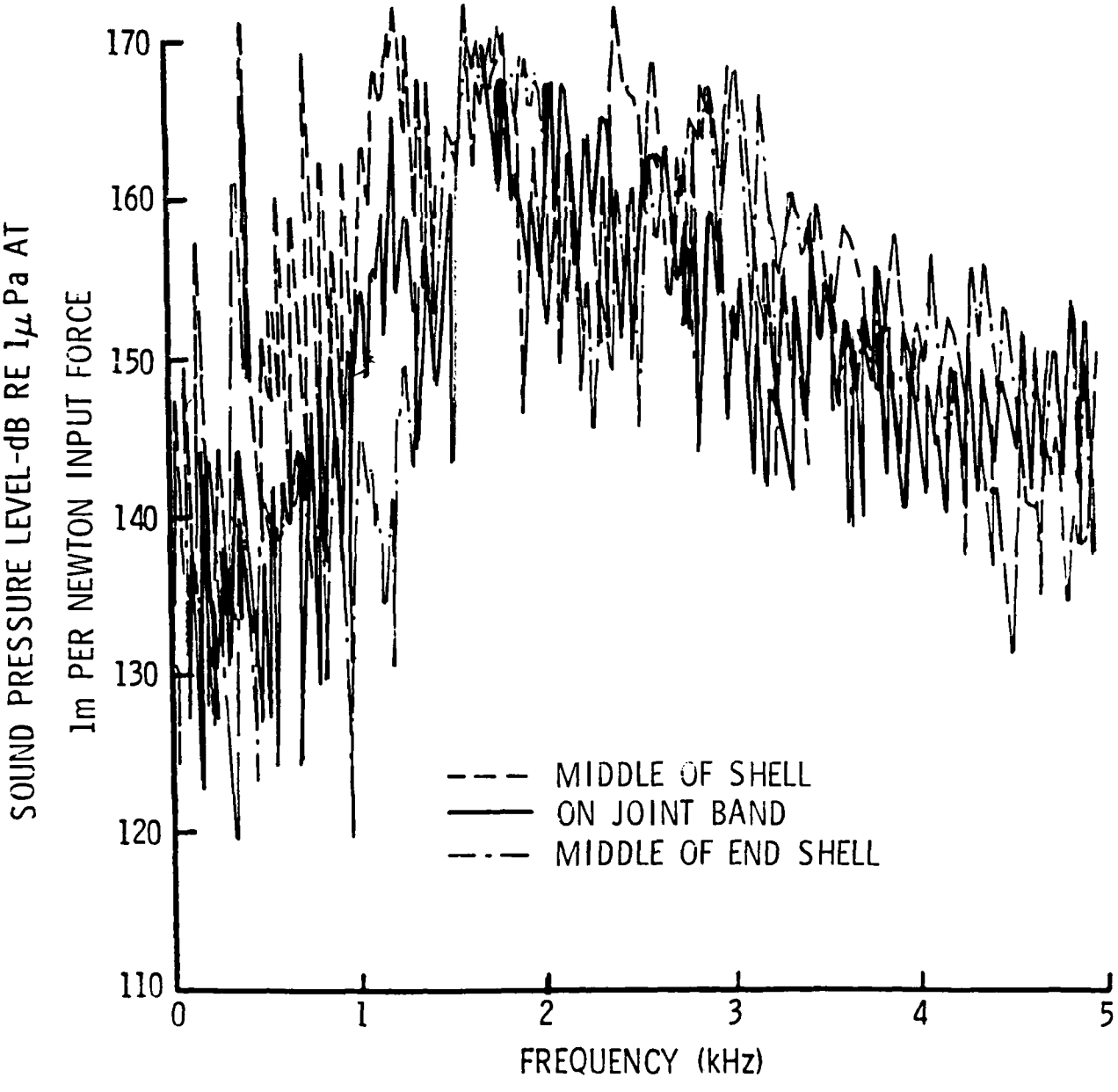

Figure 26. Effect of Drive Location on Acoustic Radiation Levels at Phone No. 1 -- Single Shell with Shakers Horizontal (ϕ = 90°) and Axial Moment Drive

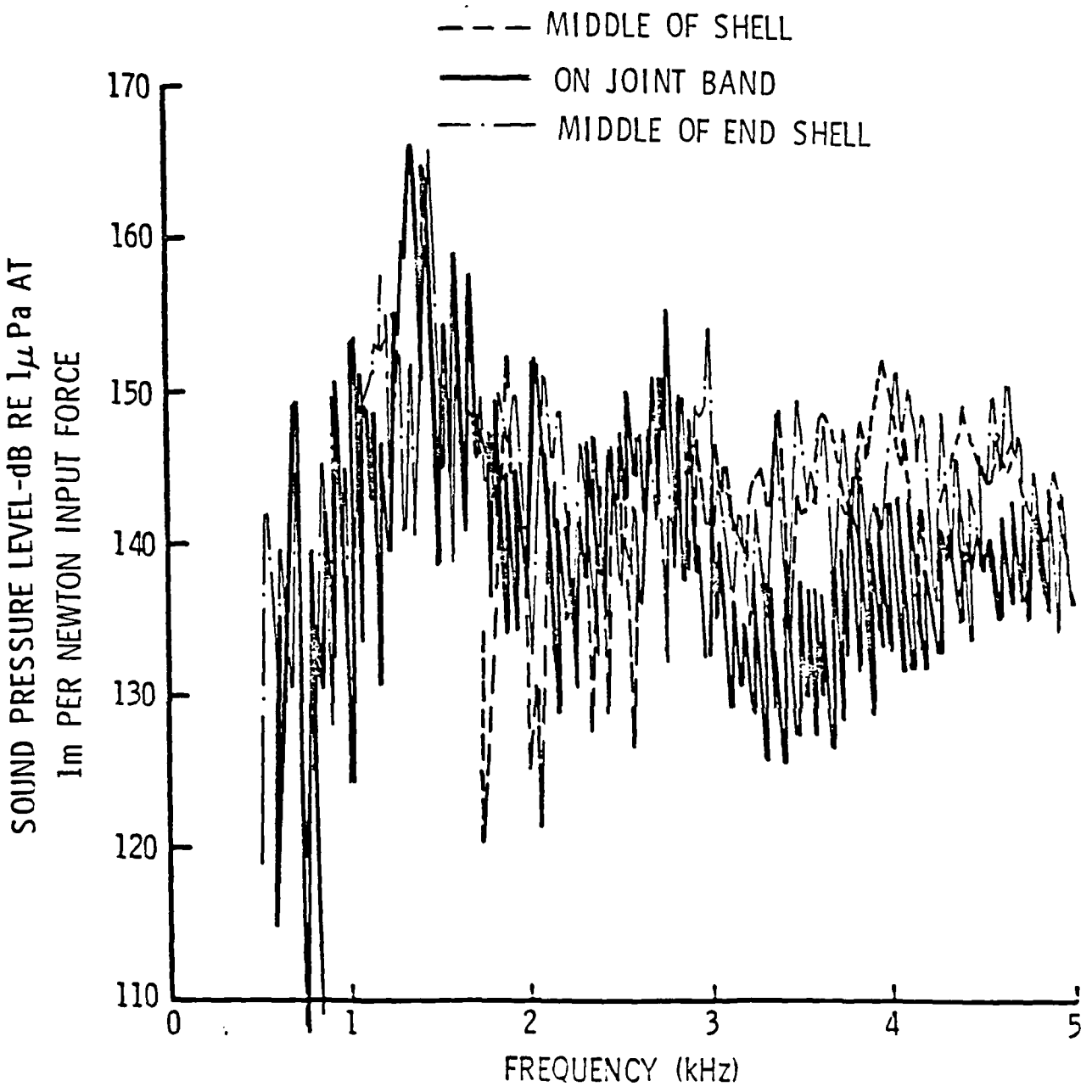

Figure 27. Effect of Drive Location on Acoustic Radiation Levels at Phone No. 1 -- Single Shell with Shakers Vertical (ϕ = 0°) and Out of Phase Longitudinal Drive

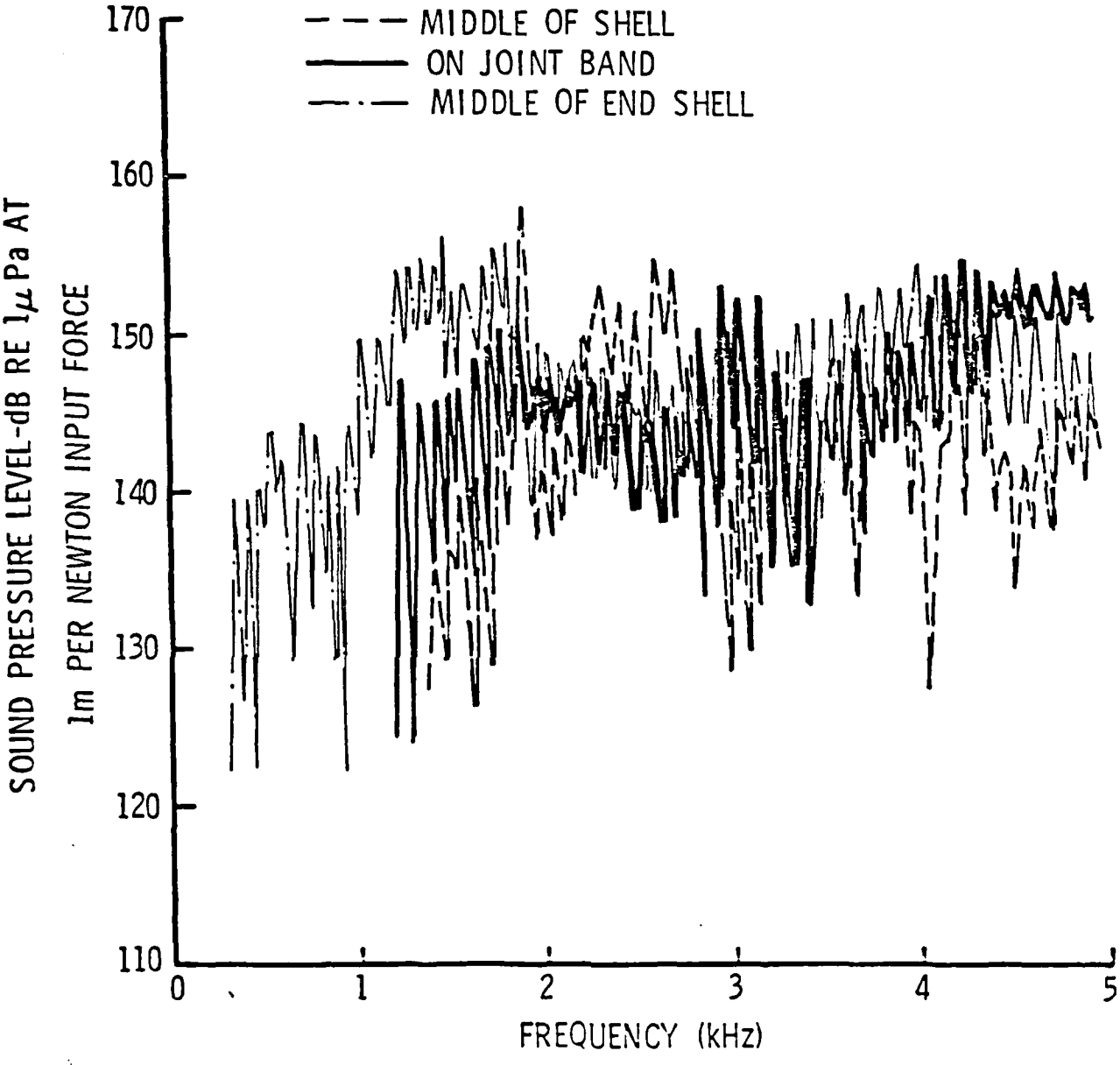

Figure 28. Effect of Drive Location on Acoustic Radiation Levels at Phone No. 1 -- Double Shell with Shakers Horizontal (ϕ = 90°) and Out of Phase Longitudinal Drive

impedance, and consequently the force-to-velocity ratio at each of the shaker locations, should be nearly equal. Therefore, the normalization to input force probably should have little affect on the data illustrated in Figs. 27 and 28. The input impedences to the shell for the two drive locations in the middle of the shell and the middle of the end shell should be lower than the shell impedance on the joint band. However, these lower impedances are not reflected clearly in the data shown in Figs. 27 and 28.

3.3 Double Shell

As illustrated in Fig. 29 for the single radial drive located in the middle of the shell assembly, the differences in the average radiation levels for the single and double shell assemblies at frequencies where peaks or valleys in the data do not occur are small. Comparison of the levels for the single and double shell assemblies with other types of drives at different locations showed results similar to those given in Fig. 29. Although the average levels do not change significantly, the outer shell does reduce the peak levels of the acoustic radiation by the single shell assembly, particularly at frequencies below 1 kHz. The peaks in the acoustic radiation levels below 1 kHz are largely controlled by the resonance response of the shell assembly. Adding the outer shell reduces the resonant response of the single shell assembly [9], which results in reduction in the acoustic radiation at resonant frequencies of the shell assembly, provided that the radiation efficiency of the shell assembly is not significantly changed by the addition of the outer shell.

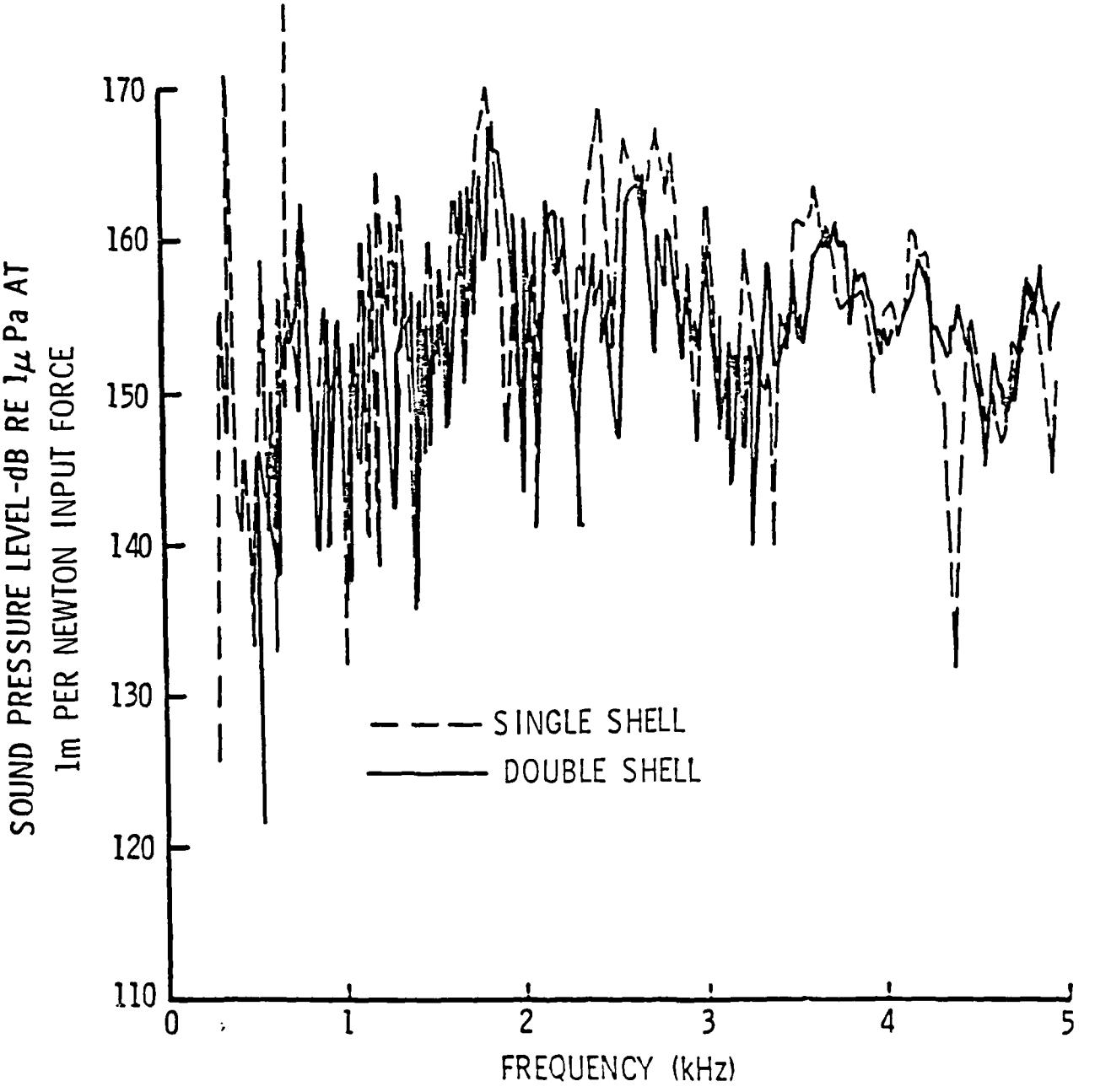

Figure 29. Effect of Outer Shell on Acoustic Radiation Levels at Phone No. 1 -- Shakers Horizontal ($\delta = 90°$) and Single Radial Drive in the Middle of the Shell

3.4 Pressure Release Layer Inside Double Shell

Acoustic radiation measurements were conducted on the double shell with 1 1/2-inch thick closed-cell styrofoam pressure released layer wrapped around the middle three inner shells. The layer was between the outer shell and the outer surface of the inner shell. Single radial and circumferential moment drives in the middle of the shell assembly and on the joint band were used in these measurements.

For the radial drives, the acoustic radiation levels shown in Fig. 30 are representative of the changes in the levels associated with adding the pressure release layer to the double shell. It was expected that the layer would reduce the acoustic radiation; however, results in Fig. 30 show that on the average, the reduction in levels is small. Because the layer reduces the water loading on the inner shell, the drive impedance should be lower so that for a given shell vibration level the force will be lower. Since the levels shown in Fig. 30 are normalized to force, the reduction in drive impedance will increase the normalized levels with the layer more than without the layer. The shaker force levels, given in Fig. 31, show that the force levels with the layer are about 5 to 10 dB below the force levels without the layer. However, as shown in Fig. 32, the vibration levels with the layer are also 5 to 10 dB below the vibration levels without the layer. Although these data do not include data on the phase between the force and velocity necessary to compute drive impedance, they do indicate that the changes in drive impedance associated with the layer are not large. Therefore, the differences in the acoustic radiation levels shown in Fig. 30 appear to be associated primarily with the layer and not a result of normalizing the data to the force input.

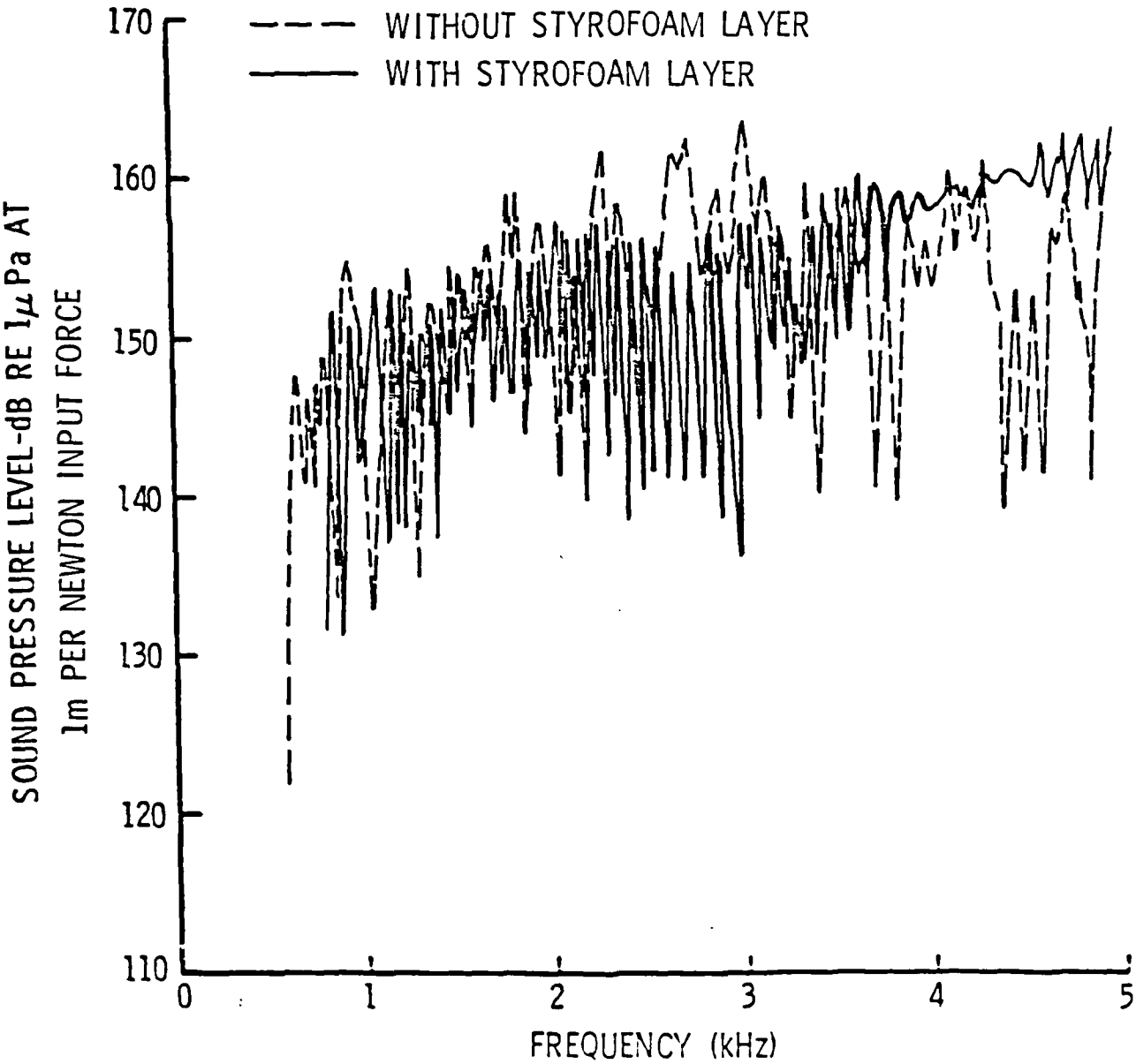

Figure 30. Effect of Styrofoam Layer on Acoustic Radiation Levels at Phone No. 1 -- Double Shell with Shakers Horizontal (ϕ = 90°) and Single Radial Drive on the Joint Band

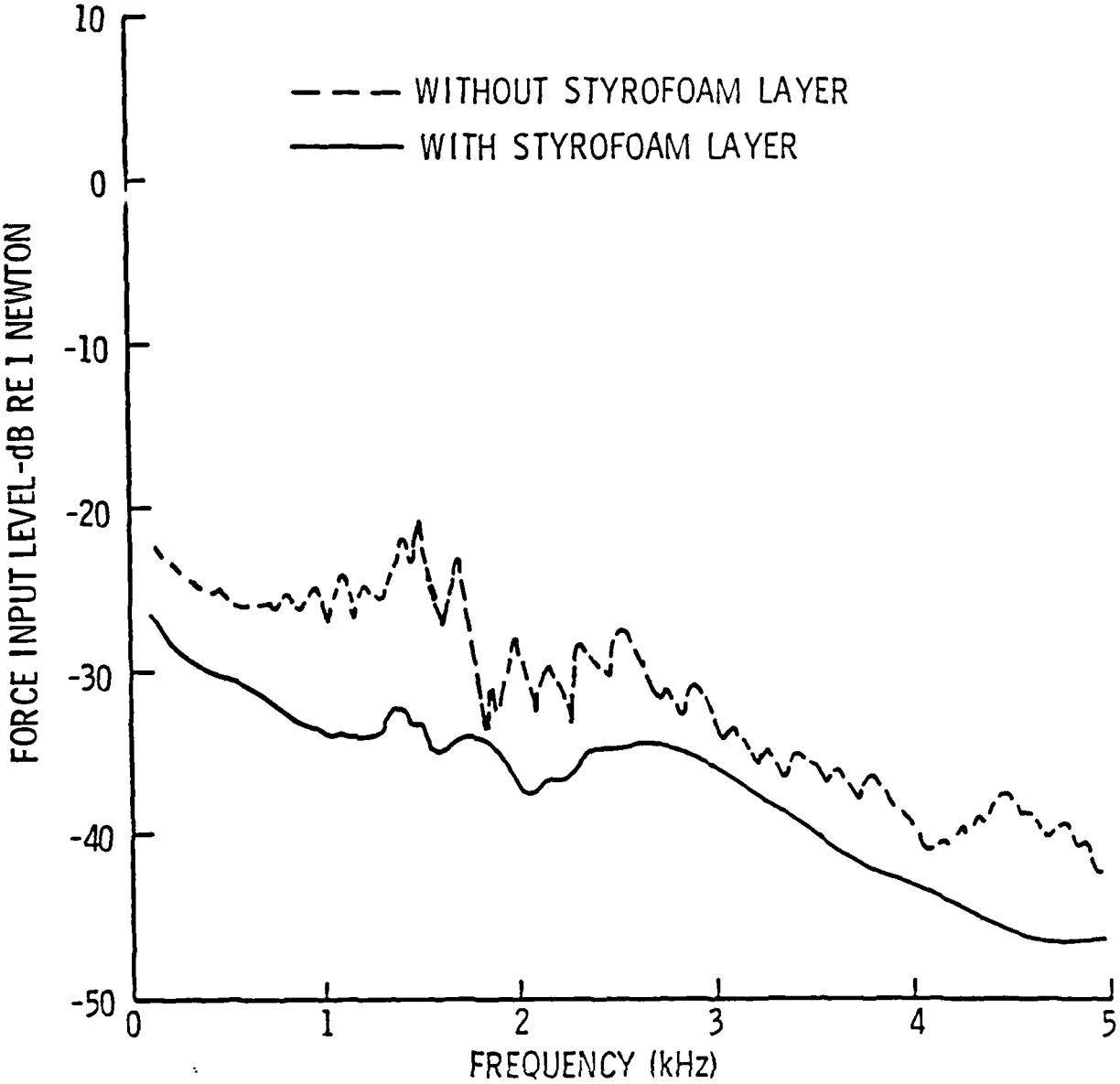

Figure 31. Force Levels at Drive Shaker with and without Styrofoam Layer -- Double Shell with Shakers Horizontal ($\phi = 90°$) and Single Radial Drive on the Joint Band

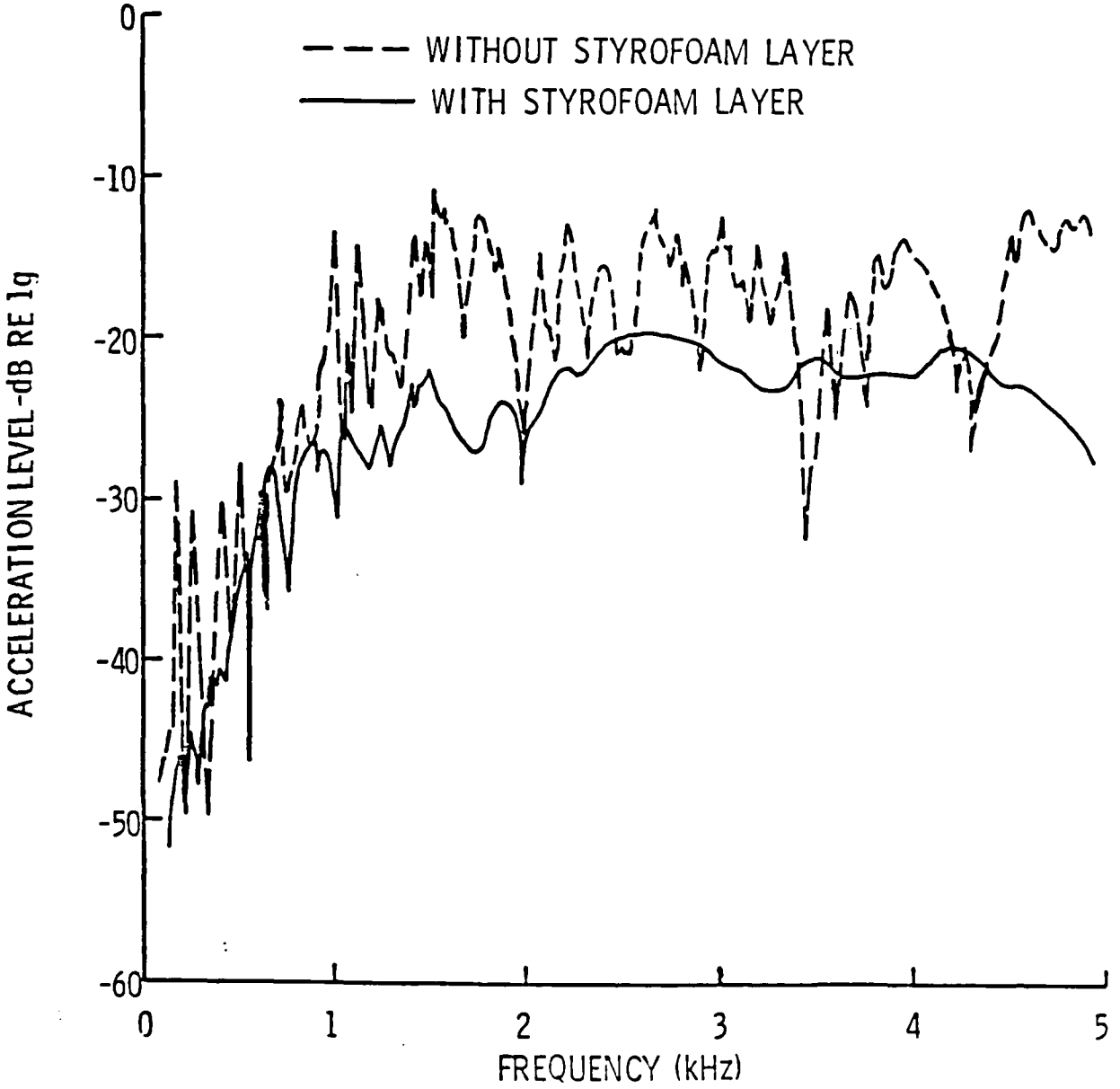

Figure 32. Acceleration Levels at Drive Shaker with and without Styrofoam Layer -- Double Shell with Shakers Horizontal (ϕ = 90°) and Single Radial Drive on the Joint Band

For the circumferential moment drives, the acoustic radiation levels increased at frequencies above 1 kHz when the layer was added, as shown in Fig. 33. A possible explanation for the increase in the levels for the circumferential moment drives and the small changes in the levels for the radial drives may lie in the transmission of the shell vibration to the outer shell through the outer shell partitions in contact with the inner shell and the acoustic radiation from the skin of the outer shell. When the layer is added between the inner and outer shell surfaces, the fluid loading on the outer shell skin is reduced, which could increase the vibration levels of the outer skin and consequently the radiation levels with the layer. However, before the hypothesis can be confirmed, data on the inner shell vibration levels, taken during the acoustic radiation measurements need to be processed and vibration levels of the outer shell relative to the inner shell vibration levels need to be measured.

3.5 Directionality at Two Measurement Hydrophones

Data on the acoustic radiation were recorded and processed for the two hydrophone locations during all of the acoustic radiation measurements at Lake Seneca. As shown in Fig. 16, hydrophone #1 was located in a direction perpendicular to the shell axis and hydrophone #2 was located in a direction parallel to the shell axis.

With the shell oriented so that the shakers were horizontal and facing hydrophone #1, the acoustic radiation levels were higher at hydrophone #1 than at hydrophone #2 at frequencies above 2 kHz for radial and moment drives located in the middle of the shell assembly. This is illustrated by the data in Fig. 34. When the drive is located in the middle of the end shell, closer to hydrophone #2, then the levels measured by the two hydrophones are nearly equal, as illustrated in Fig. 35. As shown in

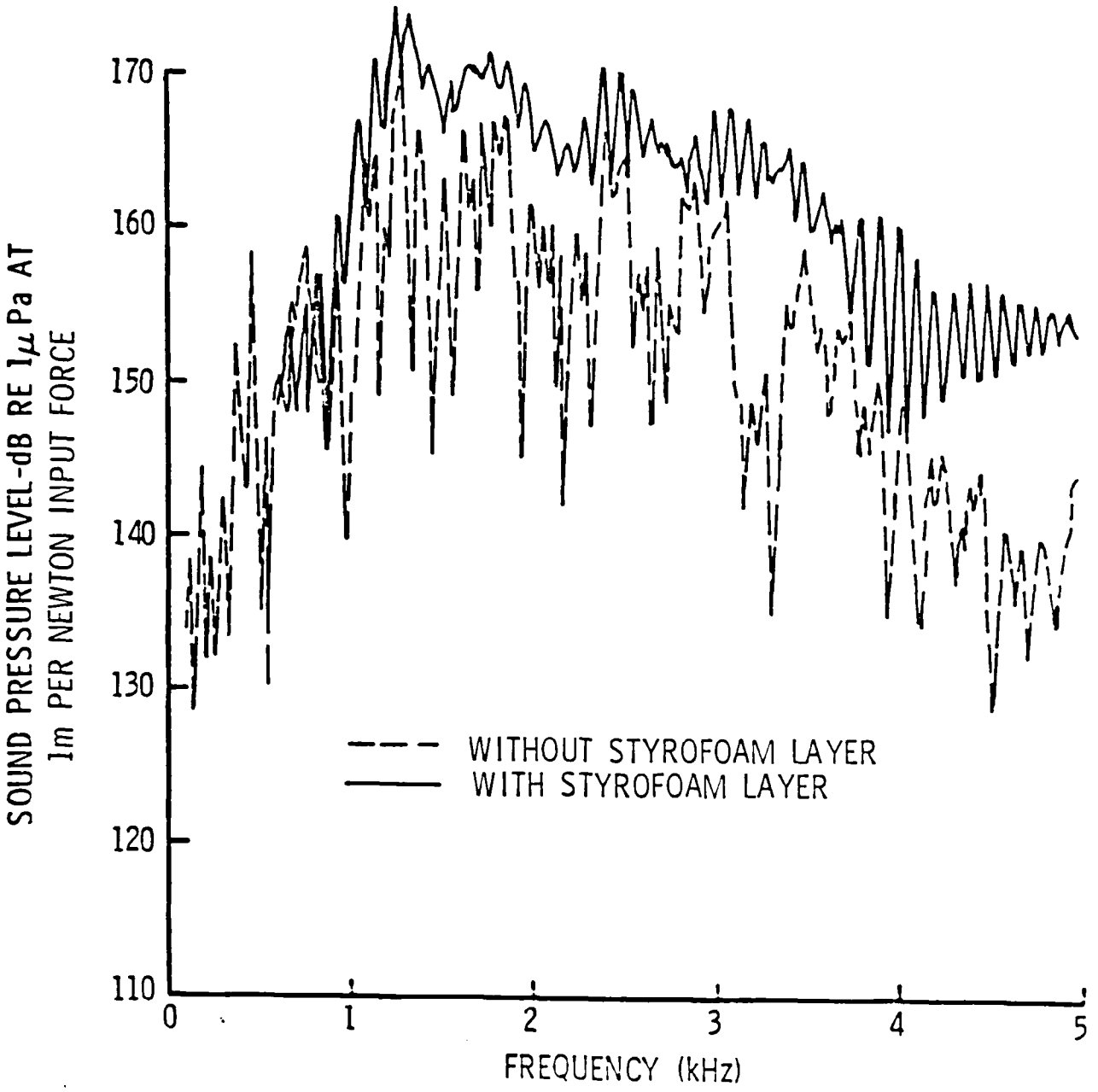

Figure 33. Effect of Styrofoam Layer on Acoustic Radiation Levels at Phone No. 1 -- Double Shell with Shakers Horizontal (ϕ = 90°) and Circumferential Moment Drive in the Middle of the Shell Assemblies

Fig. 36, when the shell is rotated about its axis so that the shakers are vertical, facing down away from the direction of hydrophone #1, the levels at the two hydrophones are nearly equal. Therefore, for the radial and moment drives, the direction of maximum radiation is in the direction of the shakers.

For the longitudinal drives, where the points of excitation are on the sides of the shell (see Fig. 13), rotating the shell so that the shakers are vertical does not change the directionality of the radiation observed at the two hydrophones. In Fig. 37, the levels at hydrophone #1 are higher than the levels at hydrophone #2 for the longitudinal drive with the shaker vertical which is not true for the other types of drives when the shakers are vertical. When the shell is rotated 90° so that the longitudinal drive shakers are horizontal, the levels at hydrophone #1 remain higher than the levels at hydrophone #2, as shown in Figure 38. For the longitudinal drive, there are two drive points at opposite sides of the shell so that the distribution of the shell vibration around the shell circumference at the drive location is probably more uniform. Therefore, the acoustic radiation is less sensitive to shell rotation about its axis than the radiation levels for the radial and moment drives which are applied at a single location.

4. Conclusions and Recommendations

The location of the drive does affect the acoustic radiation levels. The amount and direction of the changes in the acoustic radiation levels with drive location depends on the type of drive and observation position. Adding the outer shell reduced the acoustic radiation at shell resonances, but had little effect on the average radiation levels.

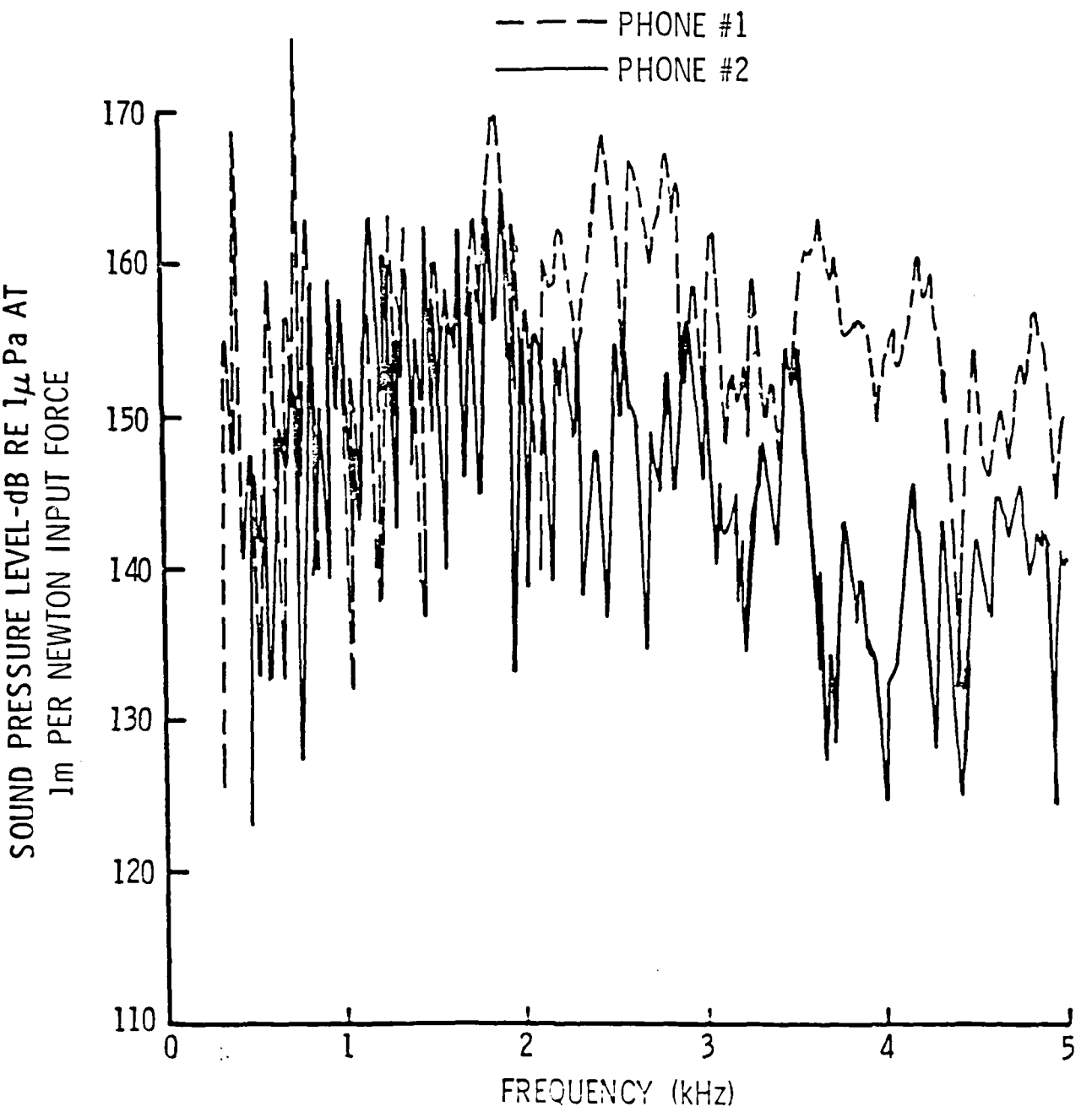

Figure 34. Directionality of Acoustic Radiation at Two Hydrophones -- Single Shell with Shakers Horizontal ($\theta = 90°$) and Single Radial Drive in Middle of Shell Assembly

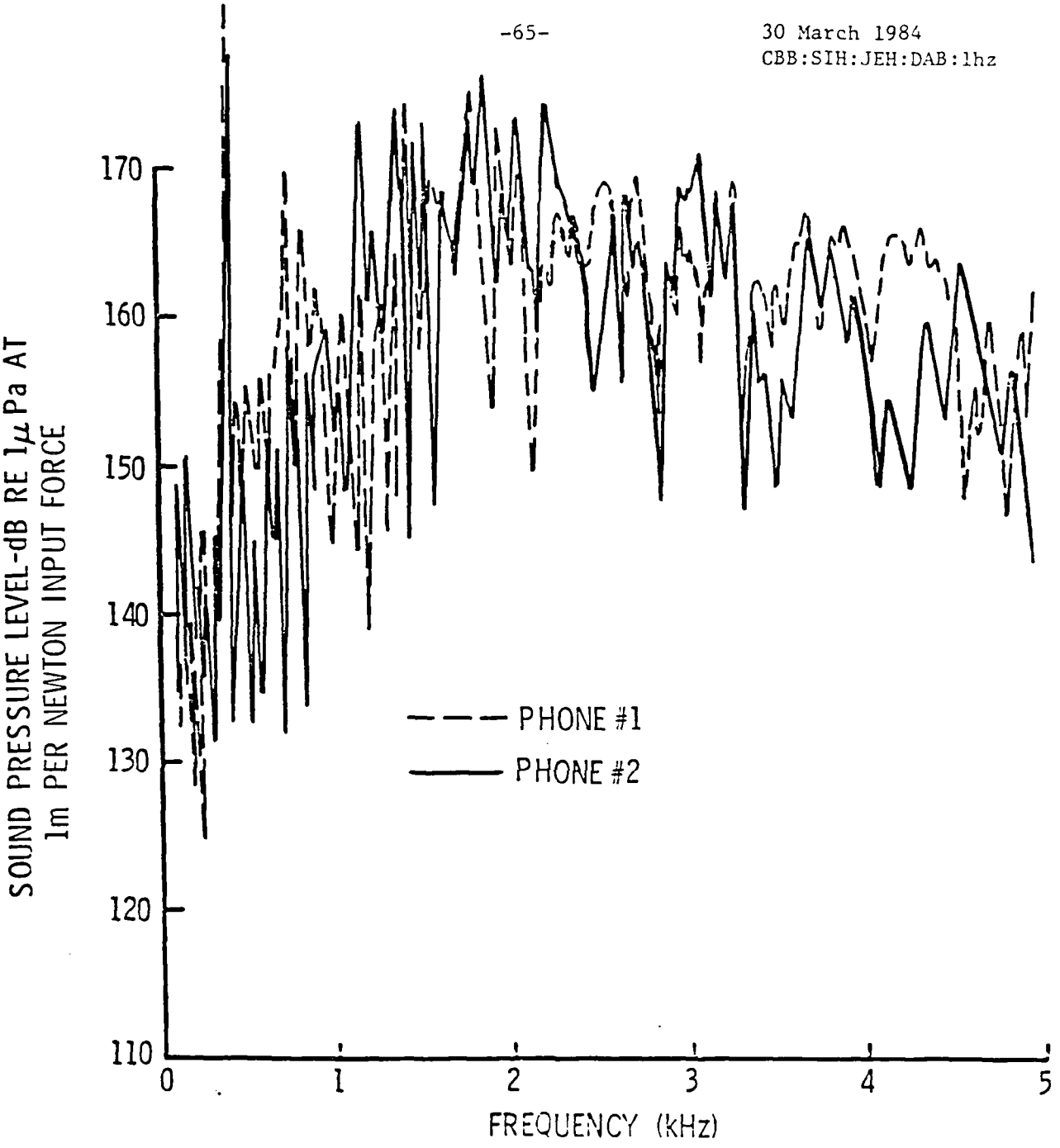

Figure 35. Directionality of Acoustic Radiation at Two Hydrophones -- Single Shell with Shakers Horizontal ($\phi = 90°$) and Single Radial Drive in Middle of End Shell

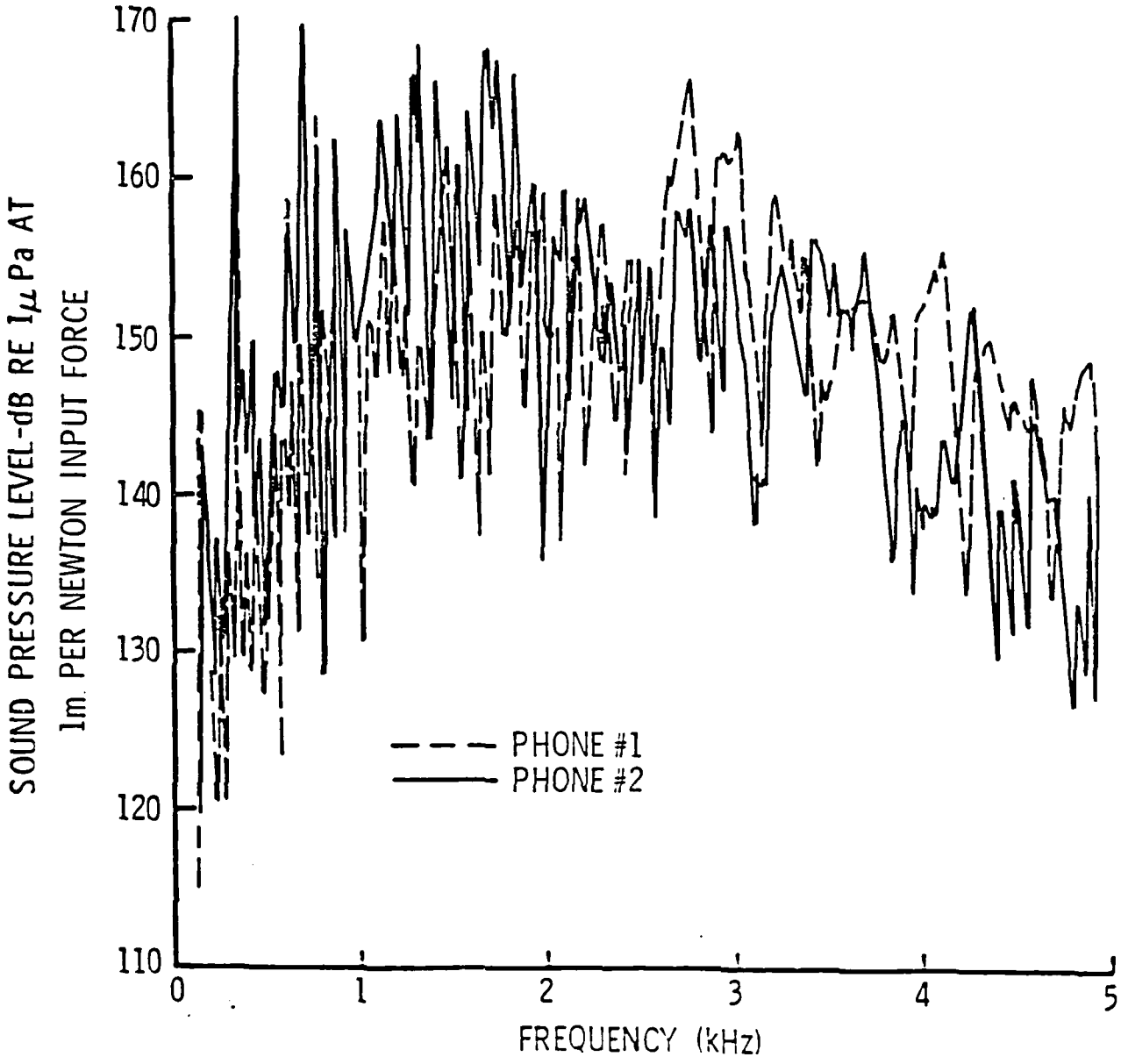

Figure 36. Directionality of Acoustic Radiation at Two Hydrophones -- Single Shell with Shakers Vertical ($\phi = 0°$) and Single Radial Drive in Middle of Shell Assembly

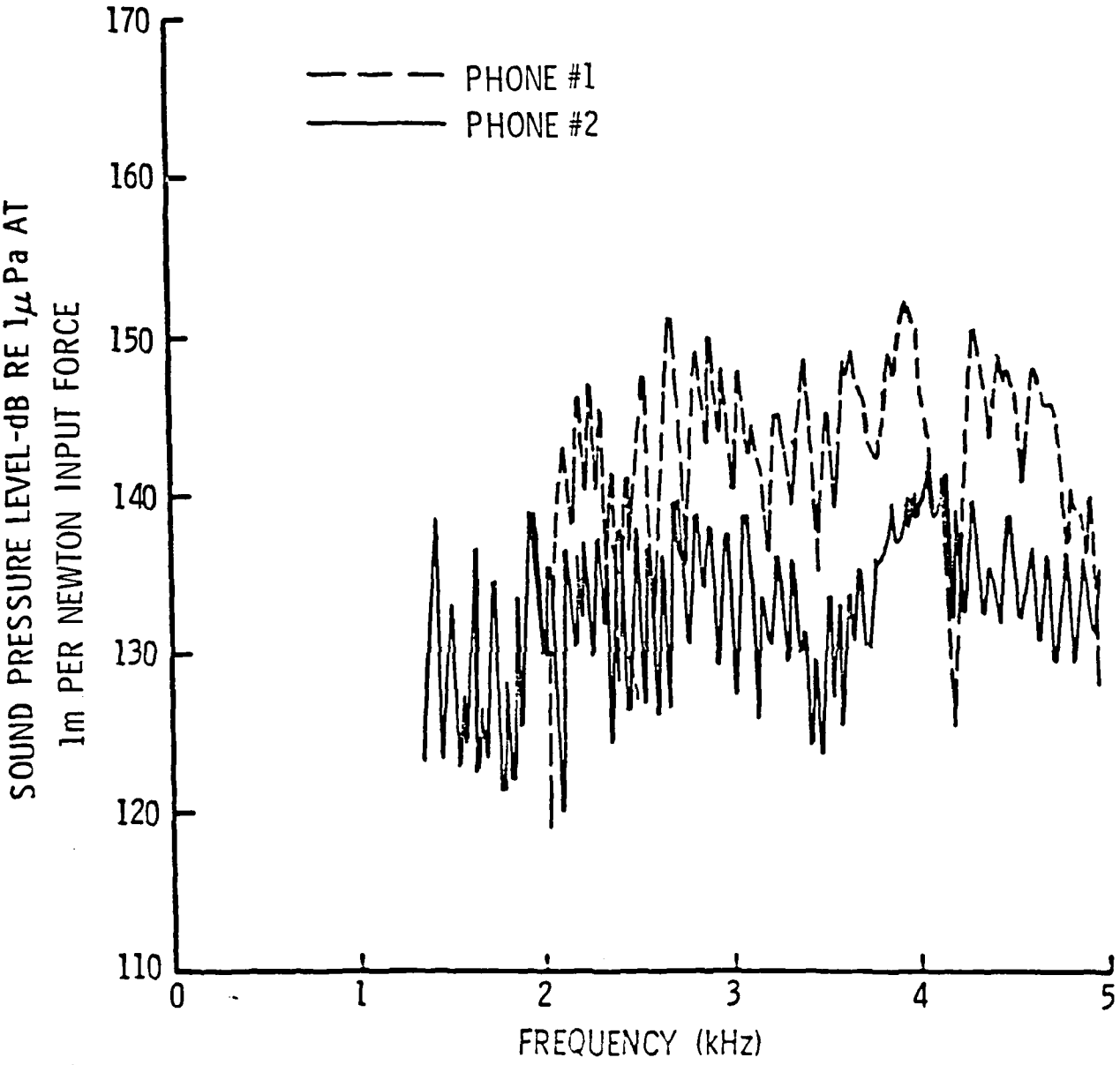

Figure 37. Directionality of Acoustic Radiation at Two Hydrophones -- Single Shell with Shakers Vertical ($\phi = 0°$) and Out of Phase Longitudinal Drive in Middle of the Shell Assembly

The styrofoam pressure release layer did not decrease the acoustic radiation from the double shell as expected. In fact, for the circumferential moment drive the layer increased the acoustic radiation.

The directionality of the acoustic radiation observed by the two measurement hydrophones indicated that the maximum radiation occurred in the direction of the shaker orientation for radial and moment drives. For the longitudinal drives, the radiation directionality is more uniform around the shell circumference.

Normalizing the acoustic radiation levels to the shaker input force does not permit comparisons of the radiated levels to be made for different types of drives. Data on both the shaker force and velocity were recorded so that the shaker output power could be computed from the amplitudes of these two signals and the phase between the signals. Because the shaker mounts will dissipate an insigificant amount of the shaker input power, the power input to the shell should be the same as the measured power output from the shakers. Input power normalization would be independent of the configuration of the shaker mounts and therefore, power-normalized acoustic radiation levels for different types of drives could be compared to assess the affect that the type of drive has on the acoustic radiation from the shell.

A large amount of data on the shell vibration was collected during all of the acoustic radiation measurements. This represents a large investment that should be used in attempts to answer some of the questions on the basic mechanisms of acoustic radiation raised in the introduction to this report that could not be answered in the analysis of only the acoustic radiation data discussed in this report. Data on the acoustic radiation spatial patterns and the shell vibration levels recorded at several frequencies during the spatial

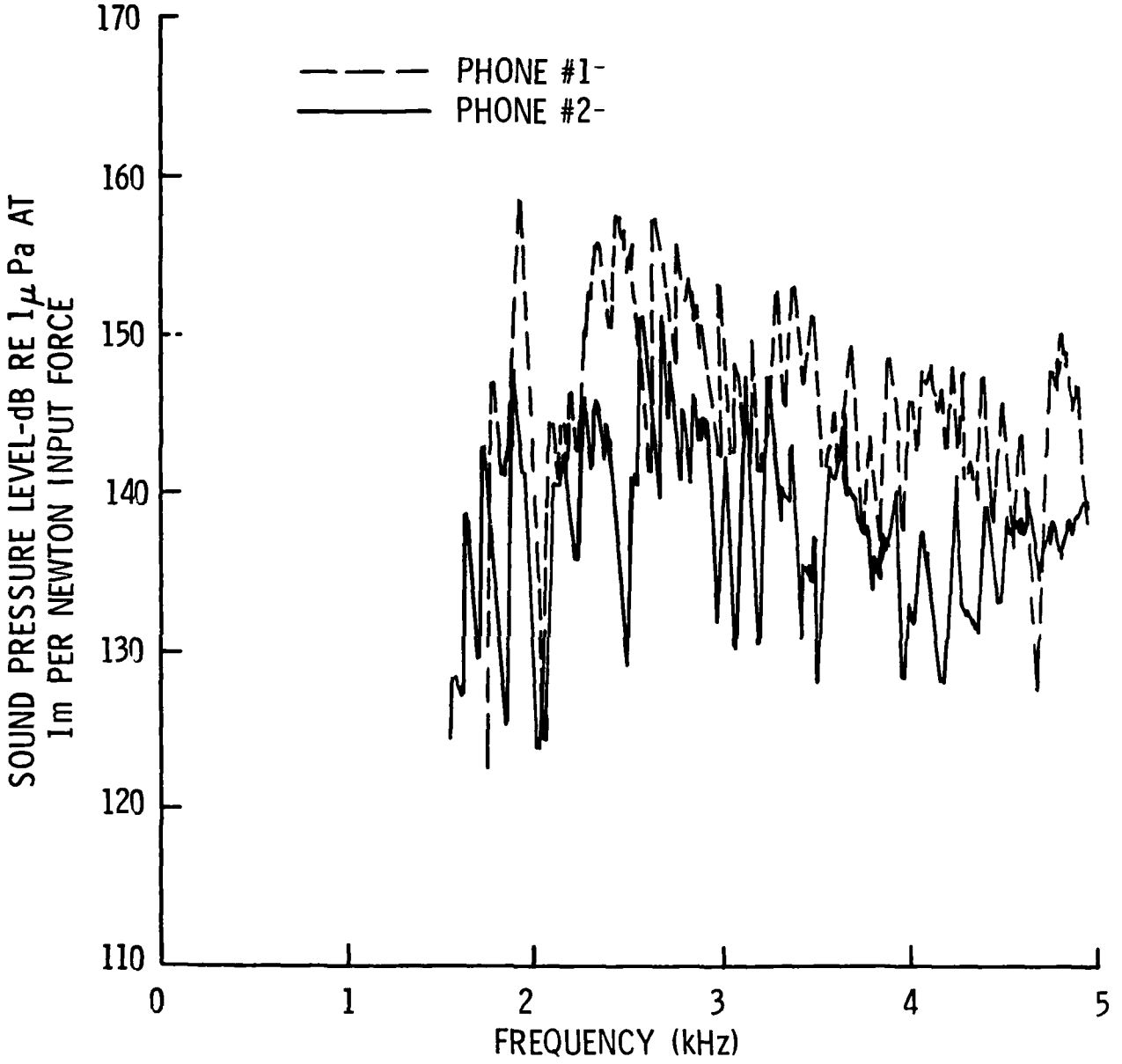

Figure 33. Directionality of Acoustic Radiation of Two Hydrophones - Single Shell with Shakers Horizontal (0=900) and out of Phase Longitudinal Drive in Middle of Shell Assembly.

sweep measurements and data on the shell vibration levels recorded during the frequency sweep measurements should be processed and analyzed to quantify some of the mechanisms of acoustic radiation from fluid-loaded ribbed finite circular cylindrical shells.

Acknowledgment

This work was supported by the Office of Naval Research, Structures Branch Code 474. The authors are grateful to Drs. N. Basdekas and A. Kushner (ONR) for helpful discussions on this work.

References

1. Maidanik, G., "Response of Ribbed Panels to Reverberant Acoustic Fields," J. Acoust. Soc. Am. 34:809-826 (1962).

2. Nayak, P. R., "Line Admittance of Infinite Isotropic Fluid-Loaded Plates," J. Acoust. Soc. Am. 47:191-201 (1970).

3. Mace, B. R., "Sound Radiation from a Plate Reinforced by Two Sets of Parallel Stiffeners," J. Sound Vibr. 71:435-441 (1980).

4. Burroughs, C. B., "Acoustic Radiation from Fluid-Loaded Infinite Circular Cylinders with Doubly Periodic Ring Supports," J. Acoust. Soc. Am. 75(3):715-722 (March 1984).

5. William, W., N. G. Parks, D. A. Moran and C. H. Sherman, "Acoustic Radiation from a Finite Cylinder," J. Acoust. Soc. Am. 36(12):2316-2322 (December 1964).

6. Sandman, B. E., "Fluid-Loading Influence Coefficients for a Finite Cylindrical Shell," J. Acoust. Soc. Am. 60(6):1256-1264 (1976).

7. Leissa, A. W., "Vibration of Shells," NASA CP-288 (1973).

8. "Measurement Plan at Lake Seneca for ONR and ACSAS" (29 September 1982).

9. Burroughs, C. B., S. I. Hayek, D. A. Bostian and J. E. Hallander, "Resonant Frequencies and Mode Shapes for Single and Double Cylindrical Shells," ARL/PSU TM 83-169, Applied Research Laboratory, The Pennsylvania State University (23 September 1983).

Appendix A: Acoustic Radiation Measurement Configurations

Table A1 lists all of the acoustic radiation measurement configurations conducted from 25 October 1982 through 17 December 1982 (Measurement Nos. 1 through 144) on all shell configurations without the styrofoam decoupling coating and from 6 June 1983 through 17 June 1983 (Measurements Nos. 163 through 178) on all shell configurations with the decoupling coating. Measurement Nos. 145 through 162 were conducted for the ACSAS Project Office during December 1982.

Table A1. Acoustic Radiation Measurement Configurations

Measurement Number	Shell Type	Shaker Location (1)	Type of Measurement (2)	Sensor Selection Switching Setting	Shell Position (3)
1	Single	(A,x)	F	C0, C1	$\phi = 0°$
2	Single	(A,x)	S	C0, C1	$\phi = 0°$
3	Single	(A,y)	F	C2, C3	$\phi = 0°$
4	Single	(A,y)	S	C2, C3	$\phi = 0°$
5	Single	(A,z)	F	C4, C5	$\phi = 0°$
6	Single	(A,z)	S	C4, C5	$\phi = 0°$
7	Single	(B,x)	F	C0, C1	$\phi = 0°$
8	Single	(B,x)	S	C0, C1	$\phi = 0°$
9	Single	(B,y)	F	C2, C3	$\phi = 0°$
10	Single	(B,y)	S	C2, C3	$\phi = 0°$
11	Single	(B,z)	F	C4, C5	$\phi = 0°$
12	Single	(B,z)	S	C4, C5	$\phi = 0°$
13	Single	(A,x)	F	C0, C1	$\phi = 90°$
14	Single	(A,x)	S	C0, C1	$\phi = 90°$
15	Single	(A,y)	F	C2, C3	$\phi = 90°$
16	Single	(A,y)	S	C2, C3	$\phi = 90°$
17	Single	(A,z)	F	C4, C5	$\phi = 90°$
18	Single	(A,z)	S	C4, C5	$\phi = 90°$
19	Single	(B,x)	F	C0, C1	$\phi = 90°$
20	Single	(B,x)	S	C0, C1	$\phi = 90°$
21	Single	(B,y)	F	C2, C3	$\phi = 90°$
22	Single	(B,y)	S	C2, C3	$\phi = 90°$
23	Single	(B,z)	F	C4, C5	$\phi = 90°$
24	Single	(B,z)	S	C4, C5	$\phi = 90°$

30 March 1984
CBB:SIH:JEH:DAB:lhz

Table A1. Acoustic Radiation Measurement Configurations (continuation)

Measurement Number	Shell Type	Shaker Location (1)	Type of Measurement (2)	Sensor Selection Switching Setting	Shell Position (3)
25	Double	(A,x)	F	C0, C1	$\phi = 0°$
26	Double	(A,x)	S	C0, C1	$\phi = 0°$
27	Double	(A,y)	F	C2, C3	$\phi = 0°$
28	Double	(A,y)	S	C2, C3	$\phi = 0°$
29	Double	(A,z)	F	C4, C5	$\phi = 0°$
30	Double	(A,z)	S	C4, C5	$\phi = 0°$
31	Double	(B,x)	F	C0, C1	$\phi = 0°$
32	Double	(B,x)	S	C0, C1	$\phi = 0°$
33	Double	(B,y)	F	C2, C3	$\phi = 0°$
34	Double	(B,y)	S	C2, C3	$\phi = 0°$
35	Double	(B,z)	F	C4, C5	$\phi = 0°$
36	Double	(B,z)	S	C4, C5	$\phi = 0°$
37	Double	(A,x)	F	C0, C1	$\phi = 90°$
38	Double	(A,x)	S	C0, C1	$\phi = 90°$
39	Double	(A,y)	F	C2, C3	$\phi = 90°$
40	Double	(A,y)	S	C2, C3	$\phi = 90°$
41	Double	(A,z)	F	C4, C5	$\phi = 90°$
42	Double	(A,z)	S	C4, C5	$\phi = 90°$
43	Double	(B,x)	F	C0, C1	$\phi = 90°$
44	Double	(B,x)	S	C0, C1	$\phi = 90°$
45	Double	(B,y)	F	C2, C3	$\phi = 90°$
46	Double	(B,y)	S	C2, C3	$\phi = 90°$
47	Double	(B,z)	F	C4, C5	$\phi = 90°$
48	Double	(B,z)	S	C4, C5	$\phi = 90°$

30 March 1984
CBB:SIH:JEH:DAB:lhz

Table A1. Acoustic Radiation Measurement Configurations (continuation)

Measurement Number	Shell Type	Shaker Location (1)	Type of Measurement (2)	Sensor Selection Switching Setting	Shell Position (3)
49	Single	(C,x)	F	C0, C1	ϕ = 0°
50	Single	(C,x)	S	C0, C1	ϕ = 0°
51	Single	(C,y)	F	C2, C3	ϕ = 0°
52	Single	(C,y)	S	C2, C3	ϕ = 0°
53	Single	(C,z)	F	C4, C5	ϕ = 0°
54	Single	(C,z)	S	C4, C5	ϕ = 0°
55	Single	(C,x)	F	C0, C1	ϕ = 0°
56	Single	(C,x)	S	C0, C1	ϕ = 0°
57	Single	(C,y)	F	C2, C3	ϕ = 0°
58	Single	(C,y)	S	C2, C3	ϕ = 0°
59	Single	(C,z)	F	C4, C5	ϕ = 0°
60	Single	(C,z)	S	C4, C5	ϕ = 0°
61	Double	(C,x)	F	C0, C1	ϕ = 0°
62	Double	(C,x)	S	C0, C1	ϕ = 0°
63	Double	(C,y)	F	C2, C3	ϕ = 0°
64	Double	(C,y)	S	C2, C3	ϕ = 0°
65	Double	(C,z)	F	C4, C5	ϕ = 0°
66	Double	(C,z)	S	C4, C5	ϕ = 0°
67	Double	(C,x)	F	C0, C1	ϕ = 90°
68	Double	(C,x)	S	C0, C1	ϕ = 90°
69	Double	(C,y)	F	C2, C3	ϕ = 90°
70	Double	(C,y)	S	C2, C3	ϕ = 90°
71	Double	(C,z)	F	C4, C5	ϕ = 90°
72	Double	(C,z)	S	C4, C5	ϕ = 90°

30 March 1984
CBB:SIH:JEH:DAB:lhz

Table A1. Acoustic Radiation Measurement Configurations (continuation)

Measurement Number	Shell Type	Shaker Location (1)	Type of Measurement (2)	Sensor Selection Switching Setting	Shell Position (3)
73	Single	(D,x)	F	C0, C1	$\phi = 0°$
74	Single	(D,x)	S	C0, C1	$\phi = 0°$
75	Single	(D,y)	F	C2, C3	$\phi = 0°$
76	Single	(D,y)	S	C2, C3	$\phi = 0°$
77	Single	(D,z)	F	C4, C5	$\phi = 0°$
78	Single	(D,z)	S	C4, C5	$\phi = 0°$
79	Single	(D,x)	F	C0, C1	$\phi = 90°$
80	Single	(D,x)	S	C0, C1	$\phi = 90°$
81	Single	(D,y)	F	C2, C3	$\phi = 90°$
82	Single	(D,y)	S	C2, C3	$\phi = 90°$
83	Single	(D,z)	F	C4, C5	$\phi = 90°$
84	Single	(D,z)	S	C4, C5	$\phi = 90°$
85	Double	(D,x)	F	C0, C1	$\phi = 0°$
86	Double	(D,x)	S	C0, C1	$\phi = 0°$
87	Double	(D,y)	F	C2, C3	$\phi = 0°$
88	Double	(D,y)	S	C2, C3	$\phi = 0°$
89	Double	(D,z)	F	C4, C5	$\phi = 0°$
90	Double	(D,z)	S	C4, C5	$\phi = 0°$
91	Double	(D,x)	F	C0, C1	$\phi = 90°$
92	Double	(D,x)	S	C0, C1	$\phi = 90°$
93	Double	(D,y)	F	C2, C3	$\phi = 90°$
94	Double	(D,y)	S	C2, C3	$\phi = 90°$
95	Double	(D,z)	F	C4, C5	$\phi = 90°$
96	Double	(D,z)	S	C4, C5	$\phi = 90°$

30 March 1984
CBB:SIH:JEH:DAB:lhz

Table A1. Acoustic Radiation Measurement Configurations (continuation)

Measurement Number	Shell Type	Shaker Location (1)	Type of Measurement (2)	Sensor Selection Switching Setting	Shell Position (3)
97	Single	(E,x)	F	C0, C1	$\phi = 0°$
98	Single	(E,x)	S	C0, C1	$\phi = 0°$
99	Single	(E,y)	F	C2, C3	$\phi = 0°$
100	Single	(E,y)	S	C2, C3	$\phi = 0°$
101	Single	(E,z)	F	C4, C5	$\phi = 0°$
102	Single	(E,z)	S	C4, C5	$\phi = 0°$
103	Single	(E,x)	F	C0, C1	$\phi = 0°$
104	Single	(E,x)	S	C0, C1	$\phi = 0°$
105	Single	(E,y)	F	C2, C3	$\phi = 0°$
106	Single	(E,y)	S	C2, C3	$\phi = 0°$
107	Single	(E,z)	F	C4, C5	$\phi = 0°$
108	Single	(E,z)	S	C4, C5	$\phi = 0°$
109	Single	(E,x)	F	C0, C1	$\phi = 90°$
110	Single	(E,x)	S	C0, C1	$\phi = 90°$
111	Single	(E,y)	F	C2, C3	$\phi = 90°$
112	Single	(E,y)	S	C2, C3	$\phi = 90°$
113	Single	(E,z)	F	C4, C5	$\phi = 90°$
114	Single	(E,z)	S	C4, C5	$\phi = 90°$
115	Single	(E,x)	F	C0, C1	$\phi = 90°$
116	Single	(E,x)	S	C0, C1	$\phi = 90°$
117	Single	(E,y)	F	C2, C3	$\phi = 90°$
118	Single	(E,y)	S	C2, C3	$\phi = 90°$
119	Single	(E,z)	F	C4, C5	$\phi = 90°$
120	Single	(E,z)	S	C4, C5	$\phi = 90°$

Table A1. Acoustic Radiation Measurement Configurations (continuation)

Measurement Number	Shell Type	Shaker Location (1)	Type of Measurement (2)	Sensor Selection Switching Setting	Shell Position (3)
121	Double	(E,x)	F	C0, C1	$\phi = 0°$
122	Double	(E,x)	S	C0, C1	$\phi = 0°$
123	Double	(E,y)	F	C2, C3	$\phi = 0°$
124	Double	(E,y)	S	C2, C3	$\phi = 0°$
125	Double	(E,z)	F	C4, C5	$\phi = 0°$
126	Double	(E,z)	S	C4, C5	$\phi = 0°$
127	Double	(E,x)	F	C0, C1	$\phi = 0°$
128	Double	(E,x)	S	C0, C1	$\phi = 0°$
129	Double	(E,y)	F	C2, C3	$\phi = 0°$
130	Double	(E,y)	S	C2, C3	$\phi = 0°$
131	Double	(E,z)	F	C4, C5	$\phi = 0°$
132	Double	(E,z)	S	C4, C5	$\phi = 0°$
133	Double	(E,x)	F	C0, C1	$\phi = 90°$
134	Double	(E,x)	S	C0, C1	$\phi = 90°$
135	Double	(E,y)	F	C2, C3	$\phi = 90°$
136	Double	(E,y)	S	C2, C3	$\phi = 90°$
137	Double	(E,z)	F	C4, C5	$\phi = 90°$
138	Double	(E,z)	S	C4, C5	$\phi = 90°$
139	Double	(E,x)	F	C0, C1	$\phi = 90°$
140	Double	(E,x)	S	C0, C1	$\phi = 90°$
141	Double	(E,y)	F	C2, C3	$\phi = 90°$
142	Double	(E,y)	S	C2, C3	$\phi = 90°$
143	Double	(E,z)	F	C4, C5	$\phi = 90°$
144	Double	(E,z)	S	C4, C5	$\phi = 90°$

End of Measurements taken from 25 October 1983 through 17 December 1983.

Table A1. Acoustic Radiation Measurement Configurations (continuation)

Measurement Number	Shell Type	Shaker Location (1)	Type of Measurement (2)	Sensor Selection Switching Setting	Shell Position (3)
163*	Double w/foam	(A,x)	F	C0, C1	$\phi = 0°$
164	Double w/foam	(A,x)	S	C0, C1	$\phi = 0°$
165	Double w/foam	(A,y)	F	C2, C3	$\phi = 0°$
166	Double w/foam	(A,y)	S	C2, C3	$\phi = 0°$
167	Double w/foam	(A,z)	F	C0, C1	$\phi = 90°$
168	Double w/foam	(A,z)	S	C0, C1	$\phi = 90°$
169	Double w/foam	(A,y)	F	C2, C3	$\phi = 90°$
170	Double w/foam	(A,y)	S	C2, C3	$\phi = 90°$
171	Double w/foam	(C,x)	F	C0, C1	$\phi = 0°$
172	Double w/foam	(C,x)	S	C0, C1	$\phi = 0°$
173	Double w/foam	(C,y)	F	C2, C3	$\phi = 0°$
174	Double w/foam	(C,y)	S	C2, C3	$\phi = 0°$

*Measurement Nos. 144 through 162 were conducted for ACSAS Project Office of ONR.

30 March 1984
CBB:SIH:JEH:DAB:lhz

Table A1. Acoustic Radiation Measurement Configurations (continuation)

Measurement Number	Shell Type	Shaker Location (1)	Type of Measurement (2)	Sensor Selection Switching Setting	Shell Position (3)
175	Double w/foam	(C,x)	F	C0, C1	ϕ = 90°
176	Double w/foam	(C,x)	S	C0, C1	ϕ = 90°
177	Double w/foam	(C,y)	F	C2, C3	ϕ = 90°
178	Double w/foam	(C,y)	S	C2, C3	ϕ = 90°

End Acoustic Radiation Measurements

30 March 1984
CBB:SIH:JEH:DAB:lhz

Table A1. Acoustic Radiation Measurement Configurations (continuation)

(1) Key to Shaker Locations

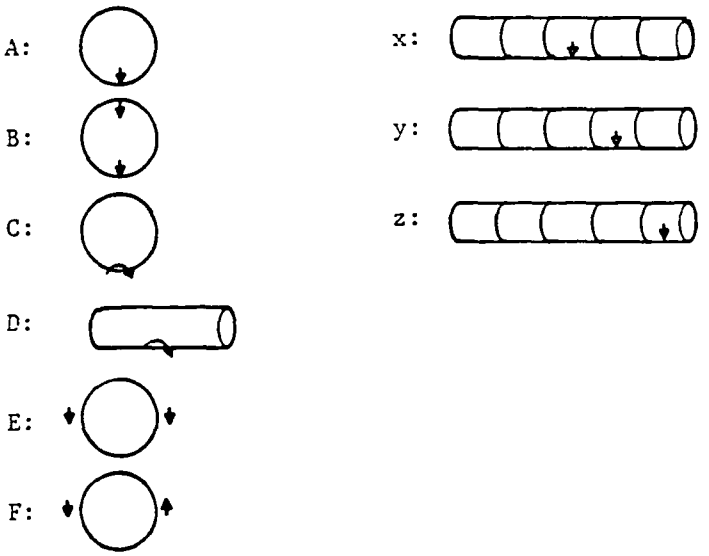

(2) Key to Type of Measurement

F. Frequency sweep from 20 Hz to 5 kHz with shell in following location (as observed from above)

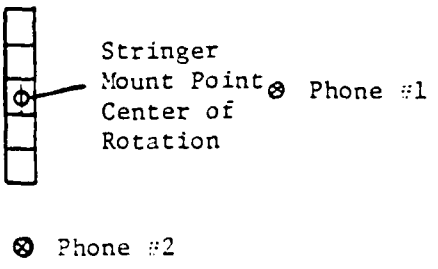

Table A1. Acoustic Radiation Measurement Configurations (continuation)

S = spatial sweep from 0° (as shown above) to 180° at frequencies where peaks in the acoustic radiation levels were observed during frequency sweep measurements.

(3) Key to Shell Position

$\phi = 0°$ with shakers vertical

$\phi = 90°$ with shakers horizontal.

Appendix B: Sample Run of Data Processing and Plotting Computer Program

In this Appendix, a printout from the computer terminal during a sample run of the data processing and plotting computer program is given. Where needed, annotation has been added. Underlining denotes user inputs. The plots for this sample run are given at the end of this Appendix.

```
Username: JEH
Password:

Please enter four (4) digit project number: 4006


WELCOME TO THE ARL VAX 11/782 VMS RELEASE 3.5 OPERATING SYSTEM


Previous logical name assignment replaced
 THE STUDENT ACCOUNT NUMBER IS 9079
ARE YOU AT A VT100, VT101?: N
  13-MAR-1984 14:41:07



VAX/VMS Interactive Users - Total = 22
     13-MAR-1984 14:41:08.39

ENTER YOUR INITIALS. -->:
$ MENU
```

} Log In

C O M M A N D M E N U

1) RETREIVE UNSCRAMBLED RAW DATA FROM STORAGE TAPES.

2) RETREIVE UNNORMALIZED CORRECTED DATA FROM STORAGE TAPES. (NOT THE SAME AS OPTION 1).

3) RUN THE MAIN PROGRAM.

4) DELETE UNSCRAMBLED 'RAW' DATA FILES.

5) DELETE UNNORMALIZED 'CORRECTED' DATA FILES.

6) DELETE PLOT FILES FROM DISK STORAGE.

7) SEND PLOTS TO THE HP PLOTTER

8) EXIT

99) LOGOUT

PLEASE ENTER YOUR SELECTION. ----> : 7
IS THERE A TAPE MOUNTED? -- : Y

30 March 1984
CBB:SIH:JEH:DAB:lhz

M A I N M E N U

```
1) TO REFINE RAW DATA.
2) TO PLOT DIFFERENCE OF TWO REFINED FILES.
3) TO PLOT A REFINED DATA FILE.
4) TO READ AND PRINT A REFINED DATA FILE.
5) TO READ AND PRINT A RAW DATA FILE.
6) TO EXIT

PLEASE ENTER YOUR SELECTION -1
<--INITIALIZING PROGRAM FLAGS-->
ENTER THE FILE TYPE. -->F
ENTER THE MEASUREMENT #. --> 141
CUT NUMBER? -->1
ENTER THE FREQUENCY(IF ANY). -->
ENTER THE TAPE CHANNEL #. --> 1

THE CURRENT STATUS IS:
EXPERIMENT TYPE          ->F
MEASUREMENT #            ->141
CUT #                    ->1
FREQUENCY #              ->0000
```

Only for spatial sweep measurements at a given frequency, otherwise return

```
CHANNEL #                ->01
```

Process shaker force data for normalizing acoustic radiation data

```
IF EVERYTHING IS FINE, PRESS RETURN.
TYPE CHANGE(C OR CH) TO DO A CORRECTION.
YOUR CHOICE? -->
IS THIS SWEEP TO 1K OR TO 5K? -->5

# OF ELEMENTS IN RAW DATA FILE =   5781

WHICH CALIBRATION FILE DO YOU CHOOSE TO USE? IT SHALL
REMAIN THE SAME THROUGHOUT THIS SESSION.

CAL FILE #? -->7
```

```
ENTER THE ITHACO GAIN ON CHANNEL # 01
                FOR MEASUREMENT # 141
                          CUT # 1    ? 0

ENTER THE CONTROL BOX NUMBER. ?00

                          DRIVE MENU

SELECT ONE OF THE FOLLOWING DRIVES:

1) RADIAL DRIVE - SINGLE
2) RADIAL DRIVE - DOUBLE IN PHASE
3) RADIAL DRIVE - DOUBLE OUT OF PHASE
4) RADIAL DRIVE - AXIAL MOMENT FOUNDATION
5) RADIAL DRIVE - CIRCUMF. MOMENT FOUNDATION
6) AXIAL MOMENT DRIVE
7) CIRCUMFERENTIAL MOMENT DRIVE.
8) LONGITUDINAL DRIVE IN PHASE.
9) LONGITUDINAL DRIVE OUT OF PHASE.  -->9

WHERE ARE THE SHAKERS LOCATED?

1) MIDDLE OF SHELL

2) ON THE JOINT BAND

3) MIDDLE OF END SHELL              -->2

IS THIS A SINGLE OR DOUBLE SHELL? -->D

WITH FOAM?---?N

WHAT IS SHAKER ORIENTATION?

PHI=0.0 (VERTICAL)

PHI=90. (HORIZONTAL)

ENTER V OR H---?H
DO YOU WISH TO CHECK THE HEADERS? --? Y
```

```
 PLOT FOR ONR FIELD MEASUREMENT NO. 141 CUT NO. 1
 FREQUENCY - 0000 HZ.



 DOUBLE SHELL WITH SHAKERS HORIZONTAL
 FORCE IN SHAKER NO. 1
 SHAKER LOCATION - ON THE JOINT BAND
 LONG. DRIVE - OUT OF PHASE


IS THIS THE CORRECT HEADER INFO? Y


NORMALIZATION MENU....SELECT ONE.


1)  INPUT FORCE
2)  INPUT VELOCITY
3)  INPUT POWER
4)  NO NORMALIZATION
5)  NO NORMALIZATION OR CALIBRATIONS.                    -->4
<--RECOVERING THE FREQUENCIES-->
<--WORKING ON THE LEVELS-->
<--CORRECT FOR GAINS, SENSITIVITIES, AND CAL TONES-->


DO YOU WISH TO PLOT THIS DATA? -->N


DO YOU WISH TO SAVE THE REFINED DATA? -->Y




SHOULD REFINED DATA BE WRITTEN TO TAPE? N
<--WRITING REFINED DATA TO A DISK DRIVE.-->


DO YOU WISH TO CHANGE ANY OF THE LOGICAL ASSIGNMENTS?


PRESS RETURN FOR NO.

TYPE 'HELP' FOR A DISCRIPTION OF THESE ASSIGNMENTS      -->

THE CURRENT STATUS IS:
EXPERIMENT TYPE          ->F
MEASUREMENT #            ->141
CUT #                    ->1
FREQUENCY #              ->0000
CHANNEL #                ->02
```

Channel number is automatically incremented by one

30 March 1984
CBB:SIH:JEH:DAB:lhz

```
IF EVERYTHING IS FINE, PRESS RETURN.
TYPE CHANGE(C OR CH) TO DO A CORRECTION.
YOUR CHOICE? -->


# OF ELEMENTS IN RAW DATA FILE =   5781



ENTER THE ITHACO GAIN ON CHANNEL # 02
                FOR MEASUREMENT # 141
                           CUT # 1    ? 0
DO YOU WISH TO CHECK THE HEADERS? --> Y

 PLOT FOR ONR FIELD MEASUREMENT NO. 141 CUT NO. 1
 FREQUENCY - 0000 HZ.
 DOUBLE SHELL WITH SHAKERS HORIZONTAL
 FORCE IN SHAKER NO. 2
 SHAKER LOCATION - ON THE JOINT BAND
 LONG. DRIVE - OUT OF PHASE

IS THIS THE CORRECT HEADER INFO? Y


NORMALIZATION MENU....SELECT ONE.


1)  INPUT FORCE
2)  INPUT VELOCITY
3)  INPUT POWER
4)  NO NORMALIZATION
5)  NO NORMALIZATION OR CALIBRATIONS.                --> 4
<--WORKING ON THE LEVELS-->
<--CORRECT FOR GAINS, SENSITIVITIES, AND CAL TONES-->



DO YOU WISH TO PLOT THIS DATA? --> N
<--WRITING REFINED DATA TO A DISK DRIVE.-->
```

Process force data from Shaker No. 1 for use to normalize acoustic radiation data (normalize to sum of force levels)

```
DO YOU WISH TO CHANGE ANY OF THE LOGICAL ASSIGNMENTS?

PRESS RETURN FOR NO,

TYPE 'HELP' FOR A DISCRIPTION OF THESE ASSIGNMENTS      -->

THE CURRENT STATUS IS:
EXPERIMENT TYPE          ->F
MEASUREMENT #            ->141
CUT #                    ->1
FREQUENCY #              ->0000
CHANNEL #                ->03

IF EVERYTHING IS FINE, PRESS RETURN.
TYPE CHANGE(C OR CH) TO DO A CORRECTION.
YOUR CHOICE? -->C
TO CHANGE A PARAMETER PRESS:

1) FOR THE EXPERIMENT TYPE.
2) FOR THE MEASUREMENT NUMBER.
3) FOR THE CUT NUMBER.
4) FOR THE CHANNEL NUMBER.
5) FOR THE FREQUENCY NUMBER.
YOUR SELECTION? -->4
ENTER THE TAPE CHANNEL #. --> 13
```

Need to go to Channel 13 for the acoustic radiation data from Phone No. 1

```
THE CURRENT STATUS IS:
EXPERIMENT TYPE          ->F
MEASUREMENT #            ->141
CUT #                    ->1
FREQUENCY #              ->0000
CHANNEL #                ->13

IF EVERYTHING IS FINE, PRESS RETURN.
TYPE CHANGE(C OR CH) TO DO A CORRECTION.
YOUR CHOICE? -->

# OF ELEMENTS IN RAW DATA FILE =    5731
<---AMBIENT FILE #141 NOT FOUND--->
CHOOSE YOUR OWN FILE #? -->Y
ENTER THE AMBIENT FILE # OF YOUR CHOICE.-- 241

AMBIENT NOISE FILE = 1POW0000.241
```

Read Ambient noise film

30 March 1984
CBB:SIH:JEH:DAB:lhz

```
ENTER THE ITHACO GAIN ON CHANNEL # 13
                FOR MEASUREMENT # 141
                            CUT # 1    ? 50
DO YOU WISH TO CHECK THE HEADERS? -->Y

 PLOT FOR ONR FIELD MEASUREMENT NO. 141 CUT NO. 1
 FREQUENCY - 0000 HZ.
 DOUBLE SHELL WITH SHAKERS HORIZONTAL
 PHONE NO. 1
 SHAKER LOCATION - ON THE JOINT BAND
 LONG. DRIVE - OUT OF PHASE


IS THIS THE CORRECT HEADER INFO? Y


NORMALIZATION MENU....SELECT ONE.


1)  INPUT FORCE
2)  INPUT VELOCITY
3)  INPUT POWER
4)  NO NORMALIZATION
5)  NO NORMALIZATION OR CALIBRATIONS.                    -->1
<--WORKING ON THE LEVELS-->
<--CORRECT FOR GAINS, SENSITIVITIES, AND CAL TONES-->



<--FILL POINTER BIN LOCATOR-->
<--SUBTRACT OFF AMBIENT NOISE-->
<--NORMALIZE THE DATA-->


DO YOU WISH TO PLOT THIS DATA? -->Y              Plot data


THE PRESENT LIMITS FOR THE FREQUENCY (X) AXIS ARE:

FMIN =      0.0000

FMAX =   4930.0000

THEY WILL BE RESET TO:

FMIN = 0.0

FMAX = 5000.

DO YOU WISH TO USE THESE INSTEAD? -- Y
<--WRITING REFINED DATA TO A DISK DRIVE.--
```

30 March 1984
CBB:SIH:JEH:DAB:lhz

```
DO YOU WISH TO CHANGE ANY OF THE LOGICAL ASSIGNMENTS?

PRESS RETURN FOR NO.

TYPE 'HELP' FOR A DISCRIPTION OF THESE ASSIGNMENTS      -->

THE CURRENT STATUS IS:
EXPERIMENT TYPE          ->F
MEASUREMENT #            ->141
CUT #                    ->1
FREQUENCY #              ->0000
CHANNEL #                ->14                    Channel number is automatically
                                                 incremented
IF EVERYTHING IS FINE, PRESS RETURN.
TYPE CHANGE(C OR CH) TO DO A CORRECTION.
YOUR CHOICE? -->


# OF ELEMENTS IN RAW DATA FILE =   5731


AMBIENT NOISE FILE = 1POW0000.941




ENTER THE ITHACO GAIN ON CHANNEL # 14
                FOR MEASUREMENT # 141
                          CUT # 1    ? 50
DO YOU WISH TO CHECK THE HEADERS? -->N
<--WORKING ON THE LEVELS-->
<--CORRECT FOR GAINS, SENSITIVITIES, AND CAL TONES-->
<--SUBTRACT OFF AMBIENT NOISE-->
<--NORMALIZE THE DATA-->


DO YOU WISH TO PLOT THIS DATA? --Y
<--WRITING REFINED DATA TO A DISK DRIVE.--      Plot data


DO YOU WISH TO CHANGE ANY OF THE LOGICAL ASSIGNMENTS?

PRESS RETURN FOR NO.

TYPE 'HELP' FOR A DISCRIPTION OF THESE ASSIGNMENTS      -- STOP   Return to
                                                                   main program
```

30 March 1984
CBB:SIH:JEH:DAB:lhz

M A I N M E N U

1) TO REFINE RAW DATA.
2) TO PLOT DIFFERENCE OF TWO REFINED FILES.
3) TO PLOT A REFINED DATA FILE.
4) TO READ AND PRINT A REFINED DATA FILE.
5) TO READ AND PRINT A RAW DATA FILE.
6) TO EXIT

PLEASE ENTER YOUR SELECTION -6
FORTRAN STOP

C O M M A N D M E N U

1) RETREIVE UNSCRAMBLED RAW DATA FROM STORAGE TAPES.

2) RETREIVE UNNORMALIZED CORRECTED DATA FROM STORAGE TAPES. (NOT THE SAME AS OPTION 1)

3) RUN THE MAIN PROGRAM.

4) DELETE UNSCRAMBLED 'RAW' DATA FILES.

5) DELETE UNNORMALIZED 'CORRECTED' DATA FILES.

6) DELETE PLOT FILES FROM DISK STORAGE.

7) SEND PLOTS TO THE HP PLOTTER

8) EXIT

PLEASE ENTER YOUR SELECTION. ----: 7
MEASUREMENT NUMBER? --: 141
CUT NUMBER? --: *
FREQUENCY? --(IF ANY):
CHANNEL NUMBER? --: *
  Job 6551 entered on queue PLOTTER
DO YOU WISH TO MAKE MORE PLOTS? --: N

Plot data from all channels

AD-A148 771 ACOUSTIC RADIATION FROM SINGLE AND DOUBLE RIBBED CIRCULAR CYLINDRICAL SHE..(U) PENNSYLVANIA STATE UNIV UNIVERSITY PARK APPLIED RESEARCH LAB.. 2/2

UNCLASSIFIED C B BURROUGHS ET AL. 30 MAR 84 F/G 20/1 NL

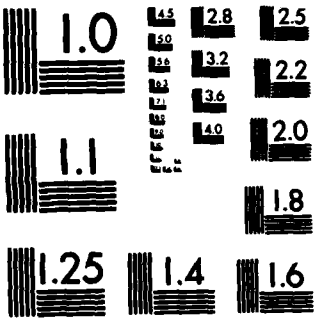

30 March 1984
CBB:SIH:JEH:DAB:lhz

COMMAND MENU

1) RETREIVE UNSCRAMBLED RAW DATA FROM STORAGE TAPES.

2) RETREIVE UNNORMALIZED CORRECTED DATA FROM STORAGE TAPES. (NOT THE SAME AS OPTION 1)

3) RUN THE MAIN PROGRAM.

4) DELETE UNSCRAMBLED 'RAW' DATA FILES.

5) DELETE UNNORMALIZED 'CORRECTED' DATA FILES.

6) DELETE PLOT FILES FROM DISK STORAGE.

7) SEND PLOTS TO THE HP PLOTTER

8) EXIT

99) LOGOUT

PLEASE ENTER YOUR SELECTION. ----->: 99

JEH logged out at 13-MAR-1984 14:55:24.94

30 March 1984
CBB:SIH:JEH:DAB:1hz

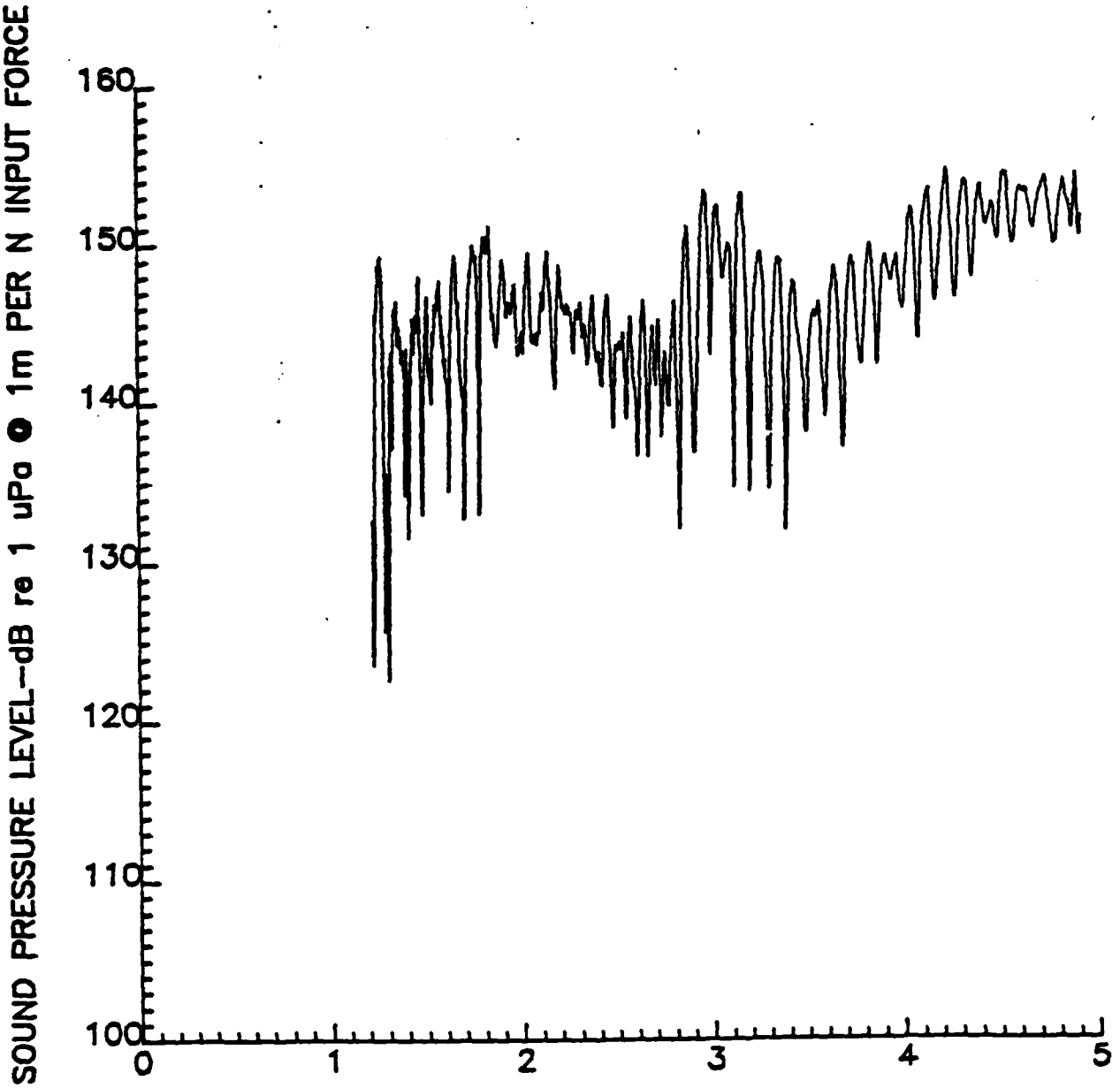

PLOT FOR ONR FIELD MEASUREMENT NO. 141 CUT NO. 1
DOUBLE SHELL WITH SHAKERS HORIZONTAL
PHONE NO. 1
SHAKER LOCATION – ON THE JOINT BAND
LONG. DRIVE – OUT OF PHASE

Figure A1. Sample Plot for Phone #1

30 March 1984
CBB:SIH:JEH:DAB:1hz

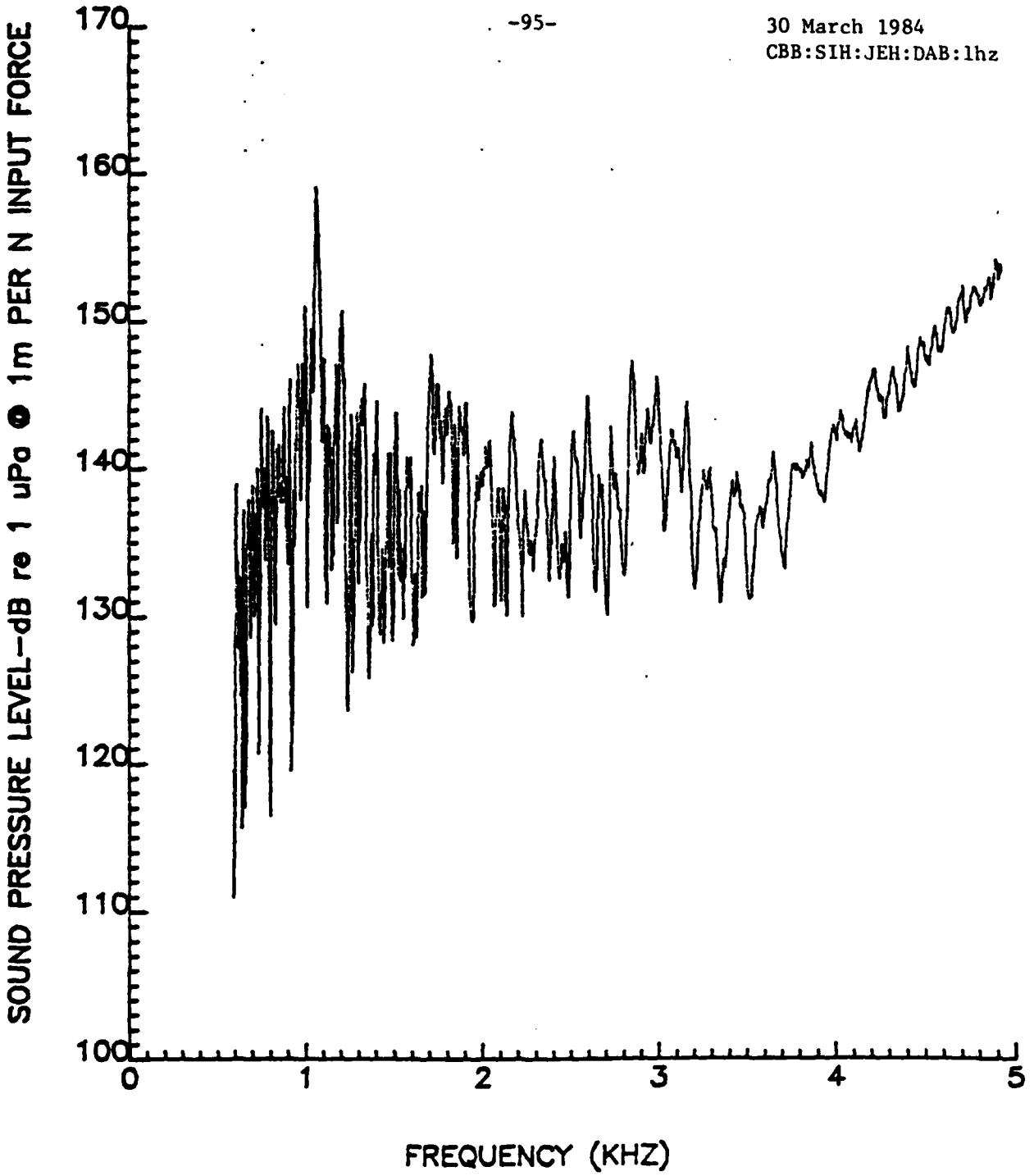

PLOT FOR ONR FIELD MEASUREMENT NO. 141 CUT NO. 1
DOUBLE SHELL WITH SHAKERS HORIZONTAL
PHONE NO. 2
SHAKER LOCATION — ON THE JOINT BAND
LONG. DRIVE — OUT OF PHASE

Figure A2. Sample Plot for Phone #2

DISTRIBUTION LIST FOR UNCLASSIFIED TECHNICAL MEMORANDUM FILE NO. 84-76
by C. B. Burroughs, S. I. Hayek, J. E. Hallander and D. A. Bostian,
dated 30 March 1984

Defense Documentation Center
5010 Duke Street
Cameron Station
Alexandria, VA 22314
(Copies 1 through 12)

Commander
Office of Naval Research
800 North Quincy Street
Department of the Navy
Arlington, VA 22217
Attn: Code 220
(Copy No. 13)

Commander
Office of Naval Research
800 North Quincy Street
Department of the Navy
Arlington, VA 22217
Attn: Code 280
(Copy No. 14)

Commander
Office of Naval Research
800 North Quincy Street
Department of the Navy
Arlington, VA 22217
Attn: Code 432
(Copies 15 through 18)

Commander
Naval Research Laboratory
Department of the Navy
Washington, DC 20375
Attn: Code 2620
(Copy No. 19)

Commander
Naval Research Laboratory
Department of the Navy
Washington, DC 20375
Attn: Code 5130
(Copy No. 20)

Commander
Naval Research Laboratory
Department of the Navy
Washington, DC 20375
Attn: Code 5132
(Copy No. 21)

Commander
Naval Research Laboratory
Department of the Navy
Washington, DC 20375
Attn: 5830
(Copy No. 22)

Commanding Officer
David W. Taylor Naval Ship
Research & Development Ctr.
Department of the Navy
Bethesda, MD 20084
Attn: Code 172
(Copy No. 23)

Commanding Officer
David W. Taylor Naval Ship
Research & Development Ctr.
Department of the Navy
Bethesda, MD 20084
Attn: Code 1844
(Copy No. 24)

Commanding Officer
David W. Taylor Naval Ship
Research & Development Ctr.
Department of the Navy
Bethesda, MD 20084
Attn: Code 1900
Copy No. 25)

Commanding Officer
David W. Taylor Naval Ship
Research & Development Ctr.
Department of the Navy
Bethesda, MD 20084
Attn: Code 1905.4
(Copy No. 26)

DISTRIBUTION LIST FOR UNCLASSIFIED TECHNICAL MEMORANDUM FILE NO. 84-76
by C. B. Burroughs, S. I. Hayek, J. E. Hallander and D. A. Bostian,
dated 30 March 1984 [continuation]

Commanding Officer
David W. Taylor Naval Ship
Research & Development Ctr.
Department of the Navy
Bethesda, MD 20084
Attn: Code 1960
(Copy No. 27)

Commanding Officer
David W. Taylor Naval Ship
Research & Development Ctr.
Department of the Navy
Bethesda, MD 20084
Attn: Code 1965
(Copies 28 and 29)

Commanding Officer
David W. Taylor Naval Ship
Research & Development Ctr.
Department of the Navy
Annapolis, MD 21402
Attn: Code 2740.1
(Copy No. 30)

Commander
Naval Surface Weapons Ctr.
Department of the Navy
White Oak, MD 20910
Attn: Code R13
(Copy No. 31)

Commander
Naval Surface Weapons Ctr.
Department of the Navy
White Oak, MD 20910
Attn: Code R14
(Copy No. 32)

Commander
Naval Surface Weapons Ctr.
Department of the Navy
White Oak, MD 20910
Attn: Code R30
(Copy No. 33)

Commander
Naval Surface Weapons Ctr.
Department of the Navy
White Oak, MD 20910
Attn: R43
(Copy No. 34)

Commander
Naval Surface Weapons Ctr.
Department of the Navy
White Oak, MD 20910
Attn: Technical Library
(Copy No. 35)

Commander
Naval Surface Weapons Ctr.
Department of the Navy
Dahlgren, VA 22448
Attn: Technical Library
(Copy No. 36)

Commanding Officer
Naval Underwater Systems Ctr.
Department of the Navy
New London, CT 06320
Attn: Code 323
(Copy No. 37)

Commanding Officer
Naval Underwater Systems Ctr.
Department of the Navy
New London, CT 06320
Attn: Code 44
(Copy No. 38)

Commanding Officer
Naval Underwater Systems Ctr.
Department of the Navy
New London, CT 06320
Attn: D. A. Bostian
(Copy No. 39)

DISTRIBUTION LIST FOR UNCLASSIFIED TECHNICAL MEMORANDUM FILE NO. 84-76
by C. B. Burroughs, S. I. Hayek, J. E. Hallander and D. A. Bostian,
dated 30 March 1984 [continuation]

Commanding Officer
Naval Underwater Systems Ctr.
Department of the Navy
New London, CT 06320
Attn: Technical Library
(Copy No. 40)

Commanding Officer
Naval Underwater Systems Ctr.
Department of the Navy
Newport, RI 02840
Attn: Code 3634
(Copy No. 41)

Commanding Officer
Naval Underwater Systems Ctr.
Department of the Navy
Newport, RI 02840
Attn: A. Harari
(Copy No. 42)

Commanding Officer
Naval Underwater Systems Ctr.
Department of the Navy
Newport, RI 02840
Attn: B. Sandman
(Copy No. 43)

Commanding Officer
Naval Underwater Systems Ctr.
Department of the Navy
Newport, RI 02840
Attn: Technical Library
(Copy No. 44)

Commander
Naval Weapons Ctr.
Department of the Navy
China Lake, CA 93555
Attn: Technical Library
(Copy No. 45)

Commander
NRL/Underwater Sound
Reference Detachment
Orlando, FL 32856
Attn: Technical Library
(Copy No. 46)

Chief of Naval Operations
Department of the Navy
Washington, DC 20350
Attn: Code OP-098
(Copy No. 47)

Commander
Naval Sea Systems Command
Department of the Navy
Washington, DC 20362
Attn: Code 05R25
(Copy No. 48)

Commander
Naval Sea Systems Command
Department of the Navy
Washington, DC 20362
Attn: Code 05R26
(Copy No. 49)

Commander
Naval Sea Systems Command
Department of the Navy
Washington, DC 20362
Attn: Code 55N
(Copy No. 50)

Commander
Naval Sea Systems Command
Department of the Navy
Washington, DC 20362
Attn: Code 63R
(Copy No. 51)

DISTRIBUTION LIST FOR UNCLASSIFIED TECHNICAL MEMORANDUM FILE NO. 84-76
by C. B. Burroughs, S. I. Hayek, J. E. Hallander and D. A. Bostian,
dated 30 March 1984 [continuation]

Commander
Naval Air Systems Command
Department of the Navy
Washington, DC 20361
Attn: Code 03D
(Copy No. 52)

Commander
Naval Air Systems Command
Department of the Navy
Washington, DC 20361
Attn: Code 7226
(Copy No. 53)

U.S. Naval Academy
Dept. of Mechanical Engineering
Annapolis, MD 21402
Attn: Technical Library
(Copy No. 54)

Naval Postgraduate School
Monterey, CA 93940
Attn: Technical Library
(Copy No. 55)

Mr. Jerome Persh
Staff Specialist for Materials
and Structures
OUSDR&E, The Pentagon
Room 3D1089
Washington, DC 20301
(Copy No. 56)

Dr. M. L. Baron
Weidlinger Associates
333 Seventh Avenue
New York, NY 10001
(Copy No. 57)

Professor G. Herrmann
Dept. of Applied Mechanics
Stanford University
Stanford, CA 94305
(Copy No. 58)

Professor J. A. Clark
Dept. of Mechanical Enginering
Catholic University of America
Washington, DC 20064
(Copy No. 59)

Professor H. Uberall
Dept. of Physics
Catholic University of America
Washington, DC 20064
(Copy No. 60)

Professor J. C. S. Yang
Dept. of Mechanical Engineering
The University of Maryland
College Park, MD 20742
(Copy No. 61)

Dr. R. D. Mindlin
Post Office Box 385
Grantham, NH 03753
(Copy No. 62)

Dr. T. L. Geers
Lockheed Missiles and Space Co.
3251 Hanover Street
Palo Alto, CA 94303
(Copy No. 63)

Dr. M. C. Junger
Cambridge Acoustical Associates
54 Ridge Avenue Extension
Cambridge, MA 02140
(Copy No. 64)

Professor R. Keltie
Dept. of Mechanical Engineering
North Carolina State University
Raleigh, NC 27650
(Copy No. 65)

DISTRIBUTION LIST FOR UNCLASSIFIED TECHNICAL MEMORANDUM FILE NO. 84-76
by C. B. Burroughs, S. I. Hayek, J. E. Hallander and D. A. Bostian,
dated 30 March 1984 [continuation]

Dr. R. S. Dunham
Anatech International Corporation
3344 North Torrey Pines Court
Suite 320
La Jolla, CA 92037
(Copy No. 66)

Professor E. Becker
Dept. of Engineering Mechanics
The University of Texas at Austin
Austin, TX 78712-1085
(Copy No. 67)

Professor P. Pinsky
Dept. of Civil Engineering
Stanford University
Stanford, CA 94305
(Copy No. 68)

Professor J. D. Achenbach
Dept. of Civil Engineering
Northwestern University
Evanston, IL 60201
(Copy No. 69)

Professor J. Awerbach
Dept. of Mechanical Engineering
and Mechanics
Drexel University
Philadelphia, PA 19104
(Copy No. 70)

Director
Applied Research Laboratory
The Pennsylvania State University
Post Office Box 30
State College, PA 16804
Attn: C. B. Burroughs
(Copies 71 and 72)

Director
Applied Research Laboratory
The Pennsylvania State University
Post Office Box 30
State College, PA 16804
Attn: S. I. Hayek
(Copies 73 and 74)

Director
Applied Research Laboratory
The Pennsylvania State University
Post Office Box 30
State College, PA 16804
Attn: R. E. Henderson
(Copy No. 75)

Director
Applied Research Laboratory
The Pennsylvania State University
Post Office Box 30
State College, PA 16804
Attn: L. R. Hettche
(Copy No. 76)

Director
Applied Research Laboratory
The Pennsylvania State University
Post Office Box 30
State College, PA 16804
Attn: B. R. Parkin
(Copy No. 77)

Director
Applied Research Laboratory
The Pennsylvania State University
Post Office Box 30
State College, PA 16804
Attn: E. J. Skudrzyk
(Copy No. 78)

Director
Applied Research Laboratory
The Pennsylvania State University
Post Office Box 30
State College, PA 16804
Attn: GTWT Files
(Copy No. 79)

Director
Applied Research Laboratory
The Pennsylvania State University
Post Office Box 30
State College, PA 16804
Attn: ARL/PSU Library
(Copy No. 80)

END

FILMED

1-85

DTIC